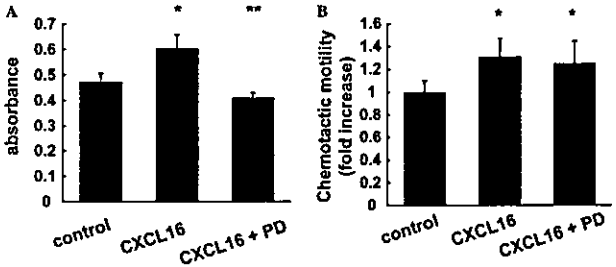

Fig. 4. MEK inhibitor suppressed CXCL16-induced proliferation, but not chemotaxis in HUVEC. (A) Cells were pretreated with or without PD98059 (25 μM) for 30 min and stimulated with 1 nM CXCL16 for 48 h. Cell proliferation was then determined by WST-1 assay. (B) CXCL16-induced chemotactic mobility of HUVEC was determined in the absence or presence of MEK inhibitor PD98059. Cells were preincubated for 30 min with or without PD98059 (25 μM) prior to treating with 1 nM CXCL16. Data A represent means ± SD, and similar results were obtained in two different experiments. Data B are expressed as fold increase over control ± SD from two different experiments with triplicate. $^{*}p < 0.05$ vs. control; $^{**}p < 0.05$ vs. CXCL16 (1 nM).

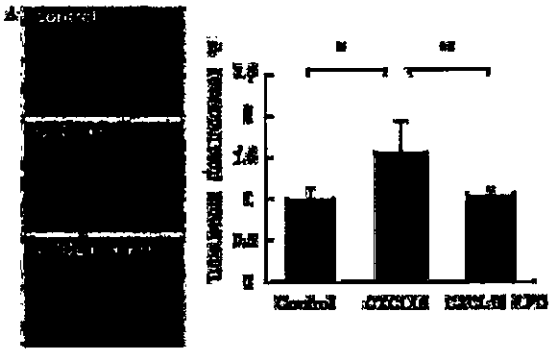

Fig. 5. MEK inhibitor inhibited CXCL16-mediated tube formation in HUVEC. (A) Cells (5×10^4/well) were pretreated with or without PD98059 (25 μM) for 30 min before stimulation with CXCL16 (1 nM). After incubation on Matrigel-coated wells for 20 h, photographs were taken under microscope (40×). Representative pictures are shown. (B) The length of tube was quantitated using Image-Pro Plus software. Data are expressed as fold increase over control ± SD from two independent experiments with triplicate determinations. $^{*}p < 0.05$ vs. control; $^{**}p < 0.05$ vs. CXCL16 (1 nM).

Acknowledgments

This study was supported by Grants-in-Aid from the Ministry of Education, Culture, Sports, Science and Technology, Japan (20045982, 12671111, 14571093, and 13307034); Center of Excellence grants from the Ministry of Education, Science, Sports and Culture of Japan (12CE2006); a research grant for health sciences from the Japanese Ministry of Health and Welfare. This study is also supported in part by Establishment of International COE for Integration of Transplantation Therapy and Regenerative Medicine (COE program of the Ministry of Education, Culture, Sports, Science and Technology, Japan). X.Z. was supported from 21st century Center of Excellent program from the Ministry of Education, Culture, Sports, Science and Technology, Japan.

References

[1] J. Folkman, Angiogenesis in cancer, vascular, rheumatoid and other disease, Nat. Med. 1 (1995) 27–31.
[2] J.R. Jackson, M.P. Seed, C.H. Kircher, D.A. Willoughby, J.D. Winkler, The codependence of angiogenesis and chronic inflammation, FASEB J. 11 (1997) 457–465.
[3] W. Risau, Mechanisms of angiogenesis, Nature 386 (1997) 671–674.
[4] F. Bussolino, A. Mantovani, G. Persico, Molecular mechanisms of blood vessel formation, Trends Biochem. Sci. 22 (1997) 251–256.

[5] M. Matloubian, A. David, S. Engel, J.E. Ryan, J.G. Cyster, A transmembrane CXC chemokine is a ligand for HIV-coreceptor Bonzo, Nat. Immunol. 1 (2000) 298–304.
[6] A. Wilbanks, S.C. Zondlo, K. Murphy, S. Mak, D. Soler, P. Langdon, D.P. Andrew, L. Wu, M. Briskin, Expression cloning of the STRL33/BONZO/TYMSTR ligand reveals elements of CC, CXC, and CX3C chemokines, J. Immunol. 166 (2001) 5145–5154.
[7] T. Shimaoka, N. Kume, M. Minami, K. Hayashida, H. Kataoka, T. Kita, S. Yonehara, Molecular cloning of a novel scavenger receptor for oxidized low density lipoprotein, SR-PSOX, on macrophages, J. Biol. Chem. 275 (2000) 40663–40666.
[8] M. Minami, N. Kume, T. Shimaoka, H. Kataoka, K. Hayashida, Y. Akiyama, I. Nagata, K. Ando, M. Nobuyoshi, M. Hanyuu, M. Komeda, S. Yonehara, T. Kita, Expression of SR-PSOX, a novel cell-surface scavenger receptor for phosphatidylserine and oxidized LDL in human atherosclerotic lesions, Arterioscler. Thromb. Vasc. Biol. 21 (2001) 1796–1800.
[9] A.C. Li, C.K. Glass, The macrophage foam cell as a target for therapeutic intervention, Nat. Med. 8 (2002) 1235–1242.
[10] O. Hofnagel, B. Luechtenborg, G. Plenz, H. Robenek, Expression of the novel scavenger receptor SR-PSOX in cultured aortic smooth muscle cells and umbilical endothelial cells, Arterioscler. Thromb. Vasc. Biol. 22 (2002) 710–711.
[11] B. Chandrasekar, S. Bysani, S. Mummidi, CXCL16 signals via Gi, phosphatidylinositol 3-kinase, Akt, I kappa B kinase, and nuclear factor-kappa B and induces cell–cell adhesion and aortic smooth muscle cell proliferation, J. Biol. Chem. 279 (2004) 3188–3196.
[12] R. Yamauchi, M. Tanaka, N. Kume, M. Minami, T. Kawamoto, K. Togi, T. Shimaoka, S. Takahashi, J. Yamaguchi, T. Nishina, M. Kitaichi, M. Komeda, T. Manabe, S. Yonehara, T. Kita, Upregulation of SR-PSOX/CXCL16 and recruitment of CD8+ T cells in cardiac valves during inflammatory valvular heart disease, Arterioscler. Thromb. Vasc. Biol. 24 (2004) 282–287.
[13] O.H. Lee, Y.M. Kim, Y.M. Lee, E.J. Moon, D.J. Lee, J.H. Kim, K.W. Kim, Y.G. Kwon, Sphingosine 1-phosphate induces angiogenesis: its angiogenic action and signaling mechanism in human umbilical vein endothelial cells, Biochem. Biophys. Res. Commun. 264 (1999) 743–750.
[14] Y.M. Kim, Y.M. Lee, H.S. Kim, J.D. Kim, Y. Choi, K.W. Kim, S.Y. Lee, Y.G. Kwon, TNF-related activation-induced cytokine (TRANCE) induces angiogenesis through the activation of Src and phospholipase C (PLC) in human endothelial cells, J. Biol. Chem. 277 (2002) 6799–6805.
[15] M. Kuzuya, S. Satake, M.A. Ramos, S. Kanda, T. Koike, K. Yoshino, S. Ikeda, A. Iguchi, Induction of apoptotic cell death in vascular endothelial cells cultured in three-dimensional collagen lattice, Exp. Cell Res. 248 (1999) 498–508.
[16] Y. Yu, J.D. Sato, MAP kinases, phosphatidylinositol 3-kinase, and p70 S6 kinase mediate the mitogenic response of human endothelial cells to vascular endothelial growth factor, J. Cell. Physiol. 178 (1999) 235–246.
[17] J.C. Groskopf, L.J. Syu, A.R. Saltiel, D.I. Linzer, Proliferin induces endothelial cell chemotaxis through a G protein-coupled, mitogen-activated protein kinase-dependent pathway, Endocrinology 138 (1997) 2835–2840.
[18] T. Shono, H. Kanetake, S. Kanda, The role of mitogen-activated protein kinase activation within focal adhesions in chemotaxis toward FGF-2 by murine brain capillary endothelial cells, Exp. Cell Res. 264 (2001) 275–283.
[19] F. Liu, A.D. Verin, P. Wang, R. Day, R.P. Wersto, F.J. Chrest, D.K. English, J.G. Garcia, Differential regulation of sphingosine-1-phosphate- and VEGF-induced endothelial cell chemotaxis. Involvement of G(ialpha2)-linked Rho kinase activity, Am. J. Respir. Cell Mol. Biol. 24 (2001) 711–719.

Editorials

See related article, pages 370–376

Apoptosis of Vascular Cells by Oxidized LDL

Involvement of Caspases and LOX-1 and Its Implication in Atherosclerotic Plaque Rupture

Noriaki Kume, Toru Kita

Atherosclerotic plaque rupture followed by thrombus formation is a key event in the onset of acute coronary syndrome.[1] Apoptotic death of smooth muscle cells in the fibrous cap of the atherosclerotic plaque, in addition to degradation of extracellular matrix proteins by matrix metalloproteinases (MMPs), appears to be involved in atherosclerotic plaque rupture.[1] Oxidized LDL (Ox-LDL) has been implicated in the pathogenesis of atherosclerosis and atherosclerotic plaque rupture by promoting lipid accumulation, proinflammatory responses, and apoptotic cell death.[2–4] In fact, apoptotic cells are present in atherosclerotic lesions.[4,5] These biological effects, including proapoptotic effects, of Ox-LDL appear to be, at least in part, mediated by cell-surface receptors for Ox-LDL.[6]

Among several different classes of oxidized LDL receptors (also designated scavenger receptors) most of which are expressed mainly by macrophages, lectin-like oxidized LDL receptor-1 (LOX-1) is a type II membrane glycoprotein and expressed by activated vascular endothelial and smooth muscle cells, as well as macrophages.[7–10] LOX-1 expression can dynamically be induced by proinflammatory and other pathological stimuli relevant to atherogenesis.[11–14] Particularly, LOX-1 is induced by its ligand Ox-LDL,[15,16] as well as proinflammatory cytokines,[11,12] thus making a positive-feedback loop to enhance the effect of Ox-LDL on vascular cells. Uptake of Ox-LDL through LOX-1 induces reactive oxygen species (ROS), reduces nitric oxide, activates NF-κB,[17,18] and thereby upregulates expression of monocyte chemoattractant protein-1 (MCP-1) and MMPs.[19–21] LOX-1–dependent uptake of Ox-LDL also induces expression of a proapoptotic factor Bax, downregulates an antiapoptotic factor Bcl-2, and induces apoptosis of cultured vascular smooth muscle cells,[15] as well as endothelial cells.[16]

In human advanced atherosclerotic lesions, but not in normal arterial walls, macrophages and smooth muscle cells in the intima, in addition to vascular endothelial cells, dominantly express LOX-1,[22] which is colocalized with Bax.[15] In the early stages of atherogenesis, LOX-1 expression is prominent in vascular endothelial cells,[22,23] and apoptosis of endothelial cells also are detected, which may be implicated in endothelial dysfunction.[4] Thus, evidence has been accumulated to indicate that vascular cell apoptosis is mediated by Ox-LDL and its receptor LOX-1, and it may be crucial for atherosclerotic plaque rupture in the advanced stage, as well as endothelial dysfunction in the early stage.

However, molecular mechanisms involved in cell apoptosis by Ox-LDL and LOX-1 interactions have not been fully understood. In this issue of *Circulation Research*, Chen et al[24] have explored the involvement of caspases and the related molecules, such as Bcl-2 and c-IAP-2, and report that activation of caspase-9 and subsequent activation of caspase-3 are responsible for Ox-LDL–induced apoptosis of cultured vascular endothelial cells through its receptor LOX-1. In addition, release of mitochondrial apoptotic proteins, such as cytochrome *c* and Smac, was associated with Ox-LDL–induced caspase activation and apoptosis. Because Ox-LDL–induced release of cytochrome *c* or Smac was blocked by antisense oligonucleotides for LOX-1 but not affected by caspase inhibitors, cytochrome *c* and Smac appear to be upstream of caspase 9 and caspase 3 or might alternatively be independent of these caspases, although LOX-1 mediates the both pathways.

Chen et al[24] have confirmed that caspase 9 is upstream of caspase 3[25] in the Ox-LDL–induced apoptosis, as shown in cytochrome *c*–dependent apoptosis by other stimuli.[26] In addition, LOX-1–dependent downregulation of Bcl-2 by Ox-LDL is also shown in this study, as shown in cultured vascular smooth muscle cells.[15] Bcl-2 appears to be the upstream of cytochrome *c* and Smac and thus may inhibit their mitochondrial release. Furthermore, c-IAP-1, an inhibitor of caspase activation, has been shown to be downregulated by Ox-LDL, depending on LOX-1, in this study (Figure). LOX-1–dependent downregulation of Bcl-2 and c-IAP-1 may depend on ROS and its downstream signals; however, these points remain to be determined. Because activation of protein kinase C,[20] mitogen-activated protein (MAP) kinases,[19] and nuclear factor-κB (NF-κB)[17] and inhibition of phosphatidylinositol 3-kinase (PI3K)/Akt,[27] as well as production of ROS,[17] are involved in Ox-LDL and LOX-1–mediated cellular events, roles of these signal transduction cascades and transcription factors in Ox-LDL–induced downregulation of Bcl-2 and c-IAP-1, as well as cell apoptosis, should also be explored. In fact, PI3K/Akt has been implicated in Ox-LDL/LOX-1–induced apoptosis.[27,28] In addition, Bax is also the upstream of cytochrome *c* and Smac release and is upregulated by Ox-LDL–LOX-1 interactions,[15] signal transduction cascades, and transcription factors involved in Ox-LDL–induced upregulation of Bax should also be examined. More importantly, future studies should be conducted to determine the effect of vascular cell apoptosis in the pathogenesis of atherosclerotic plaque rupture, thrombus formation, and the onset of acute coronary syndrome in humans or suitable animal models in vivo.

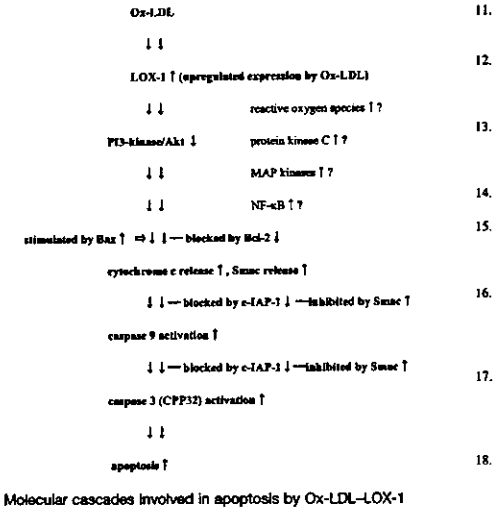

Molecular cascades involved in apoptosis by Ox-LDL–LOX-1 interactions.

References

1. Libby P. Current concepts of the pathogenesis of the acute coronary syndromes. *Circulation*. 2001;104:365–372.
2. Ross R. Atherosclerosis: an inflammatory disease. *N Engl J Med*. 1999; 1340:115–126.
3. Steinberg D. Lewis A. Conner Memorial Lecture: oxidative modification of LDL and atherogenesis. *Circulation*. 1997;95:1062–1071.
4. Norata GD, Tonti L, Roma P, Catapano AL. Apoptosis and proliferation of endothelial cells in early atherosclerotic lesions: possible role of oxidised LDL. *Nutr Metab Cardiovasc Dis*. 2002;12:297–305.
5. Kockx MM, De Meyer GR, Muhring J, Jacob W, Bult H, Herman AG. Apoptosis and related proteins in different stages of human atherosclerosis and restenosis. *Circulation*. 1998;97:2307–2315.
6. Krieger M, Acton S, Ashkenas J, Pearson A, Penman M, Resnick D. Molecular flypaper, host defense, and atherosclerosis: structure, binding properties, and functions of macrophage scavenger receptors. *J Biol Chem*. 1993;268:4569–4572.
7. Sawamura T, Kume N, Aoyama T, Moriwaki H, Hoshikawa H, Aiba Y, Tanaka T, Miwa S, Katsura Y, Kita T, Masaki T. A novel endothelial receptor for oxidised low density lipoprotein. *Nature*. 1997;386:73–77.
8. Moriwaki H, Kume N, Sawamura T, Aoyama T, Hoshikawa H, Ochi H, Nishi E, Masaki T, Kita T. Ligand specificity of LOX-1, a novel receptor for oxidized low-density lipoprotein. *Arterioscler Thromb Vasc Biol*. 1998;18:1541–1547.
9. Kataoka H, Kume N, Miyamoto S, Murase T, Minami M, Sawamura T, Masaki T, Hashimoto N, Kita T. Biosynthesis and posttranslational processing of lectin-like oxidized LDL receptor-1 (LOX-1): N-linked glycosylation affects the cell-surface expression and the ligand binding. *J Biol Chem*. 2000;275:6573–6579.
10. Kume N, Kita T. Roles of lectin-like oxidized low density lipoprotein receptor-1 (LOX-1) and its soluble forms in atherogenesis. *Curr Opin Lipidol*. 2001;12:419–423.
11. Kume N, Murase T, Moriwaki H, Aoyama T, Sawamura T, Masaki T, Kita T. Inducible expression of lectin-like oxidized low density lipoprotein receptor-1 in vascular endothelial cells. *Circ Res*. 1998;83:322–327.
12. Minami M, Kume N, Kataoka H, Morimoto M, Hayashida K, Sawamura T, Masaki T, Kita T. Transforming growth factor-β1 increases the expression of lectin-like oxidized low density lipoprotein receptor-1. *Biochem Biophys Res Commun*. 2000;272:357–361.
13. Moriwaki H, Kume N, Kataoka H, Murase T, Nishi E, Sawamura T, Masaki T, Kita T. Expression of lectin-like oxidized low density lipoprotein receptor-1 in human and murine macrophages-upregulated expression by TNF-α. *FEBS Lett*. 1998;440:29–32.
14. Kita T. LOX-1, a possible clue to the missing link between hypertension and atherogenesis. *Circ Res*. 1999;84:1113–1115.
15. Kataoka H, Kume N, Miyamoto S, Minami M, Morimoto M, Hayashida K, Hashimoto N, Kita T. Oxidized low density lipoprotein (Ox-LDL) modulates Bax/Bcl-2 through lectin-like Ox-LDL receptor-1 in vascular smooth muscle cells. *Arterioscler Thromb Vasc Biol*. 2001;21:955–960.
16. Li D, Mehta JL. Upregulation of endothelial receptor for oxidized LDL (LOX-1) by oxidized LDL and implications in apoptosis of human coronary artery endothelial cells: evidence from use of antisense LOX-1 mRNA and chemical inhibitors. *Arterioscler Thromb Vasc Biol*. 2000; 20:1116–1122.
17. Cominacini L, Pasini AF, Garbin U, Davoli A, Tosetti ML, Campagnola M, Rigioni A, Pastorino AM, Lo Cascio V, Sawamura T. Oxidized low-density lipoprotein binding to LOX-1 in endothelial cells induces the activation of NF-κB through an increased production of intracellular reactive oxygen species. *J Biol Chem*. 2000;275:633–638.
18. Cominacini L, Rigoni A, Pasini AF, Garbin U, Davoli A, Campagnola M, Pastorino AM, Lo Cascio V, Sawamura T. The binding of oxidized low-density lipoprotein (ox-LDL) to ox-LDL receptor-1 reduces the intracellular concentration of nitric oxide in endothelial cells through an increased production of superoxide. *J Biol Chem*. 2001;276:13750–13755.
19. Li D, Mehta JL. Antisense to LOX-1 inhibits oxidized LDL-mediated upregulation of monocyte chemoattractant protein-1 and monocyte adhesion to human coronary artery endothelial cells. *Circulation*. 2000; 101:2889–2895.
20. Li D, Liu L, Chen H, Sawamura T, Ranganathan S, Mehta JL. LOX-1 mediates oxidized low-density lipoprotein-induced expression of matrix metalloproteinases in human coronary artery endothelial cells. *Circulation*. 2003;107:612–617.
21. Li D, Williams V, Liu L, Chen H, Sawamura T, Antakli T, Mehta JL. LOX-1 inhibition in myocardial ischemia-reperfusion injury: modulation of MMP-1 and inflammation. *Am J Physiol*. 2002;283:H1795–H1801.
22. Kataoka H, Kume N, Miyamoto S, Minami M, Moriwaki H, Sawamura T, Masaki T, Hashimoto N, Kita T. Expression of lectin-like oxidized low density lipoprotein receptor-1 in human atherosclerotic lesions. *Circulation*. 1999;99:3110–3117.
23. Chen M, Kakutani M, Minami M, Kataoka H, Kume N, Narumiya S, Kita T, Masaki T, Sawamura T. Increased expression of lectin-like oxidized low density lipoprotein receptor-1 in initial atherosclerotic lesions of Watanabe heritable hyperlipidemic rabbits. *Arterioscler Thromb Vasc Biol*. 2000;20:1107–1115.
24. Chen J, Mehta JL, Haider N, Zhang X, Narula J, Li D. Role of caspases in Ox-LDL–induced apoptotic cascade in human coronary artery endothelial cells. *Circ Res*. 2004;94:370–376.
25. Dimmeler S, Haendeler J, Galle J, Zeiher AM. Oxidized low-density lipoprotein induces apoptosis of human endothelial cells by activation of CPP32-like proteases. *Circulation*. 1997;95:1760–1763.
26. Slee EA, Harte MT, Kluck RM, Wolf BB, Casiano CA, Newmeyer DD, Wang HG, Reed JC, Nicholson DW, Alnemri ES, Green DR, Martin SJ. Ordering the cytochrome c-initiated caspase cascade: hierarchical activation of caspases-2, -3, -6, -7, -8, and -10 in a caspase-9-dependent manner. *J Cell Biol*. 1999;144:281–292.
27. Nakagawa T, Yasuda T, Hoshokawa H, Shimizu M, Kakinuma T, Chen M, Masaki T, Nakamura T, Sawamura T. LOX-1 expressed in cultured rat chondrocytes mediates oxidized LDL-induced cell death-possible role of dephosphorylation of Akt. *Biochem Biophys Res Commun*. 2002;299:91–97.
28. Li Y, Higashi Y, Itabe H, Song Y-H, Du J, Delafontaine P. Insulin-like growth factor-1 receptor activation inhibits oxidized LDL-induced cytochrome *c* release and apoptosis via the phosphatidylinositol 3 kinase/Akt signaling pathway. *Arterioscler Thromb Vasc Biol*. 2003;23:2178–2184.

KEY WORDS: oxidized LDL ■ caspases ■ apoptosis

The opinions expressed in this editorial are not necessarily those of the editors or of the American Heart Association.

From the Department of Cardiovascular Medicine, Graduate School of Medicine, Kyoto University, Kyoto, Japan.

Correspondence to Noriaki Kume, MD, PhD, Department of Cardiovascular Medicine, Graduate School of Medicine, Kyoto University, 54 Kawahara-cho, Shogoin, Sakyo-ku, Kyoto 606-8507, Japan. E-mail nkume@kuhp.kyoto-u.ac.jp

(*Circ Res*. 2004;94:269–270.)

Circulation Research is available at http://www.circresaha.org
DOI: 10.1161/01.RES.0000119804.92239.97

Genetic subtypes of familial hemophagocytic lymphohistiocytosis: correlations with clinical features and cytotoxic T lymphocyte/natural killer cell functions

Eiichi Ishii, Ikuyo Ueda, Ryutaro Shirakawa, Ken Yamamoto, Hisanori Horiuchi, Shouichi Ohga, Kenji Furuno, Akira Morimoto, Miyoko Imayoshi, Yoshiyasu Ogata, Masafumi Zaitsu, Masahiro Sako, Kenichi Koike, Akifumi Sakata, Hidetoshi Takada, Toshiro Hara, Shinsaku Imashuku, Takehiko Sasazuki, and Masaki Yasukawa

Mutations of the perforin (*PRF1*) and *MUNC13-4* genes distinguish 2 forms of familial hemophagocytic lymphohistiocytosis (FHL2 and FHL3, respectively), but the clinical and biologic correlates of these genotypes remain in question. We studied the presenting features and cytotoxic T lymphocyte/natural killer (CTL/NK) cell functions of 35 patients for their relationship to distinct FHL subtypes. FHL2 (n = 11) had an earlier onset than either FHL3 (n = 8) or the non-FHL2/FHL3 subtype lacking a *PRF1* or *MUNC13-4* mutation (n = 16). Deficient NK cell activity persisted after chemotherapy in all cases of FHL2, whereas some patients with FHL3 or the non-FHL2/FHL3 subtype showed partial recovery of this activity during remission. Alloantigen-specific CTL-mediated cytotoxicity was deficient in FHL2 patients with *PRF1* nonsense mutations, was very low in FHL3 patients, but was only moderately reduced in FHL2 patients with *PRF1* missense mutations. These findings correlated well with Western blot analyses showing an absence of perforin in FHL2 cases with *PRF1* nonsense mutations and of MUNC13-4 in FHL3 cases, whereas in FHL2 cases with *PRF1* missense mutations, mature perforin was present in low amounts. These results suggest an association between the type of genetic mutation in FHL cases and the magnitude of CTL cytolytic activity and age at onset. (Blood. 2005;105: 3442-3448)

Introduction

Hemophagocytic lymphohistiocytosis (HLH) is characterized by fever and hepatosplenomegaly associated with pancytopenia, hypertriglyceridemia, and hypofibrinogenemia.[1-3] Histologically, infiltrations of lymphocytes and histiocytes with hemophagocytic activity are seen in the reticuloendothelial system, bone marrow, and central nervous system (CNS).[4] HLH can be classified as either primary or secondary.[5] The primary form, also known as familial hemophagocytic lymphohistiocytosis (FHL), is inherited as an autosomal recessive disorder that usually arises during infancy.

Although generally attributed to uncontrolled T-cell activation leading to the excessive production of inflammatory cytokines and abnormal macrophage activation, the pathogenesis of HLH remains controversial.[6] Thus, identifying the molecular genetic defects that underlie HLH has been a major concern for many years. Recently, mutations of the perforin (*PRF1;* MIM170280) and *MUNC13-4* genes were found in patients with FHL.[7,8] Several reports indicated that the mutation in *PRF1* occurs in about 20% to 30% of patients with FHL, thus defining the FHL2 molecular subtype.[9-13] In Japan, *MUNC13-4* mutations were identified in 6 of 16 families with non-FHL2 subtypes, suggesting an FHL3 subtype that may account for as many as 20% to 25% of all FHL cases.[14] Attempts to identify molecular genetic defects in the 45% to 50% of FHL cases that lack both *PRF1* and *MUNC13-4* mutations are under way.

Natural killer (NK) cells and cytotoxic T lymphocytes (CTLs) both rely on the Fas-FasL system and the secretion of lytic granules containing granzyme and perforin to kill virus-infected and malignant cells. Perforin is synthesized as an inactive glycosylated precursor that is subsequently cleaved at the C-terminus to yield an active mature form.[15] Perforin protein in the form of a 534–amino acid polypeptide is constitutively expressed by NK cells and CTLs. In effector-target cell interactions, intracellular perforin is secreted by a mechanism of regulated exocytosis. The secreted perforin then becomes integrated into the target-cell membrane, followed by polymerization that generates poly-perforin pores in the presence of Ca^{2+} in the plasma membrane.[16,17] This pore formation leads to the destruction of cells by osmotic lysis and by allowing entry of apoptosis-inducing granzymes.[18] The perforin gene, *PRF1*, encodes transmembrane, endothelial growth factor–like, and C2 functional domains. The C2 domain binds to phospholipids in a Ca^{2+}-dependent manner, and proteolytic cleavage of the carboxy-terminal domain uncovers the C2 domain, allowing perforin to bind to the membrane.[15] Thus, perforin is produced as a precursor form, and posttranslational processing by proteolysis and glycosylation is required for its maturation.[15] Less is known about MUNC13-4, a homolog of MUNC13-1 that functions as a priming factor for neurotransmitter release. Because of its critical role in regulating the exocytosis of lytic granules in NK cells and CTLs, MUNC13-4 is expected to play a similar role in the exocytosis of perforin-containing vesicles.[19]

The onset of FHL typically occurs within the first year of life in 70% to 80% of cases[2,20]; examples of late-onset cases,[20] as well as a case in a teenager with genetic defects in *PRF1* in the absence of clinical symptoms,[21] have also been described. NK cell function was impaired in the majority of these cases, including those considered to be late onset.[20-22] These observations suggest that the defining characteristics of FHL may vary with both the type of genetic defect and the function of NK cells or CTLs.[23,24] We therefore analyzed the relationships among the clinical features, genetic defects, and CTL/NK cell functions of FHL patients with different molecular subtypes of this disease.

From the Department of Pediatrics, Saga University, Saga, Japan; Department of Pediatrics, Kyoto Prefectural University of Medicine, Kyoto, Japan; Department of Cardiovascular Medicine, Graduate School of Medicine, Kyoto University, Kyoto, Japan; Department of Pediatrics, Graduate School of Medicine, Kyushu University, Fukuoka, Japan; Division of Molecular Population Genetics, Department of Molecular Genetics, Medical Institute of Bioregulation, Kyushu University, Fukuoka, Japan; Division of Pediatrics, Osaka General Hospital, Osaka, Japan; Department of Pediatrics, Shinshu University, Matsumoto, Japan; Division of Pediatrics, Okinawa Central Hospital, Okinawa, Japan; Research Institute, International Medical Center of Japan, Tokyo, Japan; First Department of Internal Medicine, Ehime University, Ehime, Japan.

Submitted August 26, 2004; accepted December 30, 2004. Prepublished online as *Blood* First Edition Paper, January 4, 2005; DOI 10.1182/blood-2004-08-3296.

Supported by a Grant-in-Aid for Scientific Research in Japan.

Reprints: Eiichi Ishii, Department of Pediatrics, Faculty of Medicine, Saga University, 5-1-1 Nabeshima, Saga 849-8501, Japan; e-mail: ishiie@med.saga-u.ac.jp.

The publication costs of this article were defrayed in part by page charge payment. Therefore, and solely to indicate this fact, this article is hereby marked "advertisement" in accordance with 18 U.S.C. section 1734.

Patients, materials, and methods

Patients

A total of 67 Japanese patients with HLH (34 boys and 33 girls) were registered in the study from 1994 to 2003, 10 of whom were excluded because (i) the diagnosis was not compatible with FHL by criteria of the Histiocyte Society,[3] (ii) a blood sample was not obtained, or (iii) permission for the analysis was not given by the parents. Thus, 57 patients met the diagnostic criteria for FHL and had documented informed consent, fulfilling the principal requirements for eligibility. Informed consent was provided according to the Declaration of Helsinki. Thirty-five were tested for both *PRF1* and *MUNC13-4* mutations and were the focus of the presenting analysis. The study was approved by the institutional review boards at Kyushu University, Saga University, Ehime University, and Kyoto Prefectural University. Twenty-one patients received chemotherapy according to the HLH94 protocol, which specifies a combination of dexamethasone and etoposide as induction therapy, followed by dexamethasone, etoposide, and cyclosporine A as maintenance therapy.[25] Others were managed according to the best clinical judgment of their primary physicians. Subsequently, 22 patients underwent allogeneic hematopoietic stem cell transplantation (HSCT).

Flow cytometric and genetic analyses

To analyze perforin expression, we obtained peripheral blood mononuclear cells (PBMCs) before or during treatment and performed flow cytometric analysis as described in our previous reports.[11,13] Intracellular perforin was considered deficient when less than 1.0% of $CD3^+$, $CD8^+$, or $CD56^+$ cells expressed this antigen. When perforin expression was negative, we extracted genomic DNA and used it for sequencing analysis of *PRF1* by a previously described procedure with selected primers.[11,13] Polymerase chain reaction (PCR) products were subcloned and sequenced on the ABI PRISM 377 Sequence Detection System (PE-Applied Biosystems, Foster City, CA). When perforin expression was positive and/or *PRF1* mutations were absent we performed a genetic analysis for *MUNC13-4* mutations as described in our previous report.[14] Briefly, 28 primer sets were designed to amplify the 32 exons and flanking intronic sequences of the *MUNC13-4* gene from genomic DNA. PCR products were cloned into a TA cloning vector (Invitrogen, Carlsbad, CA), and the sequences were verified on an AB13100 DNA sequencer (PE-Applied Biosystems).

Assay for NK cell activity

The NK cell activity of PBMCs was measured at diagnosis, during remission (between 2 and 6 months after diagnosis at completion of induction chemotherapy), and after HSCT by incubating cells with K562 targets for 4 hours with an effector-target (E/T) cell ratio of 20:1.[26] Target cells were also added to wells containing medium alone and to wells containing 1% Triton X-100 to determine the spontaneous and maximal levels of ^{51}Cr release, respectively. After 4 hours, 0.1 mL of supernatant was collected from each well. The percentage of specific ^{51}Cr release was calculated as (cpm experimental release − cpm spontaneous release)/(cpm maximal release − cpm spontaneous release) × 100, where cpm indicates counts per minute. At an E/T ratio of 20:1, normal values based on findings in 50 healthy children ranged from 18% to 40%, with 5% or less denoting a deficiency and 6% to 17% a moderate decrease.[26] NK cells were not routinely quantified; however, only specimens with PBM effector cell counts above 10^6 per tube were included in the analysis.

Generation of alloantigen-specific CTL lines and analysis of CTL cytotoxicity

Alloantigen-specific $CD8^+$ CTL lines were generated as previously described.[27,28] Briefly, PBMCs were obtained from FHL2 and FHL3 patients, their healthy parents, and unrelated healthy controls. These cells were cocultured with a mitomycin C (MMC)–treated B-lymphoblastoid cell line (B-LCL) established from an HLA-mismatched individual. Magnetized polystyrene beads coated with an anti-CD8 monoclonal antibody (DYNAL, Oslo, Norway) were used to isolate $CD8^+$ T lymphocytes from PBMCs that had been stimulated with allogeneic B-LCLs for 6 days. $CD8^+$ T lymphocytes, cultured in medium with interleukin-2 (Genzyme, Boston, MA), were stimulated with MMC-treated allogeneic B-LCLs 3 times at 1-week intervals; subsequently, these lymphocytes served as $CD8^+$ alloantigen-specific CTL lines. Alloantigen-specific CTL clones were generated from bulk CTL lines by a limiting dilution method as previously described.[27,28] The alloantigen specificity of CTL lines was determined by interferon-γ (IFN-γ) production in response to stimulation with allogeneic B-LCLs as described previously.[27,28] Briefly, 1×10^5 T lymphocytes were cocultured with or without 5×10^4 MMC-treated B-LCLs in 0.2 mL of RPMI 1640 medium supplemented with 10% fetal calf serum in a flat-bottomed microtiter well. In some experiments, an anti–HLA class I monoclonal antibody (w6/32) was added to wells at an optimal concentration. After 72 hours, the supernatant was collected from each well and assayed for the production of IFN-γ with an enzyme-linked immunosorbent assay (ELISA; ENDOGEN, Woburn, MA). Cytotoxic activity was determined by a 5-hour ^{51}Cr release assay as described earlier.[7] To evaluate the role of perforin in CTL-mediated cytotoxicity, we pretreated effector cells with an inhibitor of the perforin-based cytotoxic pathway, concanamycin A (CMA; Wako Pure Chemical Industries, Osaka, Japan), at a concentration of 100 nM for 2 hours before incubation with target cells.

Western blot analysis

T-cell lines established from FHL2 and FHL3 patients and a healthy control were used for Western blot analysis. Cell lysates were prepared by 1% Triton X-100 extraction. Then, the extracts (20 μg per lane each) were analyzed by the Western blot method with antiperforin (Lab Vision, Fremont, CA) and anti–MUNC13-4 rabbit polyclonal antibodies.[19] Horseradish peroxidase–labeled anti–rabbit immunoglobulin G (IgG) polyclonal antibody was used as the secondary antibody with detection by enhanced chemiluminescence (Amersham Biosciences, Piscataway, NJ).

Statistical analysis

Differences in the distribution of categorical variables (eg, age at onset, family history, CNS involvement, NK cell activity at diagnosis, NK cell activity during remission, chemotherapy, and outcome) were analyzed with the Fisher exact test. When any significant variability ($P < .05$) was observed among the 3 subgroups (FHL2, FHL3, and non-FHL2/FHL3), additional analyses were done with the Bonferroni test to identify significant differences between discrete subgroup pairs. The Student t test was used to assess CTL lytic activity in 4 patient subgroups (FHL2 nonsense, FHL2 missense, FHL3, and healthy controls) at an E/T ratio of 10:1.

Results

Comparison of genotype and phenotype in 3 different molecularly defined subgroups

Since more than 80% of all FHL patients in Japan were registered by our study group over the 10-year accrual period, the findings of this analysis are believed to reflect the actual epidemiology of FHL in Japan. Of the 57 patients who met all eligibility criteria, 11 had *PRF1* mutations and lacked perforin expression by flow cytometry, whereas 46 were positive for perforin expression (Figure 1). Thus, the frequency of the FHL2 subtype in Japan can be estimated as 19% of all FHL cases. Twenty-four of the 46 patients with perforin expression were examined for *MUNC13-4* mutations and 8 (6 of whom were described in a previous report[14]) had a positive result, suggesting that the FHL3 subtype accounts for approximately one fourth of the FHL cases in Japan. The 16 patients with neither *PRF1* nor *MUNC13-4* mutation were classified as having non-FHL2/FHL3 disease.

Selected characteristics of patients with *PRF1* mutations (FHL2), *MUNC13-4* mutations (FHL3), or neither of these defects (non-FHL2/FHL3) are summarized in Table 1. The Fisher exact test demonstrated a significant difference in age at diagnosis among the 3 subgroups (Table 1). None of the other features examined (family history, CNS involvement, NK cell activity at diagnosis, type of chemotherapy, or outcome) showed any important variability. By the Bonferroni test, patients with the FHL2 subtype had an earlier age at disease onset ($P < .01$ for comparisons with both FHL3 and non-FHL2/FHL3).

Twenty-one patients were treated entirely on the HLH94 protocol whereas the remaining 14 received alterative therapy, including steroids, cyclosporine A, etoposide, and other cytotoxic drugs. There was partial recovery of deficient NK cell activity in the FHL3 and non-FHL2/FHL3 subgroups after induction chemotherapy or during remission compared with none in the FHL2 subgroup ($P < .05$ for FHL3; $P < .1$ for non-FHL2/FHL3). This improvement was not related to the type of chemotherapy administered. Full recovery of NK cell activity was noted in all 6 patients tested after HSCT, encompassing the FHL2, FHL3, and non-FHL2/FHL3 subgroups. Of the 22 patients who underwent allogeneic HSCT, 17 have survived for 10 months to 11 years (median, 4 years): 5 FHL2 patients, 4 FHL3 patients, and 8 non-FHL2/FHL3 patients. Thus, allogeneic HSCT was effective therapy in a majority of patients who underwent this procedure, regardless of the molecular subtype. By contrast, 8 of the 13 patients treated without HSCT have died; the remaining 5 have survived for 22 months to 7 years (median, 2 years 8 months).

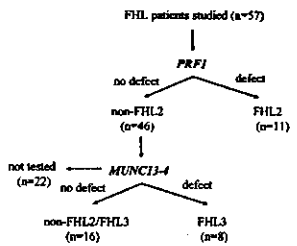

Figure 1. Classification of the FHL subtypes. *PRF1* mutations were initially classified in the 57 patients who fulfilled the diagnostic criteria of FHL. When perforin expression was positive or a *PRF1* mutation was absent, the samples were analyzed for a *MUNC13-4* mutations. The results allowed the FHL patients to be classified into 3 subtypes: FHL2 (n = 11), FHL3 (n = 8), and non-FHL2/FHL3 (n = 16).

Table 1. Characteristics of patients with the FHL2, FHL3, and non-FHL2/FHL3 subtypes of familial hemophagocytic lymphohistiocytosis

Category	No. patients with FHL2, n = 11	No. patients with FHL3, n = 8	No. patients with non-FHL2/FHL3, n = 16	P*
Age at diagnosis				.007
4-11 mo	0	6	5	
Family history				.513
Negative	6	3	10	
CNS involvement†				.713
Negative	4	3	3	
NK cell activity‡				.247
6%-17%	0	2	3	
Unknown	2	1	3	
Genetic mutation				
Nonsense/missense	1	0	0	
Donor site/donor site	0	1	0	
Acceptor site/acceptor site	0	2	0	
Acceptor site/nonsense	0	1	0	
Chemotherapy				.199
Various regimens	6	1	7	
Outcome				.292
Alive without HSCT	1	0	4	
Dead without HSCT	2	2	4	

CNS indicates central nervous system; NK, natural killer; nonsense, nonsense mutation including frameshift; missense, missense mutation; donor site, splice-donor site; acceptor site, splice-acceptor site; and HSCT, allogeneic hematopoietic stem cell transplantation.

*The Fisher exact test was used to determine the global *P* value for all 3 subgroups. By the Bonferroni test, patients with FHL2 had an earlier age at onset by comparison with either of the remaining subgroups ($P < .01$).

†Defined by neurologic symptoms and/or pleocytosis in cerebrospinal fluid.

‡NK cell activity measured at diagnosis and defined as deficient (≤ 5%), moderately decreased (6%-17%), or normal (18%-40%).

IFN-γ production and cytotoxic activity of T lymphocytes in patients with the FHL2 and FHL3 subtypes

Alloantigen-specific $CD8^+$ CTL lines were generated for all patients with available PBMCs (6 FHL2 and 2 FHL3). The antigen specificities of T-cell lines were initially examined by measuring IFN-γ production. As shown in Figure 2, all $CD8^+$ T-cell lines generated by stimulation with allogeneic B-LCLs (KIN-LCLs) produced large amounts of IFN-γ in response to stimulation with these lymphoblastoid cells but not with TAK-LCLs, which shared no HLA antigens with the KIN-LCLs. The production of IFN-γ by

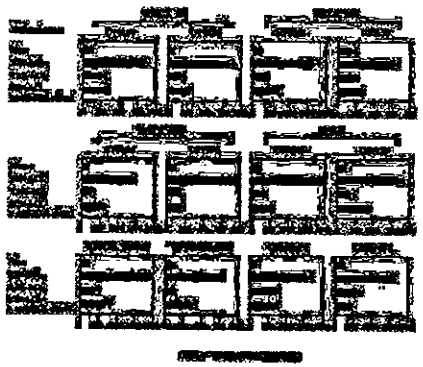

Figure 2. IFN-γ production by alloantigen-specific $CD8^+$ T-cell lines in response to stimulation with allogeneic B-LCLs. $CD8^+$ T-cell lines were generated from the PBMCs of the patients with FHL and healthy controls by stimulation with allogeneic B-LCLs (KIN-LCLs). Responder cells were cocultured with or without KIN-LCLs or TAK-LCLs, which shared no HLA antigens with KIN-LCLs, in the presence or absence of anti–HLA class I monoclonal antibody for 3 days. IFN-γ production was determined by ELISA; the results are mean values (± SD) from triplicate experiments. HLA types of B-LCLs were as follows: KIN-LCL, HLA-A01/30, B13/17, Cw6/–, DRB1*0701/*0701; TAK-LCL, HLA-A24/26, B62/–, Cw4/w9, DRB1*0405/*0901. NS indicates nonsense mutation; MS, missense mutation; and UPN, unique patient number.

the T-cell lines was clearly inhibited by anti–HLA class I monoclonal antibodies, indicating that the responses by these CTLs were alloantigen specific and HLA class I restricted.

Data on the cytotoxic activity of $CD8^+$ alloantigen-specific bulk T-cell lines generated from FHL2 and FHL3 patients, their healthy parents, and 2 healthy controls are shown in Figure 3. CTLs generated from the FHL2 patients with *PRF1* nonsense mutations (NSs; n = 2) were entirely deficient in antigen-specific cytotoxicity (percent cytotoxicity at E/T ratio of 10:1, mean 3.7 ± 1.1 SD), whereas those from the FHL3 patients (n = 2) showed very low but still detectable levels of this activity (mean 23.5 ± 2.1 SD). The cytotoxicity of CTLs generated from the patients with *PRF1* missense mutations (MSs; n = 4) was high (mean 44.0 ± 4.2 SD) compared with those of CTLs generated from FHL3 patients and patients with *PRF1* nonsense mutations but was clearly low compared with values for healthy controls and healthy parents with heterozygous mutations (mean 76.1 ± 4.7 SD). Although the patient sample in this comparison was small, statistical analysis indicated a significant difference in cytotoxicity between the FHL2 (NS)/FHL3 and FHL2 (MS) subgroups and between the FHL2 (MS) and the combined parent/healthy control groups ($P < .001$ for each comparison). Results similar to those in Figure 3 were obtained for alloantigen-specific CTL clones generated from the FHL patients and healthy controls (data not shown). The cytotoxicity of the $CD8^+$ CTL lines generated against allogeneic cells appeared to be mediated via the perforin-dependent pathway, since treatment of CTLs with CMA, a potent inhibitor of the perforin-mediated granule exocytosis cytolytic pathway, resulted in nearly complete inhibition of T-cell–mediated cytotoxicity.

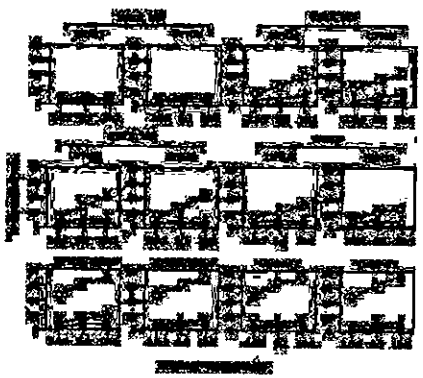

Figure 3. Cytotoxic activity of alloantigen-specific $CD8^+$ T-cell lines. $CD8^+$ T-cell lines were generated from PBMCs of the patients with FHL and healthy controls by stimulation with allogeneic B-LCLs (KIN-LCLs). Their cytotoxicity was determined against allogeneic KIN-LCLs in the presence (△) or absence (○) of CMA at a concentration of 100 nM and against allogeneic TAK-LCLs (●). Mean values and SD for triplicate experiments are reported. NS indicates nonsense mutation; MS, missense mutation; and UPN, unique patient number.

Western blot analysis for perforin and MUNC13-4 in the FHL2 and FHL3 subtypes

To account for the different patterns of CTL activity shown in Figure 3, we analyzed perforin expression in FHL patients whose CTL lines were established by Western blot analyses under reducing conditions (Figure 4A). Perforin in T cells from a healthy control and 2 FHL3 patients migrated at an apparent molecular mass of approximately 65 to 70 kDa. By contrast, the gene product associated with the *PRF1* nonsense mutation 1090.91delCT, present in 3 patients (UPN17, UPN24, and UPN42; Table 2), migrated at approximately 55 kDa. The gene product associated with the 207delC mutation (UPN24) was predicted to be an 84–amino acid peptide and therefore was too small to be seen. Gene products resulting from *PRF1* missense mutations 1228C>T (UPN42) and 1349C>T (UPN53 and UPN36) migrated at molecular masses similar to that of a healthy control, although the intensities of the bands appeared weaker compared with the control (Figure 4A). These results suggest that the mutant perforins were expressed in reduced amounts as full-length proteins with point mutations of R410W and T450M, respectively. Since a single band was also detected for UPN26 (a compound heterozygote with 949G>A and 1A>G; Table 2) at a position similar to the control, at least one of these mutants may be expressed as a full-length protein with a point mutation.

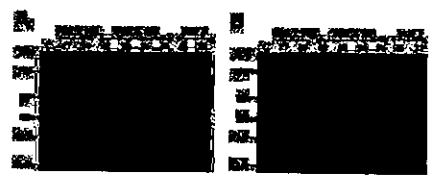

Figure 4. Perforin expression by Western blot analysis. Analysis is shown under reducing (A) or nonreducing (B) conditions in FHL patients. T cells from healthy control (C), FHL2 patients, and FHL3 patients were grown as described in "Generation of alloantigen-specific CTL lines and analysis of CTL cytotoxicity." Cell extracts of these cells (20 μg each) were analyzed by Western blot with antiperforin antibody. The data shown are representative results of 3 independent experiments. NS indicates nonsense mutation; and MS, missense mutation. The numbers above the lanes correspond to the UPNs of patients listed in Table 2.

Table 2. Relation of genotype to the cytotoxic functions of NK cells and CTLs in patients with the FHL2 or FHL3 subtypes

Subtype and UPN	Age/sex	Mutations	NK activity at diagnosis, % (% after treatment)	CTLs, %*	Western blot (active protein)	Outcome	HSCT
FHL2							
24	1 mo/F	1090.91delCT/207delC	1 (2)	3.9	Absent (p)	Alive	Y
53	7 y/F	1349C > T (mis)/1349C > T (mis)	0 (0)	46.5	Reduced (p)	Alive	Y
36†	1 mo/F	1349C > T (mis)/1349C > T (mis)	5 (5)	40.9	Reduced (p)	Alive	Y
FHL3							
23	5 mo/M	1596+1G > C/754−1G > C	19 (12)	23.8	Absent (m)	Dead	Y

Mutations in both alleles are listed in the table.
NK indicates natural killer; CTLs, cytotoxic T lymphocytes; p, perforin; mis, missense mutation; m, MUNC13-4 protein; Y, yes; N, no; and UPN, unique patient number.
*Mean CTL activity from 3 independent experiments at 10:1 of E/T ratio.
†FHL was diagnosed at 1 month of age, with relapse occurring 5 years later.

To identify the active mature form of perforin generated from the precursor of this protein, we performed Western blot analysis under nonreducing conditions (Figure 4B), as in a previous report.[15] Although the precursor forms of perforin (Figure 4B, upper bands) were detected in patients with *PRF1* missense mutations, FHL3 patients, and a healthy control, the active mature protein (Figure 4B, the lowest band) was markedly reduced in the patients with *PRF1* missense mutations, indicating that the proteolytic cleavage of perforin was inhibited. Under these conditions, the nonsense mutations (1090.91delCT and 207delC) did not yield a detectable band.

As shown in Figure 5, a single MUNC13-4 band of 120 kDa (expected size) was detected in a healthy control and all FHL2 patients but was missing in both of the FHL3 patients studied. Since the antibody used for the Western blot analysis was raised against the N-terminus of MUNC13-4 (1-262),[19] it is likely that the MUNC13-4 protein, even its N-terminal portion, was not expressed in the T cells of either of these 2 FHL3 patients.

Discussion

This study compared the frequencies, clinical features, genotypes, and CTL/NK cell functions of the FHL2 and FHL3 subtypes of familial hemophagocytic lymphohistiocytosis. Since more than 80% of all FHL cases in Japan were analyzed, the proportions of patients with *PRF1* or *MUNC13-4* mutations are likely to reflect the true epidemiology of this disorder. The FHL3 subtype appears more common than the FHL2 subtype (25% vs 19%), although this difference may vary depending on ethnic background and other factors.[9-13,29] Precise calculation of the frequency of each FHL subtype in countries outside of Japan is clearly needed.

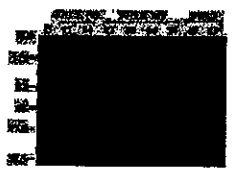

Figure 5. MUNC13-4 expression by Western blot analysis in FHL patients. Cell extracts from the T cells of healthy control (C), FHL2, and FHL3 patients (20 μg each) were analyzed by Western blot with anti-MUNC13-4 antibody. The data represent 3 independent experiments. NS indicates nonsense mutation; and MS, missense mutation. The numbers above the lanes correspond to the UPNs of patients listed in Table 2.

FHL is sometimes difficult to diagnose when the patient is a first child or lacks an affected sibling. However, several clinical findings can support this diagnosis, including an age of less than 2 years, CNS involvement, and especially defective NK cell activity,[5] which has been observed in a majority of patients.[30-32] Comparison of NK cell activity among the FHL2, FHL3, and non-FHL2/FHL3 subtypes at diagnosis did not reveal any significant differences, as most of the evaluable cases were deficient or low in this activity. However, none of the FHL2 patients showed any recovery of NK cell activity after chemotherapy, in contrast to the FHL3 and non-FHL2/FHL3 subgroups. There was no apparent relationship between the recovery of functional NK cells and the type of chemotherapy received by these patients. Our findings agree with a recent report by Schneider et al,[24] who classified patients into 4 types according to the level of NK cell activity. All cases with *PRF1* homozygous nonsense mutations lacked any evidence of NK cell activity, regardless of the type of stimulation or the length of culture.[24] Thus, *PRF1* mutations appear to play an important role in the persistence of deficient NK cell activity in FHL.[32] Whether the transience of this deficiency in the FHL3 subtype is associated with *MUNC13-4* or still unidentified mutations, or perhaps a combination of the 2, remains to be determined. The partial recovery of NK cell activity may be associated with an increased number of NK cells or their release from the external suppressive effects of chemotherapy.

Perforin deficiency in FHL2 causes severe immune defects through defective NK and CTL activities.[6,30,31] A lack of perforin expression in $CD8^+$ T cells and/or NK cells by flow cytometric analysis generally correlates with mutated *PRF1* sequences.[10,13] However, Molleran Lee et al[32] recently reported cases of late-onset FHL with *PRF1* mutations but positive expression of perforin by flow cytometry. We identified 3 novel missense mutations of *PRF1* in this study: 949G>A, 1228C>T, and 1349C>T (Table 2), and each of the affected patients, except UPN36, showed late-onset clinical manifestations. In contrast to a previous report,[33] perforin expression by $CD8^+$ or $CD56^+$ cells in our study was also negative in all patients with *PRF1* missense mutations. Feldmann et al[12] characterized the genotype and phenotype of FHL2 patients; clinical and biologic analyses did not distinguish between patients

with *PRF1* nonsense or missense mutations, although age at diagnosis was delayed in patients in the missense mutation group. It was also reported that several patients with late-onset disease had missense mutations of *PRF1*.[21,34]

In the FHL2 patients with *PRF1* missense mutations, we detected a mutant form of perforin whose molecular mass was similar to that of the wild-type protein by Western blot analysis under reducing conditions; however, as shown in Figure 4B, there was no mature form of the perforin proteins in these cases. McCormick et al[35] generated the 3-dimensional structure of the T435M *PRF1* mutant using comparative molecular modeling techniques applied to data from a single FHL patient. Their results predicted that the ability of the protein to bind Ca^{2+}, and hence its cytolytic function, would be strongly compromised. Katano et al[36] demonstrated the accumulation of an uncleaved precursor form of perforin in a patient with a *PRF1* missense mutation. Using Western blot analysis under nonreducing conditions we showed that the active mature form of perforin, the only form localized in lytic granules,[15] was absent in *PRF1* nonsense mutations and definitely reduced in all patients with *PRF1* missense mutations. These findings suggest that the missense mutations of *PRF1* lead to conformational changes in the perforin molecule that inhibit proteolytic cleavage of perforin precursors.

In our study, the cytotoxic function of CTLs in patients with *PRF1* missense mutations remained relatively intact compared with that associated with nonsense mutations of this gene. By contrast, all patients with any type of *PRF1* mutation showed a persistent deficiency in NK cell activity. Since the number and cytotoxic function of NK cells can vary depending on numerous factors, including the nature of the disease, infections, and type of treatment, measurements of NK cell activity in FHL2 cases may not accurately reflect the immune status of patients. We therefore established antigen-specific CTL lines from patients with the different subtypes of FHL and compared their cytotoxic activities. Since most of the patients with FHL are young children with an immunodeficient status, generating CTLs that are specific for viral or other recall antigens can be quite difficult; hence, we elected to generate alloantigen-specific CTL lines. The levels of cytotoxicity mediated by alloantigen-specific CTLs generated from patients with *PRF1* nonsense or missense mutations or with *MUNC13-4* mutations were clearly distinguishable from each other. Although many previous studies have relied on NK cells to examine cytolytic mediators in FHL, our findings suggest that functional analysis of antigen-specific CTLs may yield more useful insights into the immune competence of patients. Further studies with larger patient samples are needed to clarify the benefits of CTL assays in each subtype of FHL.

MUNC13-4 is a member of the *Munc13* gene family, which is required for neurotransmitter release in the small nematode *Caenorhabditis elegans*.[37] Feldmann et al[8] demonstrated that the MUNC13-4 protein colocalizes with cytotoxic granules near the site of contact between T lymphocytes and their targets and that granule exocytosis is blocked at a post-RAB27A stage in CTLs from FHL3 patients. We recently demonstrated that MUNC13-4 is a direct target of guanosine triphosphate–RAB27.[19] MUNC13-4 deficiency also results in defective cytolytic granule exocytosis despite polarization of the secretory granules and docking with the plasma membrane.[8] When we compared the cytotoxic activity of CTLs with *PRF1* or *MUNC13-4* mutations, the latter showed a lower affinity for target cells than did CTLs with *PRF1* missense mutations. The MUNC13-4 protein was not detected by Western blot analysis, indicating that its function was completely eliminated in FHL3 patients. The difference in the cytotoxic activity of CTLs may reflect the functions of the molecules responsible for FHL pathogenesis: while MUNC13-4 is a regulator of exocytosis in perforin-containing vesicles, perforin is the killing tool itself.

The only accepted curative therapy for FHL is allogeneic HSCT. Although the outcome of therapy did not differ between patients with the FHL2 or FHL3 subtype, 1 child with a *PRF1* missense mutation and 4 in the non-FHL2/FHL3 subgroup have survived without HSCT. Thus, early recognition of informative genetic defects and the cytotoxic activity of CTLs in cases of FHL may identify patients who could be spared the toxic effects of intensive chemotherapy with stem cell rescue.

Recent molecular genetic findings have demonstrated the diversity of FHL pathogenesis, but very little is known about the clinical and biologic correlations of the genetic subtypes of this disease. Although we observed a significant difference in age at onset and NK cell recovery between the FHL2 and FHL3 variants, further distinctions could not be made with any certainty. Nonetheless, the results of CTL assays performed on T-cell lines from a limited number of patients suggested an association with clinical features, type of mutation, and the subsequent production of functional proteins in FHL patients. If confirmed by studies of additional cases, the use of CTL assays to monitor the immune status of FHL patients might aid in the selection of therapy for cases without a documented genetic defect.

Acknowledgments

We thank John Gilbert for critical comments and editorial assistance; Naoko Kinukawa, Department of Medical Informatics, Kyushu University, Japan for statistical analysis of clinical parameters; and all of the members of the Japan HLH Study Group for their contributions to careful follow-up and data collection in each case. A complete list of the members of the Japan HLH Study Group appears in the "Appendix."

Appendix

The members of the Japan HLH Study Group were as follows. Yukiko Tsunematsu, MD, Department of Hematology, National Children's Hospital, Tokyo, Japan; Shuki Mizutani, MD, Department of Pediatrics, Tokyo Medical and Dental University, Tokyo, Japan; Naoko Kinukawa, Department of Pediatrics, Showa University, Tokyo, Japan; Hirokazu Kanegane, MD, Department of Pediatrics, Toyama Medical and Pharmaceutical University, Toyama, Japan; Keizo Horibe, MD, Clinical Research Center, National Nagoya Hospital, Nagoya, Japan; Ikuyo Ueda, MD and Akira Morimoto, MD, Kyoto Prefectural University, Kyoto, Japan; Naoki Sakata, MD, Department of Pediatrics, Kinki University, Osaka, Japan; Shinsaku Imashuku, MD, Department of Pediatrics, Takasago Seibu Hospital, Hyogo, Japan; Masaki Yasukawa, MD, Department of First Internal Medicine, Ehime University, Ehime, Japan; Shouichi Ohga, MD, and Toshiro Hara, MD, Department of Pediatrics, Kyushu University, Fukuoka, Japan; Nobuhiro Kimura, MD, First Department of Internal Medicine, Fukuoka University, Fukuoka, Japan; and Eiichi Ishii, MD, Department of Pediatrics, Saga University, Saga, Japan.

References

1. Loy TS, Diaz-Arias AA, Perry MC. Familial erythrophagocytic lymphohistiocytosis. Semin Oncol. 1991;18:34-39.
2. Janka GE. Familial erythrophagocytic lymphohistiocytosis. Eur J Pediatr. 1983;140:221-230.
3. Henter J, Elinder G, Ost A. Diagnostic guidelines for hemophagocytic lymphohistiocytosis. Semin Oncol. 1991;18:29-33.
4. Caballes RL, Caballes-Ponce MG, Kim DU. Familial hemophagocytic lymphohistiocytosis (FHLH). Pathology. 1997;29:92-95.
5. Filipovich AH. Hemophagocytic lymphohistiocytosis: a lethal disorder of immune regulation. J Pediatr. 1997;130:337-338.
6. Arico M, Danesino C, Pende D, Moretta L. Pathogenesis of hemophagocytic lymphohistiocytosis. Br J Haematol. 1991;114:761-769.
7. Stepp SE, Dufourcq-Lagelouse R, Le Deist F, et al. Perforin gene defects in familial hemophagocytic lymphohistiocytosis. Science. 1999;286: 1957-1959.
8. Feldmann J, Callebaut I, Raposo G, et al. Munc13-4 is essential for cytolytic granules fusion and is mutated in a form of familial hemophagocytic lymphohistiocytosis (FHL3). Cell. 2003;115:461-473.
9. Goransdotter Ericson K, Fadeeel B, Nilsson-Ardnor S, et al. Spectrum of perforin gene mutations in familial hemophagocytic lymphohistiocytosis. Am J Hum Genet. 2001;68:590-597.
10. Kogawa K, Lee SM, Villanueva J, Marmer D, Sumegi J, Filipovich AH. Perforin expression in cytotoxic lymphocytes from patients with hemophagocytic lymphohistiocytosis and their family members. Blood. 2002;99:81-86.
11. Suga N, Takada H, Ohga S, et al. Perforin defects of primary haemophagocytic lymphohistiocytosis in Japan. Br J Haematol. 2002;118:346-349.
12. Feldmann J, Le Deist F, Ouachee-Chardin M, et al. Functional consequences of perforin gene mutations in 22 patients with familial haemophagocytic lymphohistiocytosis. Br J Haematol. 2002; 117:965-972.
13. Ueda I, Morimoto A, Inaba T, et al. Characteristic perforin gene mutations of haemophagocytic lymphohistiocytosis patients in Japan. Br J Haematol. 2003;121:503-510.
14. Yamamoto K, Ishii E, Sako M, et al. Identification of novel MUNC13-4 mutations in familial hemophagocytic lymphohistiocytosis and functional analysis of MUNC13-4-deficient cytotoxic T lymphocytes. J Med Genet. 2004;41:763-767.
15. Uellner R, Zvelebil MJ, Hopkins J, et al. Perforin is activated by a proteolytic cleavage during biosynthesis which reveals a phospholipid-binding C2 domain. EMBO J. 1997;16:7287-7296.
16. Podack ER, Young JD, Cohn ZA. Isolation and biochemical and functional characterization of perforin 1 from cytolytic T-cell granules. Proc Natl Acad Sci U S A. 1985;82:8629-8633.
17. Masson D, Peters PJ, Geuze HJ, Borst J, Tschopp J. Interaction of chondroitin sulfate with perforin and granzymes of cytotoxic T-cells is dependent on pH. Biochemistry. 1990;29:11229-11235.
18. Darmon AJ, Nicholson DW, Bleackley RC. Activation of the apoptotic protease CPP32 by cytotoxic T-cell-derived granzyme B. Nature. 1995;377: 446-448.
19. Shirakawa R, Higashi T, Tabuchi A, et al. Munc13-4 is a GTP-Rab27 binding protein regulating dense core granule secretion in platelets. J Biol Chem. 2004;279:10790-10797.
20. Allen M, de Fusco C, Legrand F, et al. Familial hemophagocytic lymphohistiocytosis: how late can the onset be? Haematologica. 2001;86:499-503.
21. Clementi R, Emmi L, Maccario R, et al. Adult onset and atypical presentation of hemophagocytic lymphohistiocytosis in siblings carrying PRF1 mutations. Blood. 2002;100:2266-2267.
22. Elfe R, Janka GE, Belohradsky BH. Natural killer cell function and interferon production in familial hemophagocytic lymphohistiocytosis. Pediatr Hematol Oncol. 1989;6:265-272.
23. Arico M, Janka G, Fischer A, et al. Hemophagocytic lymphohistiocytosis: report of 122 children from the International Registry. Leukemia. 1996; 10:197-203.
24. Schneider EM, Lorenz I, Muller-Rosenberger M, Steinbach G, Kron M, Janka-Schaub GE. Hemophagocytic lymphohistiocytosis (HLH) is associated with deficiencies of cellular cytolysis but normal expression of apoptosis related transcripts. Blood. 2002;100:2891-2898.
25. Henter JI, Arico M, Egeler RM, et al. HLH-94: a treatment protocol for hemophagocytic lymphohistiocytosis. HLH Study Group of the Histiocyte Society. Med Pediatr Oncol. 1997;28:342-347.
26. Imashuku S, Hyakuna N, Funabiki T, et al. Low natural killer activity and central nervous system disease as a high-risk prognostic indicator in young patients with hemophagocytic lymphohistiocytosis. Cancer. 2002;94:3023-3031.
27. Yasukawa M, Ohminami H, Arai J, Kasahara Y, Ishida Y, Fujita S. Granule exocytosis, and not the fas/fas ligand system, is the main pathway of cytotoxicity mediated by alloantigen-specific CD4(+) as well as CD8(+) cytotoxic T lymphocytes in humans. Blood. 2000;95:2352-2355.
28. Yanai F, Ishii E, Kojima K, et al. Essential roles of perforin in antigen-specific cytotoxicity mediated by human CD4+ T lymphocytes: analysis using the combination of hereditary perforin-deficient effector cells and Fas-deficient target cells. J Immunol. 2003;170:2205-2212.
29. Janka GE, Schneider EM. Modern management of children with hemophagocytic lymphohistiocytosis. Br J Haematol. 2004;124:4-14.
30. Henter JI. Biology and treatment of familial hemophagocytic lymphohistiocytosis: importance of perforin in lymphocyte-mediated cytotoxicity and triggering of apoptosis. Med Pediatr Oncol. 2002; 38:305-309.
31. Moretta L, Moretta A, Hengartner H, et al. On the pathogenesis of perforin defects and related immunodeficiencies. Immunol Today. 2000;21:593-594.
32. Molleran Lee S, Villanueva J, Sumegi J, et al. Characterization of diverse PRF1 mutations leading to decreased natural killer cell activity in North American families with haemophagocytic lymphohistiocytosis. J Med Genet. 2004;41:137-144.
33. Schneider EM, Lorenz I, Walther P, Janka-Schaub GE. Natural killer deficiency: a minor or major factor in the manifestation of hemophagocytic lymphohistiocytosis? J Pediatr Hematol Oncol. 2003;25:680-683.
34. Busiello R, Adriani M, Locatelli F, et al. Atypical features of familial hemophagocytic lymphohistiocytosis. Blood. 2004;103:4810-4812.
35. McCormick J, Flower DR, Strobel S, Wallace DL, Beverley PC, Tchilian EZ. Novel perforin mutation in a patient with hemophagocytic lymphohistiocytosis and CD45 abnormal splicing. Am J Med Genet A. 2003;117:255-260.
36. Katano H, Ali MA, Patera AC, et al. Chronic active Epstein-Barr virus infection associated with mutations in perforin that impair its maturation. Blood. 2003;103:1244-1252.
37. Koch H, Hofmann K, Brose N. Definition of Munc13-homology-domains and characterization of a novel ubiquitously expressed Munc13 isoform. Biochem J. 2000;349(Pt 1):247-253.

THE JOURNAL OF BIOLOGICAL CHEMISTRY
Vol. 280, No. 8, Issue of February 25, pp. 7100–7106, 2005
Printed in U.S.A.

Activation of STAT3/Smad1 Is a Key Signaling Pathway for Progression to Glomerulosclerosis in Experimental Glomerulonephritis*

Received for publication, September 27, 2004, and in revised form, December 2, 2004
Published, JBC Papers in Press, December 9, 2004, DOI 10.1074/jbc.M411064200

Toshikazu Takahashi‡, Hideharu Abe‡, Hidenori Arai§, Takeshi Matsubara§, Kojiro Nagai§, Motokazu Matsuura‡, Noriyuki Ieharа§, Masayuki Yokode¶, Shinichi Nishikawa‖, Toru Kita, and Toshio Doi‡ ‡‡**

*From the ‡Department of Clinical Biology and Medicine, Course of Biological Medicine, School of Medicine, The University of Tokushima, Tokushima 770-8503, the §Department of Geriatric Medicine, ¶Translational Research Center, and **Department of Cardiovascular Medicine, Graduate School of Medicine, Kyoto University, Kyoto 606-8507, and ‖Riken Center for Development Biology, Kobe 650-0047, Japan*

Mesangial cell proliferation is a significant event in the development of progressive glomerular injuries. However, the issue of how cell proliferation is involved in the development of glomerulosclerosis is unclear. Recently, we showed that the overexpression of type IV collagen (Col IV), a major component of mesangial extracellular matrix, is transcriptionally regulated by Smad1 in diabetic glomerulosclerosis. In this study, we have demonstrated the effect of the administration of an anti-platelet-derived growth factor (PDGF) β-receptor antibody (APB5) blocking activation by the PDGF-B chain on rat glomerulonephritis and have examined the signaling pathways that regulate both glomerular cell proliferation and glomerulosclerosis *in vivo* and *in vitro*. Experimental mesangial proliferative glomerulonephritis (Thy1 GN) was induced by a single intravenous injection of anti-rat Thy-1.1 monoclonal antibody. In Thy1 GN, mesangial cell proliferation and the expression of Col IV peaked at day 6. Immunohistochemical staining for the expression of Smad1, phospho-Smad1 (pSmad1), and phospho-STAT3 (pSTAT3) revealed that the peak for glomerular Smad1 expression occurred at day 6, consistent with the peak for mesangial proliferation. The expression of pSmad1 was up-regulated at day 1, and the peak for glomerular pSmad1 expression occurred at day 4 of the disease. When treated with APB5, both mesangial proliferation and sclerosis were reduced significantly. The expression of Smad1, pSmad1, and pSTAT3 was also significantly reduced by the administration of APB5. PDGF induced both mesangial cell replication and Col IV synthesis in association with an increased expression of pSTAT3 and pSmad1 on cultured mesangial cells. In addition, APB5 reduced mesangial cell proliferation in association with decreased pSmad1, pSTAT3, and Col IV protein expressions *in vitro*. The introduction of dominant negative STAT3 significantly decreased the expression of Col IV in cultured mesangial cells. These data suggest that the activation of STAT3 and Smad1 participates in the developing process of glomerulosclerosis in experimental glomerulonephritis.

Both mesangial cell proliferation and glomerulosclerosis are major important pathological features in progressive glomerular damage. In many glomerular sclerosing diseases, mesangial cell proliferation is a critical process in progressive glomerular injuries (1, 2). Both events are observed simultaneously in most glomerular diseases; however, the issue of how cell proliferation contributes to the development of glomerulosclerosis remains unclear.

Platelet-derived growth factor (PDGF)[1] is known to be a critical mitogen for mesangial cells *in vitro* and *in vivo* (3, 4). Several lines of evidence indicate that PDGF plays a key role in the development of glomerulosclerosis not only in experimental models but also in human glomerular diseases (3). PDGF-BB has also been reported to be essential for mesangial cell proliferation (5), which is followed by development of glomerulosclerosis in the remnant kidney model (6). The introduction of a neutralizing anti-PDGF antibody has shown that both mesangial proliferation and glomerulosclerosis can be markedly ameliorated in a rat glomerulonephritis model (7), but little is known concerning the mechanisms of how the suppression of cell proliferation reduces glomerular sclerotic lesions.

Glomerulosclerosis is characterized by an increase in the levels of ECM. Col IV is a major component of expanded ECM in glomerular diseases, but the molecular mechanism of regulating Col IV gene transcription had not been cleared until our recent report in which we showed that Smad1 transcriptionally regulates the overexpression of Col IV in diabetic nephropathy (8). Smad1 directly transduces signals to downstream target genes that are related to renal damage such as osteopontin (9), inhibition of differentiation (10), and type I collagen (11) and is critically important for the development of kidney disease (12). These findings suggest that Smad1 is a critical transcriptional factor in the progression of glomerulosclerosis.

Signal transducer and activator of transcription (STAT) proteins have been shown to be involved in signaling by numerous cytokines and growth factors. It is well established that STAT3 activation is a key step in PDGF-induced mitogenesis (13). Nakashima *et al.* (14) report that transcriptional coactivator p300 physically interacts with STAT3 and Smad1, followed by the subsequent activation of the target gene transcription in astrocyte differentiation. We have postulated from these findings that PDGF is able to activate the STAT3-Smad1 cross-talk pathway in mesangial proliferative glomerulonephritis and that the process is essential for the progression of mesangial cell proliferation to glomerulosclerosis. The goal of this study was to determine how the STAT3 and Smad1 signaling pathways are involved in the development of glomerulosclerosis, using anti-PDGFβ-receptor antibody in a rat glomerulonephritis model.

* The costs of publication of this article were defrayed in part by the payment of page charges. This article must therefore be hereby marked "*advertisement*" in accordance with 18 U.S.C. Section 1734 solely to indicate this fact.

‡‡ To whom correspondence should be addressed: Dept. of Clinical Biology and Medicine, Course of Biological Medicine, School of Medicine, The University of Tokushima, 3-18-15 Kuramoto-cho, Tokushima-city 770-8503, Japan. Tel.: 81-88-633-7184; Fax: 81-88-633-9245; E-mail: doi@clin.med.tokushima-u.ac.jp.

[1] The abbreviations used are: PDGF, platelet-derived growth factor; PDGFβ-R, PDGFβ receptor; ECM, extracellular matrix; Col IV, type IV collagen; STAT, signal transducer and activator of transcription; pSmad1, phospho-Smad1; PAM, periodic acid-methenamine; PCNA, proliferating nuclear antigen; FCS, fetal calf serum; BrdUrd, bromodeoxyuridine; ELISA, enzyme-linked immunosorbent assay; GN, glomerulonephritis.

EXPERIMENTAL PROCEDURES

Animals

Male Wistar rats (CLEA Japan, Inc.) weighing 180–200 g were used in this study. Rats were housed under specific pathogen-free conditions. All animal experiments were performed in accordance with institutional guidelines, and the Review Board of Tokushima University granted ethical permission for this study.

Induction of Thy1 Glomerulonephritis

Experimental mesangial proliferative glomerulonephritis (Thy1 GN) was induced by a single intravenous injection of anti-rat Thy-1.1 monoclonal antibody (1 mg/kg) (Cedarlane Laboratories, Ontario, Canada) as described elsewhere (15). These rats were sacrificed at days 1, 2, 4, 6, and 12 (n = 6/group) after the administration of anti-Thy-1.1 antibody. Six age-matched rats were injected with vehicle only and were sacrificed as controls.

Protocol of Treatment with Anti-PDGFβ-R Antibody in Thy1 GN

A rat monoclonal anti-PDGFβ-receptor antibody (APB5) and its antagonistic effects on the PDGFβ-R signal transduction pathway *in vivo* and *in vitro* have been described previously (16, 17). The rats were injected intraperitoneally at daily intervals with 400 μg of APB5 or irrelevant isotype-matched control rat IgG after the administration of anti-Thy1.1 antibody from day 0. They were sacrificed at days 1, 2, 4, 6, and 12 (n = 6/group).

Histological Examination

Light Microscopy—After removal of the kidney, tissue blocks for light microscopy examination were fixed in methyl Carnoy's solution and embedded in paraffin. Sections (2 μm) were stained with hematoxylin and eosin, periodic acid-Schiff's reagent, and periodic acid-methenamine (PAM) silver.

Immunohistochemistry—Kidney sections were processed for immunohistochemistry following standard procedures. To study proliferating nuclear antigen (PCNA), Col IV, and Smad1, methyl Carnoy's solution-fixed and paraffin-embedded tissue blocks were used. Kidney sections were rehydrated and treated with 0.3% hydrogen peroxide in methanol for 30 min. To eliminate nonspecific staining, sections were incubated with the appropriate preimmune serum for 20 min at room temperature and then incubated with avidin D- and biotin-blocking solutions (Vector, Burlingham, CA) for 15 min each. Sections were incubated with the anti-PCNA antibody (1:200 dilution), anti-Col IV antibody (1:200 dilution), and anti-Smad1 antibody (1:100 dilution) (Santa Cruz Biotechnology) for 60 min at room temperature and then incubated with the appropriate biotinylated secondary antibodies followed by incubation with the avidin-biotin peroxidase complex (Vectastain Elite ABC kit, Vector). Peroxidase conjugates were subsequently localized using diaminobenzidine tetrahydrochloride. To study pSmad1 and pSTAT3, the tissues were snap-frozen in cold acetate in OCT compound (Miles Inc., Elkhart, IN), cut in 4-μm-thick sections, fixed in acetone for 5 min, and treated with 0.3% hydrogen peroxide in methanol for 30 min. Sections were treated in the same manner as PCNA with the following primary antibodies: anti-pSmad1 antibody (1:100 dilution) (Calbiochem) and anti-pSTAT3 antibody (1:100 dilution) (Santa Cruz Biotechnology). These antibodies react specifically with phosphorylated antigen. To evaluate the nuclear number, sections were counterstained with hematoxylin solution.

Quantitation of Light Microscopy—Glomerular morphometry was evaluated in PAM-stained tissues. The glomerular surface area and the PAM-positive area/glomerular area (%) were measured using an image analyzer with a microscope (IPAP, Image Processor for Analytical Pathology; Sumitomo Chemical Co., Osaka, Japan) as described (18–20). For each animal, 50 glomeruli were analyzed.

Quantitation of Immunohistochemistry—For the quantitation of proliferating cells (PCNA-positive cells), a blind test evaluated 50 glomeruli in each specimen, and the mean values/glomerulus were calculated. To quantitate the expression of pSmad1, pSmad1-positive cells/glomerular cell were counted, and the mean percentages of pSmad1-positive cells were calculated. For Col IV, Smad1, and pSTAT3, the brown area on an immunoperoxidase-stained section was selected for its color range, and the percentages of this area to the total mesangial area were quantitated using IPAP. In each animal, 50 glomeruli were evaluated.

Cell Culture Experiment

A glomerular mesangial cell line was established from glomeruli isolated from normal, 4-week-old mice (C57BL/6JxSJL/J) and identified according to a previously described method (21). Mesangial cells were maintained in B medium (a 3:1 mixture of minimal essential medium/F12 modified with trace elements) supplemented with 1 mM glutamine, penicillin at 100 units/ml, streptomycin at 100 mg/ml, and 20% fetal calf serum (FCS). The cultured cells fulfilled the generally accepted criteria for glomerular mesangial cells (22). Mesangial cells were plated in B medium/20% FCS onto 100-mm dishes. After 24 h of incubation, the cells were starved for 2 days in B medium/0.1% bovine serum albumin, cultured in B medium/2% FCS with 5 ng/ml of PDGF-B (Calbiochem), and then incubated with 100 ng/ml of APB5 or control rat IgG for 24 h.

Cell Proliferation Test by BrdUrd ELISA

The proliferation of mesangial cells was also determined using a colorimetric immunoassay, based on the measurement of BrdUrd incorporation during DNA synthesis (Amersham Biosciences). The BrdUrd ELISA was performed according to the manufacturer's instructions. Briefly, mesangial cells were plated out at a low density in 96-well flat-bottomed microtiter plates in B medium/10% FCS and allowed to adhere overnight. The subconfluent cells were then starved for 2 days in B medium/0.1% bovine serum albumin. 100 ng/ml of APB5 was added to cells in B medium/2% FCS with 5 ng/ml PDGF-B and 10 mM BrdUrd. After 6 h of culture, the plates were centrifuged and the cells denatured with a fixative solution and then incubated for 30 min with 1:100 diluted anti-BrdUrd monoclonal antibodies conjugated to peroxidase. After removing the antibody conjugate, substrate solutions were added for 15 min, and the reaction was terminated by adding 1 M sulfuric acid. The absorbance was measured within 5 min at 450 nm with a reference wavelength at 690 nm using an ELISA plate reader (Model550; Bio-Rad Laboratories). The blank corresponded to 100 μl of culture medium with or without BrdUrd.

Western Blot Analysis

Cultured mesangial cells were starved for 24 h in B medium/0.1% bovine serum albumin. The cells were stimulated with 5 ng/ml PDGF-BB with 100 ng/ml APB5 or control IgG for 120 min. Cells were suspended in lysis buffer, resolved by SDS-polyacrylamide gel electrophoresis, and transferred to a nitrocellulose membrane. They were subjected to Western blot using a 1:1000 dilution of antibodies for pSTAT3, 1:1000 dilution of antibodies for pSmad1, and 1:2000 dilution of antibodies for Col IV and detected using an enhanced chemiluminescence detection system (Amersham Biosciences).

Treatment of AG490 in Cultured Mesangial Cells

Cultured mesangial cells were starved for 24 h in B medium/0.1% bovine serum albumin. The cells were stimulated with 5 ng/ml PDGF-BB with 50 μM AG490 (Calbiochem), a well characterized inhibitor of STAT3 phosphorylation (23, 24), or control vehicle for 8 h. Cell lysis and Western blot analysis were performed as previously described. The proliferation of mesangial cells was also determined using a BrdUrd ELISA system.

Cell Transfection

Plasmid constructs of expression vectors of wild type STAT3 and dominant negative STAT3 were kindly provided by Jackie Bromberg (Rockefeller University) (25). Mesangial cells (60-mm dish) were transfected with an expression vector encoding wild type STAT3 (8 mg) or dominant negative STAT3 (8 mg) using Lipofectamine 2000 (Invitrogen) according to the manufacturer's instructions. After 6 h of transfection, the medium was changed to growth medium (60% Dulbecco's modified Eagle's medium, 20% F12, 20% fetal calf serum). After 48 h, cells were suspended in lysis buffer, and Western blot analysis was performed as previously described. The proliferation of transfected mesangial cells was also determined using a BrdUrd ELISA system.

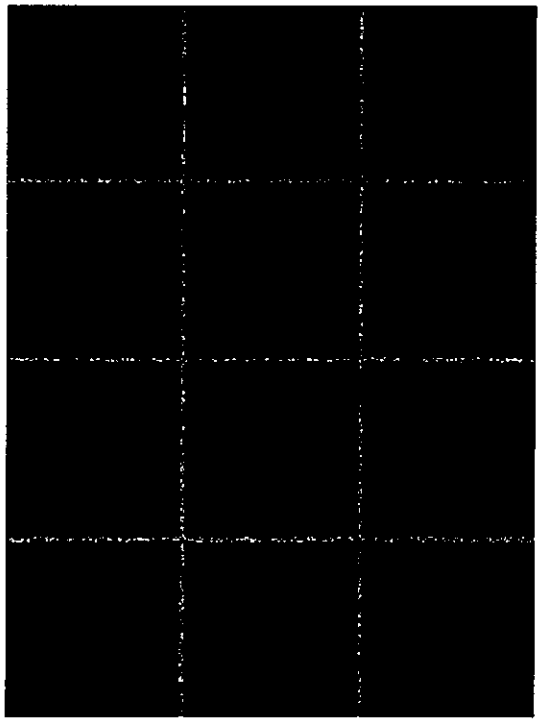

FIG. 1. **Morphological changes and effect of administration of APB5 in Thy1 GN glomeruli.** The microscopic lesions in Thy1 GN rats took the form of the diffuse proliferation of mesangial matrix and an expansion of the mesangial area. Immunohistochemical staining with anti-Col IV antibodies revealed the overexpression of Col IV in the expanded mesangial area of glomeruli from kidneys of Thy1 GN. APB5 reduced the mesangial proliferation and expression of Col IV. Thy1 GN also showed significantly positive expression of PDGF-B and PDGFβ-receptor in the glomeruli, and APB5 could reduce these overexpressions. *A–C*, PAM. *D–F*, Col IV. *G* and *H*, PDGF-B chain. *J* and *K*, PDGFβ-receptor. *A, D, G, J*, normal control rats. *B, E, H, J*, disease control rats on day 6. *C, F, I, L*, APB5-treated rats on day 6.

Statistical Analysis

All values were expressed as the mean ± S.E. and analyzed by Mann-Whitney nonparametric analysis or one-way analysis of variance with a modified *t* test. Statistical significance was defined as $p < 0.05$. Statistical analysis of the cell proliferation test and expression of Smad1 mRNA in cultured mesangial cells were done by *t* test. Quantitation of immunohistochemistry and expression of Smad1 mRNA in glomeruli were analyzed by one-way analysis of variance followed by the *post hoc* test. *p* values <0.05 were considered significant. Data are expressed as mean ± S.D.

RESULTS

Morphological Changes in Thy1 GN—We examined the *in vivo* role of Smad1 phosphorylation in glomerulonephritis. We utilized an acute model of mesangial proliferative glomerulonephritis known as Thy1 glomerulonephritis. In Thy1 GN, the proliferation of mesangial cells begins at day 2, peaks at day 6, and subsides in 12 days after the injection. Fig. 1 shows a representative light microscopic picture at day 6 for each group. The Thy1 GN group showed the increase of mesangial matrix, which peaked at day 6 (Fig. 1*B*). Increased replication of glomerular cells was assessed by immunostaining of PCNA. PCNA-positive cells were markedly increased in the Thy1 GN group and peaked at day 6 (data not shown). Col IV is a main component of the ECM in the glomerulosclerosis. Col IV was weakly visible along the glomerular basement membrane and insignificant in the mesangial area in the normal control group (Fig. 1*D*). On the other hand, the Thy1 GN group showed a strong positive reaction for Col IV in the expanded mesangial area (Fig. 1*F*).

Thy1 GN also showed overexpression of the PDGF-B and PDGFβ-receptor in the glomeruli (Fig. 1, *H* and *K*). These findings indicate that the excessive proliferation of mesangial cells, glomerular hypertrophy, and glomerular sclerotic changes occur simultaneously in glomerulonephritis induced by the anti-Thy1 antibody.

Anti-PDGFβ-receptor Antibody Inhibits Both Glomerular Cell Proliferation and Glomerulosclerosis in Vivo—APB5 inhibited the objective PDGFβ-R-mediated signaling pathway as described previously. Treatment with APB5 resulted in significant reductions of both glomerular cell numbers and glomerular PCNA-positive cells in Thy1 GN at each point studied (Figs. 1*C* and 2, *A* and *B*). Overexpression of the PDGF-B chain and PDGFβ-R were significantly reduced after the administration of APB5 (Fig. 1, *I* and *L*). APB5 treatment also reduced the increase in mesangial matrix in Thy1 GN, as assessed by the PAM-positive area/glomerular area using an image analyzer with a microscope (Fig. 2*C*). The mesangial expression of Col IV in Thy1 GN was suppressed by treatment with APB5 (Fig. 2*D*). These data indicate that APB5 is able to inhibit mesangial cell proliferation and the mesangial matrix expansion of Thy1 GN.

Time Course for the Expression of Smad1, Phospho-Smad1 (pSmad1), and Phospho-STAT3 (pSTAT3) in Thy1 GN—We examined the expression of Smad1 in a Thy1 GN rat kidney by

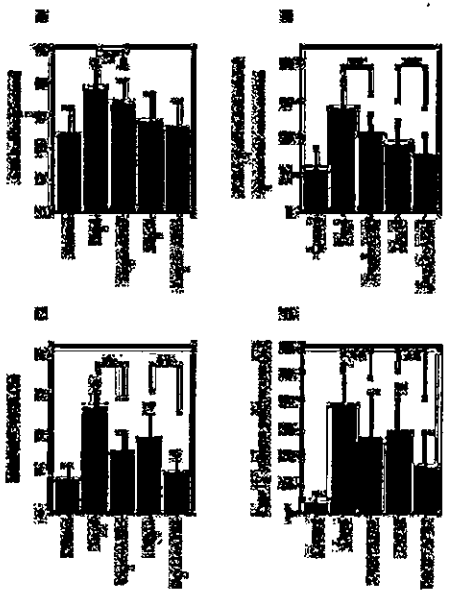

FIG. 2. **Quantitation of mesangial cell proliferation and glomerulosclerosis in Thy1 GN.** To quantitate histological changes in Thy1 GN and the effect of administration of APB5, glomerular cell number and PCNA-positive cell number were determined, and an IPAP system was used to quantitate the mesangial matrix and Col IV-positive areas. *A*, glomerular cell number. Increase in glomerular cell number was observed in Thy1 GN groups. *B*, PCNA-positive cell number of Thy1 GN. The number of PCNA-positive cells in the glomeruli of rats treated with APB5 was significantly reduced at each point studied. *C*, mesangial matrix proliferation. Mesangial matrix proliferation was observed at day 6 in Thy1 GN rats. APB5 significantly reduced this proliferation on each point studied. *D*, expression of type IV collagen. In the control group, Col IV was strongly positive in the expanded mesangial area. APB5 significantly reduced this expression. *, $p < 0.001$ *versus* Control. **, $p < 0.001$ *versus* non-treated disease control.

immunostaining. Smad1 was barely detectable in control glomeruli (Fig. 3*A*). However, in the glomerulus of Thy1 GN at day 6, Smad1 was extensively expressed with a typically expanded mesangial pattern (Fig. 3*B*). An IPAP system was used to quantitate the expression of Smad1. Glomerular Smad1 expression peaked at day 6 (Fig. 4*A*), consistent with the peak for mesangial proliferation. We next examined whether the phosphorylation and translocation of Smad1 are affected in Thy1 GN. By immunohistochemistry, pSmad1 was barely observed in the control group (Fig. 3*D*). However, in the Thy1 GN group, pSmad1 was extensive with a nuclear pattern (Fig. 3*E*). To quantitate the expression of pSmad1, the number of pSmad1-positive cells/glomerular cell was determined (Fig. 4*B*). The expression of pSmad1 was up-regulated at day 1 of Thy1 GN and glomerular pSmad1 expression peaked at day 4 of the disease, which also corresponds to the early phase of mesangial cell proliferation. Because PDGF-B and PDGFβ-R were up-regulated in Thy1 GN and APB5 reduced the overexpression, we performed immunostaining for phospho-STAT3, a transcription factor of the PDGF signaling pathway (26). The expression of pSTAT3 was extensively increased in Thy1 GN (Fig. 3, *G* and *H*) and peaked at day 6 (Fig. 4*C*).

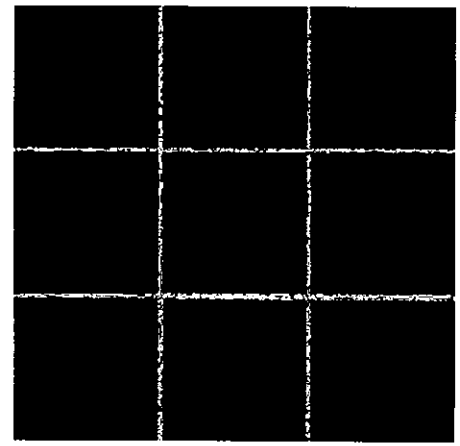

FIG. 3. **Immunohistochemical staining of Smad1, pSmad1, and pSTAT3 in Thy1 GN.** A remarkable increase in the expression of Smad1, pSmad1, and pSTAT3 was noted by immunohistochemical staining in the Thy1 rat glomeruli. pSmad1 was markedly observed with a nuclear pattern in Thy1 GN. APB5 treatment led to a significant decrease. *A–C*, Smad1. *D–F*, pSmad1. *G–I*, pSTAT3. *A, D, G*, normal control rat. *B, E, H*, untreated Thy1 rat glomeruli at day 6. *C, F, I*, treated with APB5 at day 6.

The APB5-treated groups had significantly reduced expression of Smad1 and pSmad1 proteins in glomeruli in Thy1 GN (Figs. 3, *C* and *F*, and 5, *A* and *B*). In addition, the overexpression of pSTAT3 was significantly inhibited by the administration of ABP5 at each point studied (Figs. 3*I* and 5*C*).

Effect of Anti-PDGFβ-R Antibody in Vitro—To determine whether APB5 inhibits the proliferation of mesangial cells, we examined the proliferation of mesangial cells in the absence and the presence of APB5 by using the BrdUrd ELISA system. As shown in Fig. 6*A*, the addition of APB5 suppressed PDGF-induced DNA synthesis in cultured mesangial cells. Next we examined whether the presence of phosphorylation inhibitors can prevent the actions of STAT3 in mesangial cells. AG490, an inhibitor of STAT3 phosphorylation, significantly inhibited STAT3 phosphorylation in cultured mesangial cells and mesangial proliferation (Fig. 6*B*). We also examined by Western blot analysis whether APB5 reduces the expression of pSTAT3, pSmad1, and Col IV in mesangial cells after stimulation with PDGF-B. We found that APB5 decreased phosphorylation of STAT3 and Smad1 and the expression of Col IV (Fig. 6*C*). These data suggest that STAT3 and Smad1 are involved to a significant extent in the expression of Col IV induced by stimulation of the PDGF-B signaling pathway.

Interaction between STAT3 and Smad1—To elucidate the role of the interaction between STAT3 and Smad1 for the increased expression of Col IV, transfection with a vector encoding dominant negative STAT3 was performed in cultured mesangial cells. Transfection with the dominant negative STAT3 clearly decreased the expression of pSmad1 and Col IV compared with wild type STAT3 (Fig. 6*D*). Using the BrdUrd ELISA system, we further examined whether transfection with dominant negative STAT3 reduces mesangial proliferation. The dominant negative STAT3 suppressed PDGF-induced DNA synthesis in cultured mesangial cells.

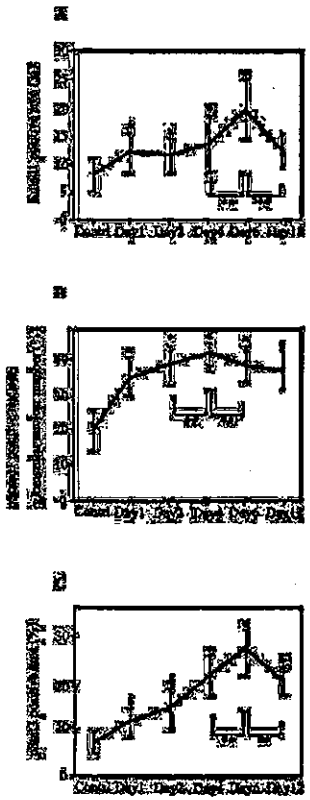

FIG. 4. **Time course of expression of Smad1, pSmad1, and pSTAT3.** Kidney sections from Thy1 GN rats on days 0, 1, 2, 4, 6, and 12 were subjected to immunohistochemical staining with antibodies against Smad1, pSmad1, and pSTAT3. *A*, expression of Smad1 in Thy1 GN. Expression of Smad1 peaked at day 6 and subsided on day 12. *B*, the time course for the ratio of pSmad1-positive cells to total glomerular cell number. Expression of pSmad1 peaked at day 4. *C*, time course of expression of pSTAT3. The ratio of pSTAT3-positive area to mesangial area increased by day 6 and subsided on day 12. *, $p < 0.001$ *versus* Control. **, $p < 0.001$ *versus* each day.

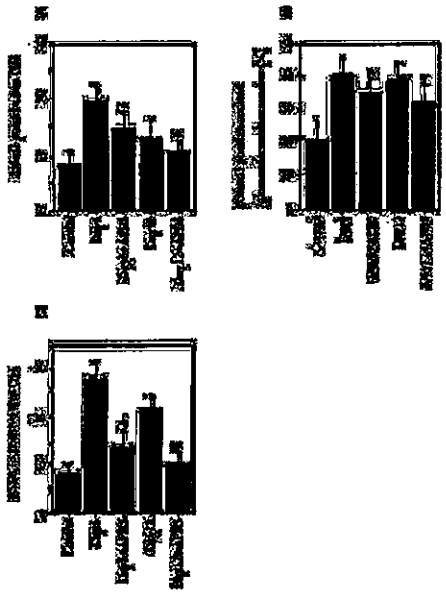

FIG. 5. **Effects of APB5 treatment on Smad1, pSmad1, and pSTAT3 expression.** Immunohistochemical staining and quantitation of Smad1, pSmad1, and pSTAT3 expression revealed treatment with APB5 reduced the expression of these proteins similar to mesangial matrix expansion and Col IV expression in glomeruli. *A*, expression of Smad1. *B*, expression of pSmad1. *C*, expression of pSTAT3. *, $p < 0.001$ *versus* non-treated disease control.

DISCUSSION

Many glomerular diseases are characterized by both mesangial cell proliferation and progressive glomerulosclerosis, but the common mechanisms related to both of these important pathological findings remain unresolved. The findings herein have shown that the activation of STAT3 and Smad1 plays a key role in regulating both of these critical events of progressive glomerular damage. Based on these findings, we have proposed a new direction of research concerning the pathogenesis and a therapeutic approach for chronic glomerulonephritis and diabetic nephropathy, which are major problems in the 21st century.

Glomerulosclerosis is characterized by an increased amount of ECM mainly in the mesangium. Col IV is one of the major components of ECM and is overproduced in glomerulosclerosis (27). We recently reported that Smad1 is a key transcriptional factor in the regulation of Col IV expression in diabetic nephropathy *in vitro* and *in vivo* (8). In Thy1 GN, Col IV is strongly expressed in the sclerotic lesions of glomeruli as previously described (19). We showed here that phosphorylated Smad1 is strongly expressed in parallel with the up-regulated expression of Col IV and the expanded ECM in this glomerulonephritis. Moreover, the area in which Smad1 is strongly expressed is consistent with the Col IV-positive area. These findings suggest that Smad1 is a critical factor in the development of glomerulosclerosis not only in diabetic nephropathy but also in glomerulonephritis as well.

Glomerulosclerosis has the pathological features of progressive glomerular injuries, including chronic glomerulonephritis, IgA nephropathy, and diabetic nephropathy. Glomerular cell proliferation at an early stage in a number of glomerular diseases progresses to the subsequent development of glomerulosclerosis, which eventually progresses to end stage glomerular damages (1, 2). This process is seen in IgA nephropathy, membranoproliferative glomerulonephritis, diabetic nephropathy, and light chain systemic diseases in humans as well as in animals such as the anti-thy1 glomerulonephritis and the rat renal ablation models (2, 28). Blocking glomerular cell proliferation with an anti-PDGF antibody (7), anti-coagulant heparin (30), or vitamin D analogue (19) has been demonstrated to abolish the subsequent development of progressive glomerulosclerosis, but responsibility for this remains unclear. In the current study, we demonstrated a possible mechanism for regulating the interaction between mesangial cell proliferation and glomerulosclerosis for these pathological processes.

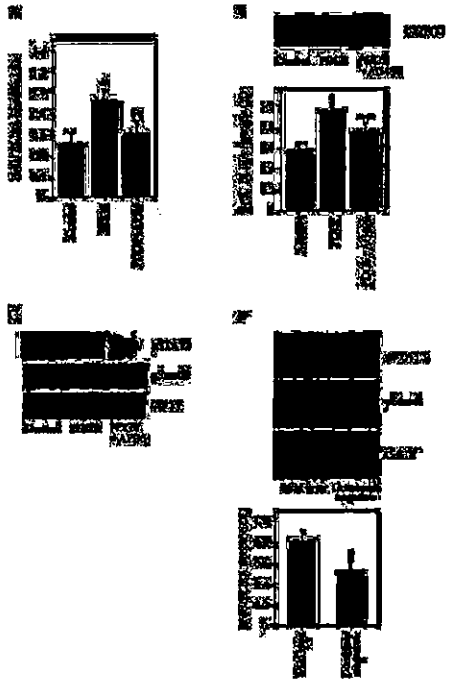

FIG. 6. **Effect of APB5 *in vivo* and Western blot analysis of transfected mesangial cells.** *A*, inhibitory effects of APB5 on mesangial cell proliferation. Addition of PDGF-B increased the proliferation of mesangial cell, and APB5 significantly inhibited this proliferation. *, $p < 0.05$ *versus* control. **, $p < 0.05$ *versus* PDGF-B-stimulated control. *B*, AG490 significantly inhibited STAT3 phosphorylation in PDGF-B-stimulated mesangial cells and mesangial proliferation. *, $p < 0.05$ *versus* Control. **, $p < 0.05$ *versus* PDGF-B-stimulated Control. *C*, Western blot analysis revealed that expression of pSTAT3, pSmad1, and Col IV protein was reduced by addition of APB5. One of three independent experiments is shown. *D*, expression of pSmad1 and Col IV protein was reduced by dominant negative STAT3. One of three independent experiments is shown. Mesangial proliferation was reduced by dominant negative STAT3. *, $p < 0.05$ *versus* wild type.

In this study, we showed that pSTAT3 is strongly expressed in mesangial proliferative lesions in Thy1 GN. Thy1 GN is a well characterized model in rats that leads to an acute phase of complement-dependent mesangial cell lysis, followed by a phase of intense mesangial cell proliferation and expansion of the mesangial matrix resembling the morphological features of human mesangial proliferative glomerulonephritis. A previous study reported that STAT3 serves as a signaling molecule in the development of glomerulonephritis (31). The current study suggests that the activation of Smad1 and STAT3 is involved in the development of glomerulosclerosis from mesangial proliferation.

A receptor for PDGF has been identified in murine and human mesangial cells (32). PDGF is a key potent mitogen for mesangial cells and is constitutively synthesized as an autocrine growth factor by these cells *in vitro* (32, 33). PDGF plays an important role in the development of pathological conditions, including glomerulonephritis, diabetic nephropathy, and progressive glomerulosclerosis *in vitro* and *in vivo* (3, 4). It has been previously reported that the activation of PDGF receptor tyrosine kinase induces the tyrosine phosphorylation of STAT3 proteins (13, 34). This activation is associated with growth regulation and differentiation (28, 29). The findings herein have demonstrated that the overexpression of phosphorylated STAT3 occurs simultaneously with the increased expressions of both PDGF and its β-receptor in this experimental glomerulonephritis and that APB5 ameliorates glomerulonephritis in association with reduced expression of PDGF, its β-receptor, and STAT3 *in vivo*. We have also shown that treatment with APB5 reduces the expression of Smad1 in Thy1 GN, indicating that the PDGF pathway can affect Smad1 production *in vivo*.

We confirmed the interaction of STAT3 and Smad1 in regulating the critical gene of glomerulosclerosis. The introduction of dominant negative STAT3 significantly decreased the expression of Col IV in cultured mesangial cells. The activation of STAT3 and Smad1 appears to be independent, although both factors are activated by PDGF. Furthermore, the activation of Smad1 appears to be involved in the activation of STAT3, based on the findings of a partial reduction of phosphorylated Smad1 by the introduction of dominant negative STAT3. These findings suggest that STAT3 activation by PDGF interacts with the overexpression of Smad1, followed by the subsequent activation of Col IV in experimental glomerulonephritis. Nakashima *et al.* (14) report that the transcriptional coactivator p300 physically interacts with STAT3 and Smad1 and that the formation of a complex between STAT3 and Smad1, bridged by p300, is involved in the cooperative signaling of the pathway. Thus, we concluded that the blocking of PDGF could affect the signaling of Smad1 and reduce the overproduction of Col IV *in vitro* and *in vivo*. The clear elucidation of both signaling pathways is essential for developing a complete understanding of the pathological process for development of progressive glomerular injury.

Therapeutic approaches for sclerosis in diverse organs are currently limited to supportive therapy to slow the loss of function of these organs. Our findings offer insights into the nature of the proliferative diseases that lead to sclerosis. Because both Smad1 and STAT3 are nearly absent in normal glomeruli, blocking Smad1 and/or STAT3 signaling may be beneficial for inhibiting the progression of various renal diseases leading to sclerosis by suppressing the pathologically activated proliferation and production of ECM.

REFERENCES

1. Fogo, A., and Ichikawa, I. (1989) *Semin. Nephrol.* **9**, 329–342
2. Striker, L. J., Doi, T., Elliot, S., and Striker, G. E. (1989) *Semin. Nephrol.* **9**, 318–328
3. Floege, J., and Johnson, R. J. (1995) *Miner. Electrolyte Metab.* **21**, 271–282
4. Doi, T., Vlassara, H., Kirstein, M., Yamada, Y., Striker, G. E., and Striker, L. J. (1992) *Proc. Natl. Acad. Sci. U. S. A.* **89**, 2873–2877
5. Barnes, J. L., and Hovey, K. A. (1990) *Lab. Investig.* **62**, 379–382
6. Floege, J., Burns, M. W., Alpers, C. E., Yoshimura, A., Pritzl, P., Gordon, K., Seifert, R. A., Bowen-Pope, D. F., Couser, W. G., and Johnson, R. J. (1992) *Kidney Int.* **41**, 297–309
7. Johnson, R. J., Raines, E. W., Floege, J., Yoshimura, A., Pritzl, P., Alpers, C., and Ross, R. (1992) *J. Exp. Med.* **175**, 1413–1416
8. Abe, H., Matsubara, T., Iehara, N., Nagai, K., Takahashi, T., Arai, H., Kita, T., and Doi, T. (2004) *J. Biol. Chem.* **279**, 14201–14206
9. Yang, X., Ji, X., Shi, X., and Cao, X. (2000) *J. Biol. Chem.* **275**, 1065–1072
10. Katagiri, T., Imada, M., Yanai, T., Suda, T., Takahashi, N., and Kamijo, R. (2002) *Genes Cells* **7**, 949–960
11. Liu, Z., Shi, W., Ji, X., Sun, C., Jee, W. S., Wo, Y., Mao, Z., Nagy, T. R., Li, Q., and Cao, X. (2004) *J. Biol. Chem.* **279**, 11313–11319
12. Dick, A., Bissu, W., and Drexler, H. (1998) *Dev. Dyn.* **211**, 293–305
13. Vignais, M. L., Sadowski, H. B., Watling, D., Rogers, N. C., and Gilman, M. (1996) *Mol. Cell. Biol.* **16**, 1759–1769
14. Nakashima, K., Yanagisawa, M., Arakawa, H., Kimura, N., Hisatsune, T., Kawabata, M., Miyazono, K., and Taga, T. (1999) *Science* **284**, 479–482

15. Bokemeyer, D., Ostendorf, T., Kunter, U., Lindemann, M., Kramer, H. J., and Floege, J. (2000) *J. Am. Soc. Nephrol.* **11**, 232–240
16. Sano, H., Sudo, T., Yokode, M., Murayama, T., Kataoka, H., Takakura, N., Nishikawa, S., Nishikawa, S., and Kita, T. (2001) *Circulation* **103**, 2955–2960
17. Sano, H., Ueda, Y., Takakura, N., Takemura, G., Doi, T., Kataoka, H., Murayama, T., Xu, Y., Sudo, T., Nishikawa, S., Nishikawa, S., Fujiwara, H., Kita, T., and Yokode, M. (2002) *Am. J. Pathol.* **161**, 135–143
18. Yamamoto, Y., Kato, I., Doi, T., Yonekura, H., Ohashi, S., Takeuchi, M., Watanabe, T., Yamagishi, S., Sakurai, S., Takasawa, S., Okamoto, H., and Yamamoto, H. (2001) *J. Clin. Investig.* **108**, 261–268
19. Makibayashi, K., Tatematsu, M., Hirata, M., Fukushima, N., Kusano, K., Ohashi, S., Abe, H., Kuze, K., Fukatsu, A., Kita, T., and Doi, T. (2001) *Am. J. Pathol.* **158**, 1733–1741
20. Nagai, K., Arai, H., Yanagita, M., Matsubara, T., Kanamori, H., Nakano, T., Ishara, N., Fukatsu, A., Kita, T., and Doi, T. (2003) *J. Biol. Chem.* **278**, 18229–18234
21. Davies, M. (1994) *Kidney Int.* **45**, 320–327
22. Striker, G. E., and Striker, L. J. (1985) *Lab. Investig.* **53**, 122–131
23. Meydan, N., Grunberger, T., Dadi, H., Shahar, M., Arpaia, E., Lapidot, Z., Leeder, J. S., Freedman, M., Cohen, A., Gazit, A., Levitzki, A., and Roifman, C. M. (1996) *Nature* **379**, 645–648
24. Bharti, A. C., Donato, N., and Aggarwal, B. B. (2003) *J. Immunol.* **171**, 3863–3871
25. Bromberg, J. F., Horvath, C. M., Besser, D., Lathem, W. W., and Darnell, J. E., Jr. (1998) *Mol. Cell. Biol.* **18**, 2553–2558
26. Schindler, C., and Darnell, J. E., Jr. (1995) *Annu. Rev. Biochem.* **64**, 621–651
27. Floege, J., Johnson, R. J., Gordon, K., Iida, H., Pritzl, P., Yoshimura, A., Campbell, C., Alpers, C. E., and Couser, W. G. (1991) *Kidney Int.* **40**, 477–488
28. Klahr, S., Schreiner, G., and Ichikawa, I. (1988) *N. Engl. J. Med.* **318**, 1657–1666
29. Meloche, S., Pelletier, S., and Servant, M. J. (2000) *Mol. Cell Biochem.* **212**, 99–109
30. Olson, J. L. (1984) *Kidney Int.* **25**, 376–382
31. Yanagita, M., Arai, H., Nakano, T., Ohashi, K., Mizuno, K., Fukatsu, A., Doi, T., and Kita, T. (2001) *J. Biol. Chem.* **276**, 42364–42369
32. Shukla, P. J., DiCorleto, P. E., Silver, B. J., and Abboud, H. E. (1988) *Am. J. Physiol.* **255**, F674–684
33. Abboud, H. E., Poptic, E., and DiCorleto, P. (1987) *J. Clin. Investig.* **80**, 676–685
34. Choudhury, G. G., Marra, F., Kiyomoto, H., and Abboud, H. E. (1996) *Kidney Int.* **49**, 19–25

Nkx2-5 mutation causes anatomic hypoplasia of the cardiac conduction system

Patrick Y. Jay,[1,2] Brett S. Harris,[3] Colin T. Maguire,[1] Antje Buerger,[2] Hiroko Wakimoto,[1] Makoto Tanaka,[2] Sabina Kupershmidt,[4] Dan M. Roden,[5] Thomas M. Schultheiss,[6] Terrence X. O'Brien,[3,7] Robert G. Gourdie,[3] Charles I. Berul,[1] and Seigo Izumo[2]

[1]Department of Cardiology, Children's Hospital, Boston, Massachusetts, USA. [2]Cardiology Division, Beth Israel Deaconess Medical Center, Boston, Massachusetts, USA. [3]Cardiovascular Developmental Biology Center, Department of Anatomy and Cell Biology, Medical University of South Carolina, Charleston, South Carolina, USA. [4]Department of Anesthesiology and [5]Department of Medicine, Vanderbilt University School of Medicine, Nashville, Tennessee, USA. [6]Division of Molecular Medicine, Beth Israel Deaconess Medical Center, Boston, Massachusetts, USA. [7]Veterans Administration Medical Center, Charleston, South Carolina, USA.

Heterozygous mutations of the cardiac transcription factor *Nkx2-5* cause atrioventricular conduction defects in humans by unknown mechanisms. We show in KO mice that the number of cells in the cardiac conduction system is directly related to *Nkx2-5* gene dosage. Null mutant embryos appear to lack the primordium of the atrioventricular node. In *Nkx2-5* haploinsufficiency, the conduction system has half the normal number of cells. In addition, an entire population of connexin40^{-}/connexin45^{+} cells is missing in the atrioventricular node of *Nkx2-5* heterozygous KO mice. Specific functional defects associated with *Nkx2-5* loss of function can be attributed to hypoplastic development of the relevant structures in the conduction system. Surprisingly, the cellular expression of connexin40, the major gap junction isoform of Purkinje fibers and a putative *Nkx2-5* target, is unaffected, consistent with normal conduction times through the His-Purkinje system measured in vivo. Postnatal conduction defects in *Nkx2-5* mutation may result at least in part from a defect in the genetic program that governs the recruitment or retention of embryonic cardiac myocytes in the conduction system.

Introduction

During cardiac development, pluripotent myocytes differentiate into specific anatomic and cellular phenotypes. For example, the atrial and ventricular lineages diversify in the precardiac mesoderm even before the heart tube has formed (1). Lineage-tracing analyses in chick embryos likewise show that the conduction system develops by recruitment of adjacent multipotent cardiac myocytes. Recruitment occurs within specific embryonic stages, starting in the central conduction system and ending with the peripheral network of Purkinje fibers (2, 3). The cells withdraw from proliferation once they join the system (3). Cell birth dating experiments suggest that the process is the same in the mouse (4). Endothelin and neuregulin-1 in the chick and mouse, respectively, may induce recruitment into the peripheral Purkinje system (5, 6), but little else is known about the mechanisms that govern the development of the conduction system.

To our knowledge, no diseases have yet been reported to perturb specifically the molecular mechanism of the embryonic formation of the conduction system. Physiologic conduction defects commonly result from drugs or mutations that affect the function of ion channels, pumps, or gap junctions, but congenital and acquired anatomic abnormalities do exist. For example, maternal lupus Ab's that cross the placenta destroy cells in the central conduction system of the fetus, causing congenital heart block. The block persists even after the Ab's are no longer present in the infant, consistent with a permanent anatomic lesion (7).

Nonstandard abbreviations used: AV nodal effective refractory period (AVERP); connexin40 (Cx40); embryonic day (E); interventricular septum (IVS); intracardiac electrogram (IEGM); stimulus (S).

Conflict of interest: The authors have declared that no conflict of interest exists.

Citation for this article: *J. Clin. Invest.* 113:1130–1137 (2004). doi:10.1172/JCI200419846.

Nkx2-5 is a transcription factor critical for cardiac development from *Drosophila* to humans (8). Heterozygous mutations of *Nkx2-5* in humans cause congenital heart disease. Mutations that affect DNA binding are associated with cardiac conduction defects or heart block (9, 10). Nkx2-5 mRNA and protein is transiently upregulated during the formation of conduction fibers relative to the surrounding myocardium in embryonic chick, mouse, and human hearts, suggesting a role in the development of the conduction system (11). We therefore hypothesized that loss of *Nkx2-5* function causes hypoplastic development of the conduction system, which in turn contributes to functional defects in the postnatal heart.

Methods

Generation of mutant strains. The *Nkx2-5$^{+/neo}$* line was generated by targeted replacement of the WT allele with the *Nkx2-5^{neo}* construct in AK7 ES cells and injection of positive clones into C57Bl/6 blastocysts, as previously described (12). To make the targeting construct, a neomycin resistance cassette flanked by loxP sequences was cloned into the first intron. An additional loxP sequence was cloned after the second exon. ES cells carrying the targeting construct were identified by Southern blot analysis using a 5′ flanking probe. Mice were genotyped by Southern blot analysis or PCR. The minK-lacZ and *Nkx2-5$^{+/-}$* lines have been previously described; each was generated by targeted replacement of the minK and *Nkx2-5* loci with β-gal (*lacZ*) (12, 13). Animal care and experiments were done in compliance with Institutional Animal Care and Use Committee guidelines and with the institutional approvals of Children's Hospital and Beth Israel Deaconess Medical Center.

Total RNA was purified from the ventricular myocardium of WT and *Nkx2-5$^{+/neo}$* mice for Northern blot analysis of Nkx2-5 and GAPDH mRNA expression by TRIzol extraction. Total RNA (10 μg) was electrophoresed on an agarose gel and transferred onto a nylon membrane (Hybond-N; Amersham Biosciences, Piscataway, New Jersey, USA). The membrane was then hybridized, washed, and imaged by standard methods using ^{32}P-labeled probes for Nkx2-5 or GAPDH.

β-Gal staining and assay. Hearts that expressed minK-lacZ were stained with X-gal for examination of the conduction system as previously described (13). Microscopic sections were obtained from stained hearts embedded in paraffin and eosin counterstained. Hearts viewed in whole mount were dehydrated in a graded methanol series and cleared in benzyl alcohol-benzyl benzoate (1:1). All embryos and mice were genotyped for *Nkx2-5* and minK-lacZ gene dosage; all comparisons using the minK-lacZ marker were made between hearts bearing equal copy numbers of the minK-lacZ allele, that is, heterozygotes or homozygotes.

Total minK-lacZ enzymatic activity in fetal hearts was quantified by a colorimetric assay. Hearts were dissected from embryonic day 14.5 (E14.5) embryos, washed in PBS, and homogenized in reporter lysis buffer (Promega Corp., Madison, Wisconsin, USA). β-Gal substrate (pH 7.3, 200 mM $NaPO_4$, 2 mM $MgCl_2$, 100 mM β-mercaptoethanol, 1.33 mg/ml o-nitrophenyl-β-D-galactopyranoside) was mixed with an equal volume of the homogenate and incubated at 37°C for 30 minutes. The reactions were stopped with 1 M Na_2CO_3. The absorption of the reaction was measured at 420 nm. Measurements were normalized to protein concentration determined by Bradford assays.

Connexin immunohistochemistry. Hearts were snap-frozen in liquid nitrogen, embedded in OCT, and sectioned (8-μm thickness). Alternate consecutive sections were histochemically stained with H&E. Immunofluorescent labeling followed previously described methods (2, 3). In brief, sections were incubated in primary Ab's overnight at 4°C. The primary Ab's used were guinea pig anti-rat connexin40 (Cx40), rabbit anti-chick Cx40 (5), rabbit anti-Cx43 (Sigma-Aldrich, St. Louis, Missouri, USA), and guinea pig anti-Cx45 (14). Secondary Ab's used were goat anti-rabbit Alexa 488 (Molecular Probes Inc., Eugene, Oregon, USA), goat anti-guinea pig TRITC, and goat anti-guinea pig cy5 (Jackson ImmunoResearch Laboratories Inc., West Grove, Pennsylvania, USA). Sections were counterstained with wheat germ agglutinin-TRITC to label cell membranes and Hoechst 33258 to label nuclei (Sigma-Aldrich). Representative laser-scanning confocal microscopy images at similar short-axis levels of the heart were obtained without knowledge of the *Nkx2-5* genotype. Cx40 particle number and size were calculated from ten sections for each heart. Quantitative image analysis was performed using NIH Image (Research Services Branch, National Institutes of Mental Health, Bethesda, Maryland, USA) as described previously (15).

Surface and intracardiac electrophysiology. In vivo cardiac electrophysiologic recordings were obtained in mice at 3 weeks, 7 weeks, and 1 year of age. Three-week-old mice were the youngest age at which their size permitted insertion of the intracardiac catheter. The mice were anesthetized with intraperitoneal pentobarbital (0.033 mg/g). A surface multilead ECG was obtained through subcutaneous limb leads. ECG signals were sampled at 2,000 Hz, yielding 1 ms time resolution.

Intracardiac electrogram (IEGM) were obtained by passing a 0.54-mm diameter (1.7 French) octapolar electrode catheter (CIBer mouse EP; NuMed Inc., Hopkinton, New York, USA) into the right heart via the internal jugular vein. The eight electrodes spaced 0.5 mm apart directly contact the endocardial surface of the heart. Bipolar recordings of the atrial and ventricular depolarization were obtained from adjacent electrodes in the superior right atrium just past the superior vena cava and right ventricular apex, respectively. Recordings of the His bundle were obtained by manipulations of the catheter to obtain a triphasic signal from the middle electrodes. The His amplitude was measured from the maximal signal obtained from the bipolar IEGM from the middle electrodes. Proper catheter placement was confirmed by visual inspection through a sternotomy at the end of studies.

The cardiac intervals, RR, PR, QRS, and QT, were measured from the surface ECG. The intracardiac intervals, AV, AH, and HV, were measured from the onset of deflection of the atrial, His, and right-ventricular IEGM signals. During normal sinus rhythm, the "A" recording measured from the superior right atrium near the sinus node should be coincident with the onset of the PR interval. In practice, the A measured anywhere in the right atrium of the mouse is nearly simultaneous with the onset of the P wave on the surface ECG.

Standard clinical electrophysiological pacing protocols were used to determine all basic electrophysiological parameters (16–18). The AV-His-Purkinje conduction properties were assessed by rapid atrial pacing at fixed rates; each subsequent train of stimuli was delivered at 5-ms shorter decrements. The minimum paced cycle length that maintained 1:1 AV conduction and the maximum cycle length that caused 2:1 AV block were determined for each animal. The 1:1 cycle length is the minimum coupling interval in which AV conduction is maintained with a constant AV interval. The 2:1 cycle length is the maximal interval that causes every other ventricular beat to be refractory to the paced atrial beat. The AV nodal effective refractory period (AVERP) was determined by an S1S2 protocol in which an eight-beat train of stimuli (S1) at 150-ms intervals was followed by a stimulus (S2) at a progressively shorter coupling interval; AVERP was defined as the maximal S1S2 coupling interval that failed to propagate to the ventricle. All recordings and measurements were made without knowledge of genotype.

Statistical analysis. Numerical data are presented as mean plus or minus SEM. Statistical significance for differences between groups was set at P values less than 0.05 as determined by the Student's two-sided t test.

Results

To examine the anatomy of the embryonic and postnatal conduction system, we used two independent sets of molecular markers. First, we crossed *Nkx2-5* haploinsufficient mice (*Nkx2-5$^{+/neo}$*) with minK-KO mice in which the minK-coding region was replaced with β-gal (minK-lacZ). MinK-lacZ labels the nuclei of conduction system myocytes, as determined by their anatomic location and coexpression with the gap junction protein connexin40 (13, 19). The *Nkx2-5^{neo}* allele, originally created for Cre-recombinase–mediated conditional deletion experiments, retains a neomycin-resistance cassette and flanking loxP sites in the noncoding regions. The allele unintentionally caused loss of function, presumably because of the neomycin-resistance cassette, as previously reported for other genes (20, 21). *Nkx2-5$^{+/neo}$* hearts have half as much Nkx2-5 mRNA as WT (Figure 1A). *Nkx2-5$^{neo/neo}$* embryos were morphologically identical to previously described homozygous *Nkx2-5* KO (*Nkx2-5$^{-/-}$*) embryos (12). The hearts of *Nkx2-5$^{neo/neo}$* embryos at E9.5 had arrest of cardiac development after partial looping, a bulbous atrium and ventricle, a wide AV canal, and a stenotic outflow tract. No viable

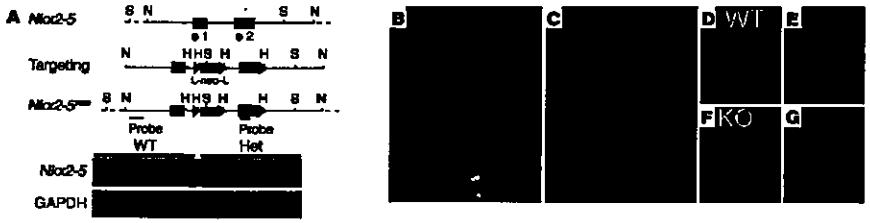

Figure 1
The absence of the AV node primordium in *Nkx2-5*–null mutant embryos. (**A**) Schematic diagram of the *Nkx2-5* genomic structure, targeting construct, and *Nkx2-5*^{neo} allele and Northern blot analysis demonstrating a 50% reduction in Nkx2-5 mRNA in the *Nkx2-5*$^{+/neo}$ adult ventricular myocardium. (**B**) WT *Nkx2-5* E9.5 embryos that carry the minK-lacZ gene show blue X-gal staining in the inner curvature of the AV canal (arrow). (**C**) *Nkx2-5*$^{neo/neo}$ E9.5 embryos show abnormal development of the heart tube and no minK-lacZ activity in the AV canal region where the AV node primordium is expected (arrow); staining is normal in the somites (arrowhead). In situ hybridization for minK mRNA and the corresponding bright-field images demonstrate expression throughout the myocardium of WT (**D** and **E**) and *Nkx2-5*$^{neo/neo}$ (**F** and **G**) embryos. All images are representative of three or more embryos or mice. Comparisons of minK-lacZ expression were made between animals with identical copy numbers of the reporter allele. **B** and **C** show minK-lacZ homozygotes; heterozygotes yield similar results. WT, *Nkx2-5* WT; Het, *Nkx2-5*$^{+/neo}$; KO, *Nkx2-5*$^{neo/neo}$; H, HindIII; N, NotI; S, SpeI; e 1, exon; e 2, exon 2; L, loxP sequence; neo, pGK neomycin resistance cassette. Probe denotes fragments used for Southern blot analysis. Scale bars: 200 μm (**B** and **C**), 100 μm (**D**–**G**).

Nkx2-5$^{neo/neo}$ mice were recovered after E10, as was originally reported for two other *Nkx2-5* KO strains (12, 22). Progeny resulting from a double-heterozygous (*Nkx2-5*$^{+/neo}$-minK$^{+/lacZ}$) cross have 0–2 copies of the minK-lacZ allele and the *Nkx2-5* WT allele. For the second independent set of conduction cell markers, we examined in the *Nkx2-5*$^{+/-}$ line the expression of Cx40, Cx45 (23, 24). *Nkx2-5*$^{+/-}$ mice were not crossed to the minK-lacZ strain because both KO alleles were replaced with lacZ.

Agenesis or hypoplasia of the central conduction system in Nkx2-5 KO mice

The primordium of the AV node resides at the lesser curvature of the AV canal in the looping heart tube (25, 26). At E9.5, the cells in the region express minK-lacZ in *Nkx2-5* WT embryos (Figure 1B). In contrast, E9.5 *Nkx2-5*$^{neo/neo}$ embryos show no cells that express minK-lacZ in the AV region (Figure 1C). The absence of marked cells suggests that the primordium is itself absent, but we cannot exclude the possibility that the primordial AV node cells uniquely require Nkx2-5 for transcription of the minK-lacZ gene. Two observations suggest that transcription at the minK locus does not require Nkx2-5 in general. First, the somites, which lack Nkx2-5, express minK-lacZ. Second, minK mRNA is expressed throughout the myocardium of both WT (Figure 1, D and E) and *Nkx2-5*$^{neo/neo}$ embryos (Figure 1, F and G), as previously described (27).

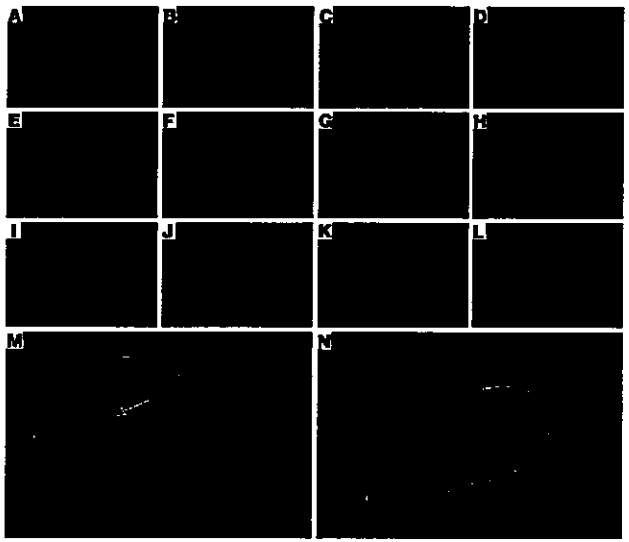

Figure 2
Hypoplasia of the central conduction system in heterozygous *Nkx2-5* KO mice. Histologic sections of adult hearts demonstrate the blue, X-gal–stained cells of the AV node (**A** and **B**) and His bundle (**C** and **D**) in WT (**A** and **C**) and *Nkx2-5*$^{+/neo}$ (**B** and **D**) hearts bearing one minK-lacZ allele. The histology of the AV node and His bundle were also examined by H&E and immunohistochemical staining of WT (**E**, **F**, **I**, **J**) and *Nkx2-5*$^{+/-}$ (**G**, **H**, **K**, **L**) hearts. Cx40 (TRITC, red) and Cx43 (FITC, green) label conductive and contractile myocytes, respectively. The AV node (**F** and **H**) and His bundle tissues (**J** and **L**) are circled. Consecutive sister sections from the same AV nodes were double-labeled for Cx40 (FITC, green) and Cx45 (TRITC, red) (circled in **M** and **N**). In the WT node (**M**), a small population of Cx40$^+$/Cx45$^+$ cells is present (arrow), but a larger population bearing Cx45 alone predominates. In the *Nkx2-5*$^{+/-}$ node (**N**) the Cx40$^+$/Cx45$^+$ cells are present, but the population expressing Cx45 alone is absent. Images shown are representative of at least three separate animals. HET, *Nkx2-5*$^{+/-}$ or *Nkx2-5*$^{+/neo}$; AVN, AV node; His, His bundle. Scale bars: 100 μm.

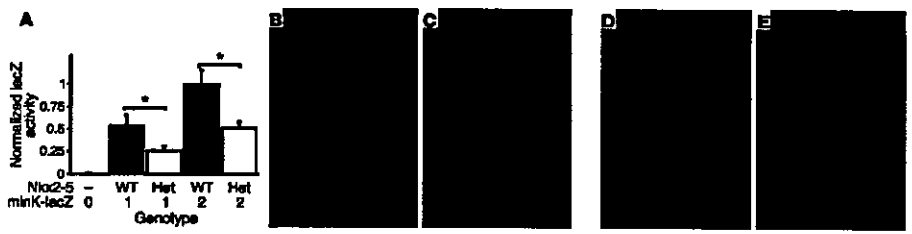

Figure 3
Hypoplasia of the peripheral conduction system in *Nkx2-5*$^{neo/+}$ mice revealed by minK-lacZ expression. (**A**) In E14.5 hearts minK-lacZ enzymatic activity is proportional to minK-lacZ (copy numbers 0, 1, or 2) and *Nkx2-5* gene dosage. Whole-mount images of minK-lacZ–stained neonatal hearts contrast the dense Purkinje fiber network in WT (**B** and **D**) compared with the hypocellular system in *Nkx2-5*$^{+/neo}$ mice (**C** and **E**). Sections show that the prominent blue X-gal stain shown in the whole mount is the peripheral conduction system at the interventricular septum (**D** and **E**). The hearts shown were from minK-lacZ homozygotes; heterozygotes yield similar results. The images shown are representative of at least three hearts. $P < 0.05$.

Nkx2-5 haploinsufficient mice form a smaller central conduction system. When viewed in frontal (four-chamber) histologic sections, the AV node is located posterior to and immediately above the interventricular septum (IVS). The His bundle extends anteriorly from the AV node along the crest of the IVS. The AV node and His bundle express minK-lacZ and Cx40 and Cx45. Serial sections through adult hearts demonstrate that the AV node and His bun-

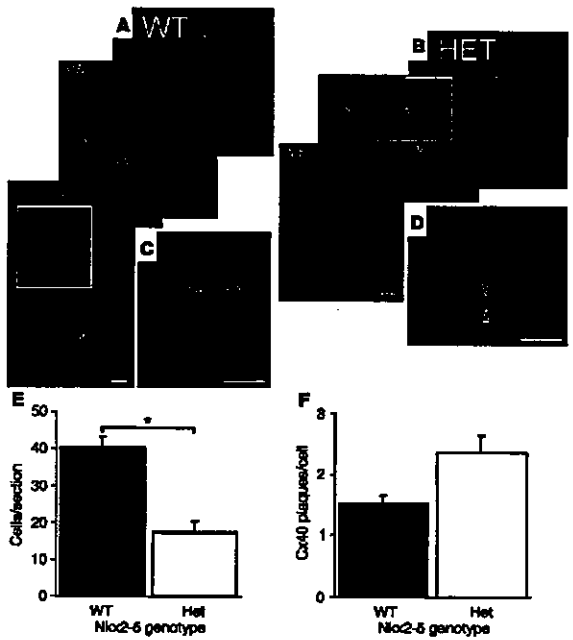

Figure 4
Cx40 immunohistochemistry confirms hypoplasia of the peripheral Purkinje system and normal cellular expression levels of Cx40 in *Nkx2-5*$^{+/-}$ mice. Montage confocal images demonstrate Cx40 expression as red, punctate staining in the subendocardial Purkinje fibers of WT (**A** and **C**) and *Nkx2-5*$^{+/-}$ (**B** and **D**) left ventricular myocardium. The distribution of Cx40 in the *Nkx2-5*$^{+/-}$ myocardium is considerably smaller than in WT (arrows in **A** and **B**). Higher magnification images of the boxed areas in **A** and **B** reveal the increased thickness of Purkinje fiber layers (arrowheads) in the WT (**C**) compared with *Nkx2-5*$^{+/-}$ heart (**D**). LV, left ventricle. Scale bars: 100 μm. (**E**) Cell counts within Cx40-positive domains reveal that Purkinje cell numbers are reduced by approximately half within sections of *Nkx2-5*$^{+/-}$ ventricles ($P < 0.05$). (**F**) *Nkx2-5*$^{+/-}$ and WT Purkinje cells contain approximately the same the number of Cx40 particles per cell. Three hearts each from WT and *Nkx2-5*$^{+/-}$ animals were examined.

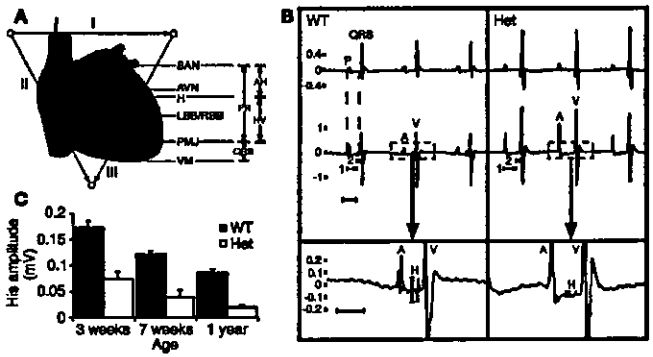

Figure 5
ECG correlates of anatomic structures in the cardiac conduction system in WT and *Nkx2-5*$^{+/-}$ mice. (**A**) Schematic diagram of the cardiac conduction system and ECG intervals as symbolized by the surface vectors I, II, and III and the intracardiac catheter. (**B**) Representative surface and intracardiac electrogram from a WT and *Nkx2-5*$^{+/-}$ mouse. The upper and middle tracings are simultaneous surface ECGs and IEGMs. The lower tracing shows the intracardiac recording at higher magnification and demonstrates the difference in His bundle signal amplitude between WT and *Nkx2-5*$^{+/-}$ mice. Atrial (P, A) and ventricular (QRS, V) depolarizations are depicted. The IEGM shows His (H) depolarization. Atrio-His and His-ventricular intervals are denoted (1 and 2). Note that ventricular depolarization or QRS interval begins immediately after the HV interval. (**C**) The amplitude of His depolarization is diminished in *Nkx2-5*$^{+/-}$ mice at all ages examined ($P < 0.0001$ in all age groups). AV, atrial-ventricular; AH, atrio-His; HV, His-ventricular; LBB/RBB, left and right bundle branch; PMJ, Purkinje-myocyte junction; SAN, sinoatrial node; VM, ventricular myocardium.

dle in *Nkx2-5*$^{+/nlacZ}$ mice are smaller and have fewer minK-lacZ^{+} cells than the WT mice (Figure 2, A and B). Cross sections of the His bundle demonstrate the size difference most clearly. Compare the wispy strand of the *Nkx2-5*$^{+/nlacZ}$ heart to the wide bundle of the WT at the crest of the ventricular septum where the bundle branches first diverge (Figure 2, C and D). Cx40 expression similarly delineated the larger AV node and His bundle of the WT (Figure 2, B–J) compared with the *Nkx2-5*$^{+/-}$ mice (Figure 2, G–L).

The normal mouse AV nodal region contains two cell populations or compartments as defined by gap junction isoform expression (28). The proximal, posterior compartment expresses Cx45 but not Cx40. The distal, anterior compartment, which connects to the His bundle, expresses both Cx40 and Cx45. In the WT, there is a discrete fascicular structure that contains a smaller Cx40^{+}/Cx45^{+} and a larger Cx40^{-}/Cx45^{+} compartment (Figure 2M). The *Nkx2-5*$^{+/-}$ node has only the distal Cx40^{+}/Cx45^{+} compartment (Figure 2N). The proximal Cx40^{-}/Cx45^{+} compartment is absent or severely attenuated. Qualitatively similar levels of Cx40 and Cx45 were present in the remaining Cx40^{+}/Cx45^{+} compartment of *Nkx2-5*$^{+/-}$ and WT mice. The Cx40^{+}/Cx45^{+} region reveals a high degree of overlap of the immunofluorescent green Cx40 (FITC) and red Cx45 (TRITC) signals, yielding a yellow signal when merged. The colocalization indicates that a cell in the AV node can express both connexin isoforms and that the two connexins are usually present in the same gap-junctional plaques, as previously reported (28).

Hypocellularity of the peripheral conduction system in heterozygous Nkx2-5 KO mice

By E14 the peripheral conduction system has developed (29). Although *Nkx2-5*–null murant embryos die around E10, the heterozygotes survive to birth. For an initial assessment of the conduction system in E14.5 WT and *Nkx2-5*$^{+/nlacZ}$ embryos we measured minK-lacZ activity in whole-heart lysates. As expected, homozygous minK-lacZ embryos had twice as much lacZ activity as heterozygotes given equivalent *Nkx2-5* gene dosages. *Nkx2-5* haploinsufficiency was also associated with a proportionate reduction in lacZ activity (Figure 3A). Hypocellularity of the peripheral Purkinje network in *Nkx2-5*$^{+/nlacZ}$ hearts is largely the cause of the reduced enzymatic activity. Compare the dense blue staining of the AV ring and interventricular septum of newborn WT mice (Figure 3, B and D) to the sparser network in the *Nkx2-5*$^{+/nlacZ}$ heart (Figure 3, C and E). Hence, individual fibers of the left and right bundle branch radiations can be discerned in the mutant (Figure 3C) but not the WT mouse (Figure 3B).

Quantification of Purkinje cells in WT and *Nkx2-5*$^{+/-}$ hearts was obtained by Cx40 immunohistochemistry. Distinct subendocardial clusters of Cx40^{+} myocytes, corresponding to Purkinje cells, were located in the ventricular septum. *Nkx2-5*$^{+/-}$ hearts had fewer fibers, each of which had fewer cells when compared with WT hearts (Figure 4, A–D). *Nkx2-5*$^{+/-}$ ventricles had approximately half as many Cx40^{+} Purkinje cells as the WT (Figure 4E), which parallels the quantitative reduction in minK-lacZ activity in E14.5 *Nkx2-5*$^{nlacZ/+}$ mice (Figure 3A). The discrete plaquelike structure and near crystalline packing of gap junction channels within a plaque permit quantification of connexins by immunofluorescent confocal microscopy (30). Surprisingly, no difference in the number of Cx40 plaques per Purkinje cell was noted between *Nkx2-5*$^{+/-}$ and WT (Figure 4F). Cx40 plaque size and fluorescence intensity levels were comparable between the WT and *Nkx2-5*$^{+/-}$ cells (data not shown).

Conduction and electrophysiologic abnormalities in Nkx2-5 haploinsufficiency

Propagation of the heartbeat through the conduction system can be followed by surface ECG and IEGM (Figure 5). The hypoplastic central and peripheral conduction systems in *Nkx2-5* KO mice were associated with physiologic abnormalities at each affected level. ECG measurements were obtained in mice ranging from 3 weeks to 1 year of age. *Nkx2-5*$^{+/nlacZ}$ and *Nkx2-5*$^{+/-}$ mice of both sexes showed similar conduction and electrophysiologic abnormalities (data not shown). Ventricular repolarization, as determined by the rate-corrected QT interval (31), was the same in *Nkx2-5*$^{+/-}$ and WT mice (Table 1).

The PR interval reflects conduction from the sinus node to the onset of ventricular myocardial activation. The PR is composed of the intracardiac AH and HV intervals, corresponding to conduction from the atrium to the His bundle and from the His bundle to the Purkinje-ventricular myocyte junction. *Nkx2-5*$^{+/-}$ mice have a prolonged PR interval at age 7 weeks and older (Table 1). The prolonged PR interval in *Nkx2-5*$^{+/-}$ mice resulted from prolongation of the AH interval. Because the durations of the P wave were equal in WT and *Nkx2-5*$^{+/-}$ mice, which indicates similar atrial conduction velocities, the prolonged PR must result from a defect in the AV node. *Nkx2-5*$^{+/-}$ mice, age 7 weeks and older, also have longer 1:1 and 2:1 cycle lengths and AV node effective refractory periods than the WT as determined by rapid atrial pacing. The differences further demonstrate diminished AV node function in *Nkx2-5*$^{+/-}$ mice (Table 2). *Nkx2-5*$^{+/-}$ mice as old as 2 years do not progress beyond first-degree AV block (data not shown). Curiously, 3-week-old *Nkx2-5*$^{+/-}$ mice have a normal PR interval and AV node function as assessed by atrial pacing. Autonomic influences are unlikely to obscure any intrinsic cardiac defect because β-adrenergic and cholinergic blockade did not elicit a difference between the WT and heterozygous 3-week-old mice (data not shown).

The His signal amplitude on the IEGM was markedly diminished in *Nkx2-5* haploinsufficient mice as young as 3 weeks, when they were large enough to permit intravenous insertion of the electrode catheter. All WT mice had an easily detected His signal, whereas all *Nkx2-5* haploinsufficient mice had a small or undetectable signal (Figure 5). The difference was so clear that the *Nkx2-5* genotype could be predicted by visual inspection of the His signal in mice of any age. For example, the genotype was correctly determined by a blinded observer in all 57 one-year-old mice based solely on the His signal (21 *Nkx2-5*$^{+/-}$, 14 *Nkx2-5*$^{+/nlacZ}$, 22 *Nkx2-5*$^{+/+}$). Normalization for the amplitude of the atrial or ventricular electrogram did not affect the results (data not shown.)

The HV interval, measured between the initial deflections of the His and ventricular signals, predominantly reflects conduction through the His-Purkinje system to the Purkinje-myocyte junction in the right ventricular apex. WT and *Nkx2-5*$^{+/-}$ mice had similar intervals at all ages (Table 1). Therefore, the conduction velocities of WT and *Nkx2-5*$^{+/-}$ Purkinje fibers are the same.

The QRS interval, which continues after the HV, represents depolarization of the entire ventricular myocardium. Depolarization begins at the Purkinje-myocyte junction and ends at the myocyte farthest from a terminal Purkinje-myocyte junction. *Nkx2-5*$^{+/-}$ mice at all ages showed a significantly prolonged QRS interval (Table 1).

Table 1
Cardiac conduction intervals in *Nkx2-5*$^{+/-}$ and WT mice

	ECG				IEGM			
	HR (bpm)	PR (ms)	QRS (ms)	QTm (ms)	HR (bpm)	AH (ms)	HV (ms)	AVI (ms)
3 weeks old								
Het (20, 8)	333 ± 10	38.2 ± 0.9	15.0 ± 0.4	22.0 ± 0.6	284 ± 8	30.1 ± 0.9	10.1 ± 0.5	40.2 ± 1.2
WT (18, 12 mice)	310 ± 12	39.0 ± 1.0	13.4 ± 0.4	21.2 ± 0.5	271 ± 16	32.2 ± 1.5	11.2 ± 0.3	43.4 ± 1.5
P values	NS	NS	0.01	NS	NS	NS	NS	NS
7 weeks old								
Het (13, 11)	345 ± 11	44.4 ± 1.0	15.7 ± 0.7	19.3 ± 0.7	320 ± 19	44.0 ± 3.3	10.5 ± 0.6	54.5 ± 3.2
WT (9, 9)	357 ± 11	39.8 ± 1.1	12.9 ± 0.3	19.7 ± 0.8	327 ± 17	34.6 ± 1.4	10.3 ± 0.6	44.9 ± 1.4
P values	NS	0.006	0.003	NS	NS	0.03	NS	0.02
1 year old								
Het (21, 9)	358 ± 15	50.0 ± 1.4	17.0 ± 0.4	25.4 ± 0.5	319 ± 18	45.2 ± 1.9	11.7 ± 0.6	56.9 ± 1.5
WT (20, 20)	373 ± 10	44.6 ± 1.2	12.5 ± 0.3	24.4 ± 0.4	338 ± 8	36.0 ± 1.0	11.8 ± 0.4	47.9 ± 1.2
P values	NS	0.004	< 0.001	NS	NS	0.0001	NS	0.0005

ECG and IEGM intervals were obtained in mice at 3 and 7 weeks and 1 year of age. The intracardiac AV interval is physiologically equivalent to the surface PR interval, but appears longer than the PR because the mice are more sedated for catheter placement. Numbers in parentheses indicate the number of mice recorded for surface and intracardiac ECG values, respectively. Intracardiac ECG data include only those mice in which a His signal was detected. Data represent mean plus or minus SEM. HET, *Nkx2-5*$^{+/-}$; AVI, AV interval; bpm, beats per minute; QTm, QT interval corrected for heart rate.

Table 2
Impaired atrioventricular conduction in *Nkx2-5*$^{+/-}$ mice

	AV node functional intervals		
	1:1 (ms)	2:1 (ms)	AVERP (ms)
3 weeks old			
Het (9)	125.0 ± 5.1	100.6 ± 3.8	97.8 ± 6.9
WT (12)	123.3 ± 4.4	97.1 ± 3.3	87.7 ± 3.8
P values	NS	NS	NS
7 weeks old			
Het (12)	132.9 ± 3.8	103.3 ± 2.7	98.6 ± 3.3
WT (9)	118.9 ± 3.0	91.7 ± 2.4	85.6 ± 3.7
P values	0.01	0.01	0.02
1 year old			
Het (21)	128.3 ± 3.6	93.3 ± 3.0	92.8 ± 4.1
WT (20)	116.3 ± 2.7	88.7 ± 2.7	76.0 ± 3.1
P values	0.002	0.03	< 0.001

Rapid atrial pacing reveals diminished AV node function in *Nkx2-5*$^{+/-}$ compared with WT mice. The 1:1 and 2:1 cycle lengths are the minimal and maximal right atrial pacing intervals in which the ventricular beat follows each paced beat at a constant interval or skips every other beat, respectively. To determine AVERP, the right atrium is given a train of eight beats (S1, 150-ms cycle length) followed by a single beat (S2) at incrementally shorter intervals after the last S1. AVERP is the S1S2 interval in which the AV node fails to propagate the S2 beat. Data are presented as mean plus or minus SEM. Het, *Nkx2-5*$^{+/-}$.

Discussion

Mutations of *Nkx2-5* cause atrioventricular conduction defects in humans and a mouse KO model. The current work suggests an anatomic basis for conduction defects present in *Nkx2-5* loss of function. *Nkx2-5* gene dosage affects the number of myocytes in the murine conduction system. Null mutant embryos entirely lack the minK-lacZ–expressing cells in the lesser curvature of the heart that

are probably the progenitors of the AV node. Haploinsufficient embryos and adults have cellular hypoplasia of the central and peripheral conduction systems, as marked by minK-lacZ or Cx40 and Cx45 expression. In addition, a group of $Cx40^{-}/Cx45^{+}$ cells is strikingly absent in the *Nkx2-5*$^{+/-}$ AV node. Thus, either *Nkx2-5* mutant embryos recruit fewer myocytes into the conduction system, or myocytes are lost after recruitment, perhaps by apoptosis. If Nkx2-5 affects recruitment, then Nkx2-5 might regulate specification of a small population of recruiting cells or a component of an inductive signaling pathway. Diminished proliferation of conduction cells probably cannot explain hypoplasia in the *Nkx2-5* KO mouse because the myocytes exit the cell cycle during recruitment (2, 4).

The physiologic data show that heterozygous *Nkx2-5* KO mice have defects in the AV node, His bundle, and intraventricular conduction. The results differ from a previous report in which only PR prolongation was found in a specific strain and sex of *Nkx2-5* KO mice (32). One potential explanation is that the high temporal resolution (1 ms) in this study permitted detection of interval differences relevant to the rapid murine heart rate.

The His bundle demonstrates the clearest relationship between structural and functional defects in the heterozygous *Nkx2-5* mutant conduction system. Heterozygous *Nkx2-5* KO mice have thin His bundles, as defined by either minK-lacZ or Cx40 expression. Intracardiac electrogram consistently demonstrate a low amplitude signal of His depolarization in the heterozygous KO mice at any age, which is most directly explained by the wispiness of the bundle. We have not observed any consistent difference in the anatomy or structure of the atrioventricular septum that could affect the course of the electrode catheter or its ability to measure the His bundle signal in *Nkx2-5* mutant mice. Diminished cellular depolarization in the His bundle is possible, but this would only compound the effect of a thin His bundle.

A second direct relationship can be drawn between the low density of peripheral Purkinje cells and the prolonged QRS interval in *Nkx2-5* KO mice. The low density of Purkinje cells is suggested by comparison of minK-lacZ expression in WT and *Nkx2-5*$^{+/nlz}$ hearts and confirmed by direct counts of $Cx40^{+}$ myocytes. The hypocellular Purkinje network in heterozygous *Nkx2-5* KO mice could cause prolongation of the QRS interval because each terminal Purkinje cell must depolarize a larger region of contractile myocardium where conduction is slow relative to the Purkinje fibers.

A seeming paradox arises from the prolonged QRS in the presence of a normal HV interval in the *Nkx2-5* mutant mice. Based on the definitions of the QRS and HV intervals, however, the observation is consistent with the fact that conduction velocity through a Purkinje fiber and the number of terminal Purkinje fibers that depolarize the ventricles are separate variables. The HV interval, which largely represents conduction through the His-Purkinje system, indicates that individual Purkinje fibers in the *Nkx2-5* mutant mouse conduct normally. The QRS extends beyond the HV to include ventricular depolarization after the Purkinje-myocyte junction. We suggest that the prolonged QRS results from the decreased ratio of terminal Purkinje cells to contractile myocardial volume in *Nkx2-5* mutant hearts. The prolonged QRS cannot be attributed to the downregulation of Cx43, the major gap junction isoform in the contractile myocardium, because it is normally expressed in *Nkx2-5*$^{+/-}$ mice (33).

Interestingly, the size of the region ultimately depolarized by each terminal Purkinje cell can explain QRS durations across species with large and small hearts. For example, humans and mice have a predominantly subendocardial distribution of Purkinje fibers. As would be predicted, the QRS durations in humans and mice, about 90 and 12 ms, respectively, scale with the thicknesses of their left ventricular wall, approximately 9 and 1 mm. In contrast, the bovine heart is four times larger than the human heart, but the QRS durations are similar, probably because the bovine Purkinje network extends from the subendocardium almost to the epicardium (34). Prolonged QRS intervals have not been described in human *Nkx2-5* mutation, but the small interval differences present in mutant mice might be subclinical in patients for whom recognition of larger prolongations are more relevant, such as complete right bundle branch block.

The relationship between a small AV node that lacks $Cx40^{-}/Cx45^{+}$ cells and prolongation of the PR or AH intervals in *Nkx2-5* mutant mice is less clear because the onset of PR prolongation and AV nodal functional defects, that is, longer-paced 1:1 and 2:1 block cycle lengths and increased AVERP, occurs between 3 and 7 weeks of age. As WT mice age, the PR interval prolongs independently of the heart rate. The mechanistic basis is unknown, but maturational changes of AV node physiology in association with hypoplasia or absence of the $Cx40^{-}/Cx45^{+}$ cell population could cause the atrioventricular conduction defect present in the *Nkx2-5* mutant mice. For example, changes in the cellular distribution of gap junctions have been described in the terminal crest from the right atrium of neonatal, weanling, and adult rabbits (35).

A limitation of the current work is that we have not excluded changes in every protein that participates in the action potential. Still, the downregulation of Cx40, the predominant gap junction protein in the conduction system, does not seem to occur in the conduction system of *Nkx2-5* heterozygotes and hence cannot cause the prolonged PR and QRS intervals, as could be reasonably supposed (36). Homozygous Cx40 KO mice have slow conduction through the Purkinje system and Purkinje-myocyte junction that manifests as prolonged HV and QRS intervals (37, 38). Heterozygous Cx40 KO mice have normal conduction despite having half-normal Cx40 protein levels, indicating that a greater than 50% reduction is necessary to cause a conduction defect (39). In *Nkx2-5*$^{+/-}$ and WT mice the number of Cx40 particles per Purkinje cell is the same, consistent with their equivalent HV intervals. The expression of Cx40 and Cx45 in the $Cx40^{+}/Cx45^{+}$ compartment of the AV node likewise appears similar. The observations by no means disprove the transcriptional regulation of Cx40 by Nkx2-5 but do demonstrate that half-normal gene dosage is sufficient for specific expression of Cx40 in the conduction system.

In summary, the number of myocytes that ultimately become conduction cells depends upon *Nkx2-5* gene dosage. Hypoplasia of anatomic structures in the conduction system of heterozygous *Nkx2-5* KO mice likely contributes to diminished AV node function and PR prolongation and can completely explain electrophysiologic defects such as a small His bundle-depolarization signal and intraventricular conduction delay. For the His bundle and peripheral Purkinje system, it is unnecessary to invoke a role for Nkx2-5 in the transcriptional regulation of a channel or gap junction such as Cx40.

Acknowledgments

We thank Olga Rozhitskaya, Maria Rivera, Laura Barbosky, and Daniel Iaun-bor Chen for their assistance. J. Barhanin kindly provided the minK in situ probe. This work is supported by grants from the NIH (to P.Y. Jay, R.G. Gourdie, and S. Izumo), the Marram and Carpenter Fund for Innovation and the Charles H. Hood Foundation (to P.Y. Jay), and the Deutsche Akademie der Naturforscher Leopoldina (to A. Buerger).

Received for publication August 20, 2003, and accepted in revised form February 17, 2004.

Address correspondence to: Patrick Jay, Department of Cardiology, Children's Hospital and Department of Pediatrics, Harvard Medical School, 300 Longwood Avenue, Boston, Massachusetts 02115, USA. Phone: (617) 355-8571; Fax: (617) 975-5268; E-mail: patrick.jay@childrens.harvard.edu.

1. Wang, G.F., and Stockdale, F.E. 1999. Chamber-specific gene expression and regulation during heart development. In *Heart development*. R.P. Harvey and N. Rosenthal, editors. Academic Press. San Diego, California, USA. 357–369.
2. Cheng, G., et al. 1999. Development of the cardiac conduction system involves recruitment within a multipotent cardiomyogenic lineage. *Development.* **126**:5041–5049.
3. Gourdie, R.G., Mima, T., Thompson, R.P., and Mikawa, T. 1995. Terminal diversification of the myocyte lineage generates Purkinje fibers of the cardiac conduction system. *Development.* **121**:1423–1431.
4. Sedmera, D., et al. 2003. Spatiotemporal pattern of commitment to slowed proliferation in the embryonic mouse heart indicates progressive differentiation of the cardiac conduction system. *Anat. Rec. 274A*:773–777.
5. Gourdie, R.G., Wei, Y., Kim, D., Klatt, S.C., and Mikawa, T. 1998. Endothelin-induced conversion of embryonic heart muscle cells into impulse-conducting Purkinje fibers. *Proc. Natl. Acad. Sci. U. S. A.* **95**:6815–6818.
6. Rentzsch, S., et al. 2002. Neuregulin-1 promotes formation of the murine cardiac conduction system. *Proc. Natl. Acad. Sci. U. S. A.* **99**:10464–10469.
7. Askanase, A.D., et al. 2002. Spectrum and progression of conduction abnormalities in infants born to mothers with anti-SSA/Ro-SSB/La antibodies. *Lupus.* **11**:145–151.
8. Jay, P.Y., Powell, A.J., Sherwood, M.C., and Izumo, S. 2003. Nkx2-5 and congenital heart disease. In *The molecular basis of inborn errors of development*. C.J. Epstein, R.P. Erickson, and A. Wynshaw-Boris, editors. Oxford University Press. New York, New York, USA. 607–614.
9. Schott, J.J., et al. 1998. Congenital heart disease caused by mutations in the transcription factor NKX2-5. *Science.* **281**:108–111.
10. Benson, D.W., et al. 1999. Mutations in the cardiac transcription factor NKX2.5 affect diverse cardiac developmental pathways. *J. Clin. Invest.* **104**:1567–1573.
11. Thomas, P.S., et al. 2001. Elevated expression of Nkx-2.5 in developing myocardial conduction cells. *Anat. Rec.* **263**:307–313.
12. Tanaka, M., Chen, Z., Bartunkova, S., Yamasaki, N., and Izumo, S. 1999. The cardiac homeobox gene Csx/Nkx2.5 lies genetically upstream of multiple genes essential for heart development. *Development.* **126**:1269–1280.
13. Kuperschmidt, S., et al. 1999. Replacement by homologous recombination of the minK gene with lacZ reveals restriction of minK expression to the mouse cardiac conduction system. *Circ. Res.* **84**:146–152.
14. Coppen, S.R., Dupont, E., Rothery, S., and Severs, N.J. 1998. Connexin45 expression is preferentially associated with the ventricular conduction system in mouse and rat heart. *Circ. Res.* **82**:232–243.
15. Barker, R.J., Price, R.L., and Gourdie, R.G. 2002. Increased association of ZO-1 with connexin43 during remodeling of cardiac gap junctions. *Circ. Res.* **90**:317–324.
16. Maguire, C.T., Bevilacqua, L.M., Wakimoto, H., Gehrmann, J., and Berul, C.I. 2000. Maturational atrioventricular nodal physiology in the mouse. *J. Cardiovasc. Electrophysiol.* **11**:557–564.
17. Berul, C.I., et al. 2001. Ventricular arrhythmia vulnerability in cardiomyopathic mice with homozygous mutant myosin-binding protein C gene. *Circulation.* **104**:2734–2739.
18. Berul, C.I., Aronovitz, M.J., Wang, P.J., and Mendelsohn, M.E. 1996. In vivo cardiac electrophysiology studies in the mouse. *Circulation.* **94**:2641–2648.
19. Kondo, R.P., Anderson, R.H., Kupershmidt, S., Roden, D.M., and Evans, S.M. 2003. Development of the cardiac conduction system as delineated by minK-lacZ. *J. Cardiovasc. Electrophysiol.* **14**:383–391.
20. Gage, P.J., Suh, H., and Camper, S.A. 1999. Dosage requirement of Pitx2 for development of multiple organs. *Development.* **126**:4643–4651.
21. Meyers, E.N., Lewandoski, M., and Martin, G.R. 1998. An Fgf8 mutant allelic series generated by Cre- and Flp-mediated recombination. *Nat. Genet.* **18**:136–141.
22. Lyons, I., et al. 1995. Myogenic and morphogenetic defects in the heart tubes of murine embryos lacking the homeo box gene Nkx2-5. *Genes Dev.* **9**:1654–1666.
23. Gourdie, R.G., et al. 1993. The spatial distribution and relative abundance of gap-junctional connexin40 and connexin43 correlate to functional properties of components of the cardiac atrioventricular conduction system. *J. Cell Sci.* **105**:985–991.
24. Gourdie, R.G., Green, C.R., Severs, N.J., Anderson, R.H., and Thompson, R.P. 1993. Evidence for a distinct gap-junctional phenotype in ventricular conduction tissues of the developing and mature avian heart. *Circ. Res.* **72**:278–289.
25. Viragh, S., and Challice, C.E. 1977. The development of the conduction system in the mouse embryo heart. II. Histogenesis of the atrioventricular node and bundle. *Dev. Biol.* **56**:397–411.
26. Viragh, S. and Challice, C.E. 1977. The development of the conduction system in the mouse embryo heart. I. The first embryonic A-V conduction pathway. *Dev. Biol.* **56**:382–396.
27. Franco, D., et al. 2001. Divergent expression of delayed rectifier K(+) channel subunits during mouse heart development. *Cardiovasc. Res.* **52**:65–75.
28. Coppen, S.R., Severs, N.J., and Gourdie, R.G. 1999. Connexin45 (alpha 6) expression delineates an extended conduction system in the embryonic and mature rodent heart. *Dev. Genet.* **24**:82–90.
29. Viragh, S., and Challice, C.E. 1982. The development of the conduction system in the mouse embryo heart. IV. Differentiation of the atrioventricular conduction system. *Dev. Biol.* **89**:25–40.
30. Green, C.R., Peters, N.S., Gourdie, R.G., Rothery, S., and Severs, N.J. 1993. Validation of immunohistochemical quantification in confocal scanning laser microscopy: a comparative assessment of gap junction size with confocal and ultrastructural techniques. *J. Histochem. Cytochem.* **41**:1339–1349.
31. Mitchell, G.F., Jeron, A., and Koren, G. 1998. Measurement of heart rate and Q-T interval in the conscious mouse. *Am. J. Physiol.* **274**:H747–H751.
32. Biben, C., et al. 2000. Cardiac septal and valvular dysmorphogenesis in mice heterozygous for mutations in the homeobox gene Nkx2-5. *Circ. Res.* **87**:888–895.
33. Tanaka, M., et al. 2002. A mouse model of congenital heart disease: cardiac arrhythmias and atrial septal defect caused by haploinsufficiency of the cardiac transcripton factor Csx/Nkx2.5. *Cold Spring Harb. Symp. Quant. Biol.* **67**:317–325.
34. Oosthoek, P.W., Viragh, S., Lamers, W.H., and Moorman, A.F. 1993. Immunohistochemical delineation of the conduction system. II: The atrioventricular node and Purkinje fibers. *Circ. Res.* **73**:482–491.
35. Litchenberg, W.H., et al. 2000. The rate and anisotropy of impulse propagation in the postnatal terminal crest are correlated with remodeling of Cx43 gap junction pattern. *Cardiovasc. Res.* **45**:379–387.
36. Bruneau, B.G., et al. 2001. A murine model of Holt-Oram syndrome defines roles of the T-box transcription factor Tbx5 in cardiogenesis and disease. *Cell.* **106**:709–721.
37. VanderBrink, B.A., et al. 2000. Connexin40-deficient mice exhibit atrioventricular nodal and infra-Hisian conduction abnormalities. *J. Cardiovasc. Electrophysiol.* **11**:1270–1276.
38. Tamaddon, H.S., et al. 2000. High-resolution optical mapping of the right bundle branch in connexin40 knockout mice reveals slow conduction in the specialized conduction system. *Circ. Res.* **87**:929–936.
39. Kirchhoff, S., et al. 1998. Reduced cardiac conduction velocity and predisposition to arrhythmias in connexin40-deficient mice. *Curr. Biol.* **8**:299–302.

R353Q Polymorphism, Activated Factor VII, and Risk of Premature Myocardial Infarction in Japanese Men

Masakazu Ogawa, MD; Satoshi Abe, MD; Sadatoshi Biro, MD; Masahiko Saigo, MD; Takashi Kihara, MD; Shiro Setoyama, MD**; Tatsuru Matsuoka, MD; Hitoshi Toda, MD; Hiroyuki Torii, MD; Yoshihiko Atsuchi, MD; Yoshifumi Toyama, MD; Shigeki Tateishi, MD; Shinichi Minagoe, MD; Ikuro Maruyama, MD*; Chuwa Tei, MD

Background The association between myocardial infarction (MI) and the R353Q polymorphism of the Factor VII (FVII) gene, which reportedly influences FVII concentrations, activated Factor VII (FVIIa), or FVII antigen (FVIIag), remains controversial.

Methods and Results The present case–control study in 127 Japanese men with their first MI at or before 45 years of age and 150 matched healthy controls was designed to clarify this association in premature MI. R353Q polymorphism was determined by polymerase chain reaction, and plasma concentrations of FVIIa and FVIIag were assayed. The distribution of the RR, RQ, and QQ genotypes with respect to R353Q polymorphism was 117, 10, and 0 in the patients, and 131, 17, and 2 in the controls. The Q allele was negatively associated with premature MI (odds ratio=0.41, p=0.038). The plasma concentration of FVIIa was slightly higher in patients (55.1±40.9 U/L) than in controls (44.8±20.2 U/L), but not significantly (p=0.078); the plasma concentration of FVIIag did not differ between patients (88.7±15.7%) and controls (87.0±9.0%) (p=0.557). Plasma FVIIa concentrations were influenced by R353Q polymorphism (p<0.001).

Conclusions The Q allele may be protective against premature MI. (*Circ J* 2004; **68**: 520–525)

Key Words: Coronary risk factor; Factor VII; Genotype; Premature myocardial infarction; R353Q polymorphism

Factor VII (FVII) is the first enzyme in the extrinsic pathway of the blood coagulation system. Activation of the extrinsic coagulation pathway plays a key role in hemostasis[1] and thus FVII contributes to the occurrence of thrombotic events. Although most FVII circulates in plasma in the zymogen form, small but significant amounts of activated FVII (FVIIa) also are present, and appear to serve as a primer for triggering the extrinsic cascade[2–5] The Northwick Park Heart Study suggested that FVII coagulant activity is independently associated with risk of coronary events in middle-aged men[6,7] and several additional studies have linked elevated concentrations of FVII in plasma to coronary heart disease[8–14] Thus, FVII has become recognized as a hemostatic coronary risk factor.

Plasma FVII concentrations are influenced by both genetic and environmental factors. Green et al reported a strong association between a common polymorphism in exon 8 of the FVII gene (R353Q polymorphism) and plasma FVII[15] which has been confirmed by several other studies[8,9,16–23] especially with respect to FVIIa[24] However, the association between R353Q polymorphism of the FVII gene and myocardial infarction (MI) remains controversial. The contribution of the coagulation system to the pathogenesis of MI can be studied most readily in patients with premature MI, who have less atherosclerotic coronary stenosis than elderly patients[25–28]

We performed a case–control study to determine whether plasma FVIIa concentrations and R353Q polymorphism are associated with risk of premature MI.

(Received April 25, 2003; revised manuscript received March 2, 2004; accepted March 8, 2004)

*Departments of Cardiovascular, Respiratory and Metabolic Medicine, and *Laboratory and Molecular Medicine, Graduate School of Medicine, Kagoshima University and **Kagoshima Prefectural Comprehensive Health Center, Kagoshima, Japan*

Mailing address: Satoshi Abe, MD, Department of Cardiovascular, Respiratory and Metabolic Medicine, Graduate School of Medicine, Kagoshima University, 8-35-1 Sakuragaoka, Kagoshima 890-8520, Japan. E-mail: abe@m2.kufm.kagoshima-u.ac.jp

Methods

Study Population

We investigated 129 consecutive Japanese male patients treated as outpatients at Kagoshima Coronary Care Unit Network (2000–2003), with a first MI occurring before the age of 45 years (mean±SD, 40.4±4.5 years old) and giving informed consent. We angiographically confirmed occlusion or significant stenosis of a coronary artery in all patients. Of the 129 patients, 2 patients, one had Kawasaki disease and another had a coronary artery anomaly, were excluded. The remaining 127 patients (premature MI patients) had a mean age of 43.9±5.1 years at study entry, 3.3±3.8 years after initial MI. Coronary angiography showed single-vessel disease in 93 (73.2%), and multivessel disease in 34 (26.8%). Oral anticoagulant agents were administered to 33 patients. Control subjects were 150 consecutive age-matched healthy Japanese men (43.8±5.1 years old at entry), who underwent a medical checkup at Kagoshima Prefectural Comprehensive Health Center and gave informed consent. None of the control subjects had coronary heart disease according to their medical history or electrocardiography, and none took an oral anticoagulant. This study protocol was approved by the Ethics Committee of Kagoshima University.

Table 1 Characteristics of the Premature MI Patients and Control Subjects

Characteristics	Premature MI patients	Control subjects	p value
No.	127	150	
Age at MI, years	40.4±4.5		
Age at study entry, years	43.9±5.1	43.7±5.1	NS
Total number of coronary risk factors*	1.9±0.8	1.4±0.8	<0.001
Hypertension present (%)	17 (13.4)	24 (16.0)	NS
Hypercholesterolemia present (%)	79 (62.2)	66 (44.0)	0.003
Diabetes mellitus present (%)	29 (22.8)	9 (6.0)	<0.001
Smoking history (%)	110 (86.6)	110 (73.3)	0.006

MI, myocardial infarction. Values are means±SD for continuous variables. NS, not significant.
**Total number of coronary risk factors represents the sum of hypertension, hypercholesterolemia, diabetes mellitus, and smoking (maximum, 4).*

Identification of Conventional Coronary Risk Factors

Hypertension, hypercholesterolemia, diabetes mellitus, and smoking history were evaluated as conventional coronary risk factors. Hypertension was defined by a systolic blood pressure at entry of at least 140 mmHg, a diastolic pressure at least 90 mmHg, a past history of hypertension, or receiving antihypertensive medication. Hypercholesterolemia was defined by a serum total cholesterol concentration at entry of at least 220 mg/dl, a past history of hypercholesterolemia, or receiving lipid-lowering medication. Diabetes mellitus was defined by a fasting plasma glucose concentration at entry of at least 126 mg/dl, a past history of diabetes mellitus, or receiving hypoglycemic medications.

Laboratory Measurements and Techniques

Blood sampling was performed gently by 3 expert physicians at study entry. Samples were collected from all subjects between 07.00 and 11.00 h after an overnight fast, and also 20 min later in a separate syringe. Blood samples were centrifuged for 10 min (3,000 G, 4°C) and divided into plasma, serum, and blood cells. Each was dispensed into a plastic tube respectively and frozen at –80°C until analysis. Plasma concentrations of FVIIa and FVII antigen (FVIIag) were measured using a double-antibody enzyme-linked immunosorbent assay (Roche Diagnostics, Basel, Switzerland)[4] and a coagulation time method (Roche Diagnostics), respectively.

Detection of R353Q Polymorphism

R353Q polymorphism was detected as described by Green et al[15] Amplified fragments were digested with 5 U of *MspI* (New England BioLabs, Beverly, MA, USA) and then subjected to electrophoresis on a 2% agarose gel. Fragments of 205 bp (the R allele) and 272 bp (the Q allele) were detected. Genotypes were defined as RR, RQ, and QQ.

Statistical Analysis

Differences in baseline characteristics between the premature MI patients and control subjects were assessed using chi-square test for categorical variables and by unpaired t-test for continuous variables. Because the distributions of the plasma concentrations of FVIIa and FVIIag were skewed, logarithmic transformation was performed. Log FVIIa and log FVIIag were compared between groups by unpaired t-test. To estimate the contribution of various risk factors to the occurrence of premature MI, multivariate logistic regression analysis was performed with FVIIa, FVIIag, hypertension, hypercholesterolemia, diabetes mellitus, and smoking status as independent variables. The frequencies of genotypes in the premature MI and control groups were compared using the chi-square test with the values predicted by Hardy-Weinberg equilibrium. Frequencies of alleles and genotypes (RR genotype vs RQ+QQ genotypes) were compared using the chi-square test between the premature MI and control groups. The odds ratio (OR) was calculated with a 95% confidence interval (95%CI). Multivariate logistic regression analysis including hypertension, hypercholesterolemia, diabetes mellitus, and smoking status was performed to assess the association between the R353Q polymorphism and the occurrence of premature MI. The effect of the Q allele, with the R allele chosen as the reference allele, was analyzed by the introduction of 3 dummy variables (0, 1, and 2) coding respectively for the number of Q alleles. Categorical independent variables (hypertension, hypercholesterolemia, diabetes mellitus, and smoking status) also were coded as dummy variables (0 for absence and 1 for presence). The association of plasma FVIIa and FVIIag concentrations with each genotype was analyzed with one-way analysis of variance.

Values for continuous variables are expressed as means± SD. A p-value of less than 0.05 was considered to be statistical significant. All computations were carried out with the STAT View-J 5.0 (SAS Institute, NC, Cary, USA) or STATA 7.0 (Stata Corporation, College Station, USA).

Results

Characteristics of the Study Population

Characteristics of the premature MI patients and control subjects are shown in Table 1. There was no significant difference in age at entry between the 2 groups. Patients showed significantly higher prevalences of hypercholesterolemia, diabetes mellitus, and smoking than control subjects (p<0.01), and had a greater number of conventional coronary risk factors than control subjects (p<0.001). Family history was recognized in 7.1% of MI patients.

R353Q Polymorphism and Premature MI

The frequencies of the genotypes and alleles of the R353Q polymorphism are shown in Table 2. The distribution of genotypes was virtually identical to that predicted by the Hardy-Weinberg equilibrium, in both the MI patients (p=0.644) and control subjects (p=0.113). Because

Table 2 Plasma FVIIa and FVIIag Concentrations, and the Distribution of Genotypes and Alleles of R353Q Polymorphism of the Factor VII Gene Between the Premature MI Patients and Control Subjects: Risk of Premature MI

Variable	Premature MI patients	Control subjects
FVIIa (U/L)	55.1±40.7	44.8±20.2
FVIIag (%)	88.7±15.7	87.0±9.0
Genotype, no. (%)		
RR	117 (92.1)	131 (87.3)
RQ	10 (7.8)	17 (11.3)
QQ	0 (0)	2 (1.3)
RQ+QQ	10 (7.8)	19 (12.7)
Alleles, no. (%)		
R	244 (96.1)	279 (93.0)
Q	10 (3.9)	21 (7.0)

FVIIa, activated factor VII; FVIIag, factor VII antigen; MI, myocardial infarction.
Values are means±SD for continuous variables.

Table 3 Risk of Premature Myocardial Infarction for R353Q Polymorphism by Multivariate Logistic Regression Analysis

Variable	OR (95% CI)	p value
Q allele	0.41 (0.18–0.95)	0.038
Hypertension	0.86 (0.42–1.76)	NS
Hypercholesterolemia	1.87 (1.13–3.10)	0.016
Diabetes mellitus	5.37 (2.27–12.74)	<0.001
Smoking status	2.43 (1.25–4.70)	0.009

OR, odds ratio; CI, confidence interval.
The multivariate logistic regression analysis included the Q allele of R353Q polymorphism and hypertension, hypercholesterolemia, diabetes mellitus and smoking history. All independent variables were coded as dummy variables (for R353Q polymorphism, 0 for RR, 1 for RQ, and 2 for QQ; for hypertension, hypercholesterolemia, diabetes mellitus, and smoking history: 0 for absence and 1 for presence).

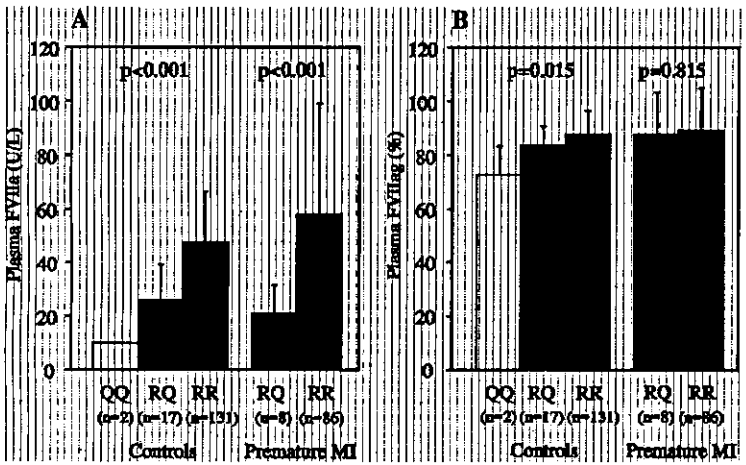

Fig 1. Plasma concentrations of FVIIa (A) and FVIIag (B) according to R353Q polymorphism. QQ, RQ, and RR refer to the respective genotypes. Values are means±SD. FVIIa, activated factor VII; FVIIag, factor VII antigen; MI, myocardial infarction.

the QQ genotype was not seen in premature MI patients, the distribution of genotypes was compared between the RR and the RQ+QQ genotypes. No significant difference in frequency of the RQ+QQ genotype or the Q allele was seen between the 2 groups.

The results of logistic regression analysis including the Q allele, hypertension, hypercholesterolemia, diabetes mellitus, and smoking are shown in Table 3. In the multivariate analysis including the 4 conventional coronary risk factors, the Q allele was significantly associated with the occurrence of premature MI (OR 0.41; p=0.038, r^2=0.01). There were no significant interactions between the Q allele and conventional risk factors.

Ten premature MI patients with the Q allele had 2.7±1.2 conventional risk factors, significantly more (p=0.002) than 19 control subjects with the Q allele (1.5±0.7). All premature MI patients with the Q allele had a history of smoking, and none had hypertension. No significant difference in prevalence of diabetes mellitus or hypercholesterolemia was noted (data not shown).

Plasma FVII and Premature MI

Plasma concentrations of FVIIa and FVIIag were compared between MI patients not receiving anticoagulant agents and control subjects. The plasma FVIIa concentrations in the patients (55.1±40.7 U/L) were slightly higher than those in control subjects (44.8±20.2 U/L), but not significant (p=0.078). Plasma FVIIag concentrations showed no significant difference between the 2 groups (88.7±15.7% vs 87.0±9.0%, p=0.557) (Table 2).

In multivariate logistic regression analysis including plasma concentrations of FVIIa and FVIIag and the presence of hypertension, hypercholesterolemia, diabetes mellitus, and past or present smoking status with respect to

premature MI, plasma FVIIa and FVIIag concentrations showed no significant association with risk of premature MI (p=0.102 and 0.810, respectively).

R353Q Polymorphism and FVII

Plasma concentrations of FVIIa and FVIIag in the various genotypes are compared in Fig 1. In the control subjects, plasma FVIIa concentrations for the QQ, RQ, and RR genotypes were 9.7±0.7 U/L, 26.0±13.2 U/L, and 47.8±12.3 U/L, respectively. Plasma FVIIag concentrations were 72.5±10.6%, 83.6±7.2%, and 87.6±9.0%, respectively. R353Q polymorphism, then, showed significant associations with FVIIa (p<0.001) and FVIIag (p=0.015). In MI patients, plasma FVIIa concentrations for the RQ genotype (21.0±9.8 U/L) were significantly lower (p<0.001) than those with the RR genotype (58.3±41.0 U/L). However, plasma FVIIag concentrations showed no significant difference between the 2 genotypes (87.5±15.7% vs 88.8±15.8%, respectively, p=0.815).

Discussion

The findings of the multivariate logistic regression analysis that included the conventional coronary risk factors of hypertension, hypercholesterolemia, diabetes mellitus, and smoking suggest that R353Q polymorphism is significantly associated with the risk of premature MI in the present study population. Plasma FVIIa concentrations in the patients were slightly higher than those in control subjects, but not significantly. Therefore, the Q allele of R353Q polymorphism might protect against premature MI in Japanese men.

Several studies have suggested that FVII is a coronary risk factor[5–14] but it has not been established by consensus that R353Q polymorphism of the FVII gene is associated with the risk of MI. Therefore, we conducted the present case–control study analyzing FVII genotypes. Although most FVII circulates in the zymogen form, a priming role in triggering the coagulation cascade has been assigned to the smaller amounts of circulating FVIIa[2–5] Because FVIIa is the first active protease in the extrinsic pathway of the coagulation cascade, plasma FVIIa concentrations may be important for determining the occurrence of thrombotic events such as thrombosis after rupture of an atherosclerotic plaque. Kario et al reported that plasma FVIIa concentrations were increased in patients with cardiovascular disease[9] and Philippou et al observed increased FVIIa in patients with acute coronary syndromes[10] However, the increase of FVIIa has not been sufficiently established as a hemostatic coronary risk factor. In our previous study, we found activation of the coagulation cascade, evaluated by the ratio of tissue factor and tissue factor pathway inhibitor in premature MI, but could not confirm the increase of plasma FVIIa[29]

In the present study of premature MI in Japanese men, we observed significant associations for R353Q polymorphism, but not for plasma FVIIa (p=0.078). Many studies have not recognized associations between plasma R353Q polymorphism or FVIIa and cardiovascular disease[23,30–34] The Framingham Heart Study reported that R353Q polymorphism was not significantly associated with cardiovascular disease, and suggested that R353Q polymorphism might be in linkage disequilibrium with other polymorphisms of the FVII gene or with another as-yet-unidentified gene located near the FVII gene[23] Recently, significant associations between polymorphisms of the FVII gene and MI, coronary artery disease, or cardiac events after intervention have been confirmed[35–40] Iacoviello et al suggested that R353Q and the hypervariable region 4 polymorphisms influenced the risk of MI in families with a history of thrombosis[35] Girelli et al reported that there were significantly more heterozygotes and homozygotes for the Q and A2 alleles among those who had not had a MI than among those who had had an infarction (p=0.01 for R353Q)[36] However, there have been no studies showing a significant association between R353Q polymorphism of FVII and premature MI.

Among there are many studies of the polymorphisms of genes and coronary heart disease in Japanese[41–43] as far as we know there have been only 2 studies investigating the genotypes of coagulation factor VII and coronary heart disease. Tamaki et al reported that polymorphisms of factor VII gene were not associated with the risk of MI[34] whereas Shimokata et al found a significant association between FVII polymorphism and coronary artery disease, but not MI[40] Therefore, we are the first to recognize a significant association with the risk of MI in Japanese.

Many studies have reported fewer stenotic atheromatous lesions on the coronary angiograms of younger MI patients compared with the elderly[25–28] Because atherosclerosis plays a reduced role in premature MI, prothrombotic factors become relatively important[27,44–47] Therefore, we selected relatively young Japanese men as study subjects. In the present study, the relation of R353Q polymorphism to the risk of premature MI was significant when considered together with the presence of conventional coronary risk factors. The discrepancy between our results and previous Japanese studies may be caused by the difference in the age of the study subjects. The mean ages of patients in studies by Tamaki et al and Shimokata et al were 59 years and 63 years, respectively. Because the role of FVII in the pathogenesis of MI might be less significant than conventional coronary risk factors in elderly Japanese, the previous 2 Japanese studies that included many elderly patients did not recognize the significant associations between R353Q polymorphism and MI. In contrast to hypercholesterolemia, diabetes mellitus, and smoking, all of which increased risk in this study, the Q allele seemed to be protective against premature MI. In contrast to the present results, when Moor et al and Ardissino et al assessed R353Q polymorphism in young survivors of MI, they found no significant differences in the prevalence of R353Q polymorphism between patients with premature MI and control subjects[8,32] In Taiwan, Li et al reported that R353Q polymorphism was an independent risk predictor of subsequent cardiac events in the young survivors of MI, but there was no difference in the prevalence of this polymorphism between patients and controls[39] The reason for disagreement between these study findings is not clear, but may involve differences of ethnicity and the prevalence of established coronary risk factors in the subjects.

Premature MI patients with the Q allele who otherwise might have had a reduced risk of MI had a significantly greater number of conventional coronary risk factors than control subjects with the Q allele. Recently, Iacoviello et al reported that smoking doubled the risk of MI in subjects with the Q allele[48] In the present study, all premature MI patients with the Q allele were current or former smokers. The Q allele presumably could not counter the increased risk of MI from smoking.

Study Limitations

The study was retrospective in design and had small statistical power (0.28) because of its small scale. We need more than 450 young MI patients to obtain results with sufficient statistical power (type II error <0.20) and we will continue the present study protocol to obtain a sufficient number of patients. Although the distribution of the Q allele in the control subjects was similar to that previously described in Japanese (12.6% by Tamaki et al; 17.6% by Shimokawa et al)[20,21,35,40] the number of controls in our study was also low. Therefore, we cannot establish the FVII gene as the protective factor of MI. Large prospective epidemiologic studies are necessary to clarify the associations between polymorphism of the FVII gene, plasma FVIIa, and risk of MI.

In addition, among several polymorphisms we examined only the R353Q polymorphism of the FVII gene. Other polymorphisms of the FVII gene such as the hypervariable region 4[49] and the decanucleotide insertion/deletion polymorphism[37,50-52] which is located in the promoter region of the FVII gene and influences its transcription, may have influenced the association. Recently, Peyvandi et al reported that a novel polymorphism in intron 1a of the FVII gene (G73A) might protect against premature MI[53] Therefore, these polymorphisms of the FVII gene also need to be analyzed. Because antiplatelet agents do not have direct effects on the coagulation cascade, we measured factor VII concentrations without interrupting these agents, which were being administered to the majority of cases. To strictly exclude the effects of antiplatelet agents, it is necessary to take blood samples from patients not receiving antiplatelet agents.

In conclusion, R353Q polymorphism of FVII, which importantly influences plasma FVIIa concentrations, may protect against premature MI.

Acknowledgments

We thank Drs Tsuminori Yamashita, Masato Maeda, Hiroshi Kaieda, Tsuyoshi Yamaguchi, Seiki Harada, Hiroyuki Fujisaki, Hideaki Fukunaga, Hirohisa Shono, Toshiko Maki, Tetsuro Muranaga, Kozo Shiraishi, and Ktyotake Arikawa for their kind help. We also thank Ms Noriko Yoshihara, and Mr Hirobumi Okamura for measuring the biochemical parameters.

References

1. Fuster V, Corti R, Badimon JJ. Therapeutic targets for the treatment of atherothrombosis in the new millennium: Clinical frontiers in atherosclerosis research. *Circ J* 2002; **66:** 783–790.
2. Seligsohn U, Kasper CK, Osterud B, Rapaport SI. Activated factor VII: Presence in factor IX concentrates and persistence in the circulation after infusion. *Blood* 1979; **53:** 828–837.
3. Nakagaki T, Foster DC, Berkner KL, Kisiel W. Initiation of the extrinsic pathway of blood coagulation: Evidence for the tissue factor dependent autoactivation of human coagulation factor VII. *Biochemistry* 1991; **30:** 10819–10824.
4. Morrissey JH, Macik BG, Neuenschwander PF, Comp PC. Quantitation of activated factor VII levels in plasma using a tissue factor mutant selectively deficient in promoting factor VII activation. *Blood* 1993; **81:** 734–744.
5. Morrissey JH. Tissue factor interactions with factor VII: Measurement and clinical significance of factor VIIa in plasma. *Blood Coagul Fibrinol* 1995; **6:** S14–S19.
6. Meade TW, Mellows S, Brozovic M, Miller GJ, Chakrabarti RR, North WRS, et al. Haemostatic function and ischaemic heart disease: Principal results of the Northwick Park Heart Study. *Lancet* 1986; **2:** 533–537.
7. Meade TW, Ruddock V, Stirling Y, Chakrabarti R, Miller GJ. Fibrinolytic activity, clotting factors, and long-term incidence of ischaemic heart disease in the Northwick Park Heart Study. *Lancet* 1993; **342:** 1076–1079.
8. Moor E, Silveira A, van't Hooft F, Suontaka AM, Eriksson P, Blomback M, et al. Coagulation factor VII mass and activity in young men with myocardial infarction at a young age: Role of plasma lipoproteins and factor VII genotype. *Arterioscler Thromb Vasc Biol* 1995; **15:** 655–664.
9. Kario K, Miyata T, Sakata T, Matsuo T, Kato H. Fluorogenic assay of activated factor VII: Plasma factor VIIa levels in relation to arterial cardiovascular diseases in Japanese. *Arterioscler Thromb* 1994; **14:** 265–274.
10. Philippou H, Adami A, Amersey RA, Stubbs PJ, Lane DA. A novel specific immunoassay for plasma two-chain factor VIIa: Investigation of FVIIa levels in normal individuals and in patients with acute coronary syndromes. *Blood* 1997; **89:** 767–775.
11. Hoffman CJ, Miller RH, Lawson WE, Hultin MB. Elevation of factor VII activity and mass in young adults at risk of ischemic heart disease. *J Am Coll Cardiol* 1989; **14:** 941–946.
12. de Sousa JC, Azevedo J, Soria C, Barros F, Ribeiro C, Parreira F, et al. Factor VII hyperactivity in acute myocardial thrombosis: A relation to the coagulation activation. *Thromb Res* 1988; **51:** 165–173.
13. Redondo M, Warzke HH, Stucki B, Sulzer I, Biasiutti FD, Binder BR, et al. Coagulation factors II, V, VII, and X, prothrombin gene 20210G→A transition, and factor V Leiden in coronary artery disease: High factor V clotting activity is an independent risk factor for myocardial infarction. *Arterioscler Thromb Vasc Biol* 1999; **19:** 1020–1025.
14. Broadhurst P, Kelleher C, Hughes L, Imeson JD, Raftery EB. Fibrinogen, factor VII clotting activity and coronary artery disease severity. *Atherosclerosis* 1990; **85:** 169–173.
15. Green F, Kelleher C, Wilkes H, Temple A, Meade T, Humphries S. A common genetic polymorphism associated with lower coagulation factor VII levels in healthy individuals. *Arterioscler Thromb* 1991; **11:** 540–546.
16. Saha N, Liu Y, Heng CK, Hong S, Low PS, Tay JSH. Association of factor VII genotype with plasma factor VII activity and antigen levels in healthy Indian adults and interaction with triglycerides. *Arterioscler Thromb* 1994; **14:** 1923–1927.
17. de Maat MPM, Green F, de Knijff P, Jespersen J, Kluft C. Factor VII polymorphisms in populations with different risks of cardiovascular disease. *Arterioscler Thromb Vasc Biol* 1997; **17:** 1918–1923.
18. Bernardi F, Marchetti G, Pinotti M, Arcieri P, Baroncini C, Papacchini M, et al. Factor VII gene polymorphisms contribute about one third of the factor VII levels variation in plasma. *Arterioscler Thromb Vasc Biol* 1996; **16:** 72–76.
19. Hunault M, Arbini AA, Lopaciuk S, Carew JA, Bauer KA. The Arg353Gln polymorphism reduces the level of cagulation factor VII: In vivo and in vitro studies. *Arterioscler Thromb Vasc Biol* 1997; **17:** 2825–2829.
20. Takamiya O. Genetic polymorphism (Arg353A→Gln) in coagulation factor VII gene and factor VII levels (coagulant activity, antigen and binding ability to tissue factor) in 101 healthy Japanese. *Scand J Clin Lab Invest* 1995; **55:** 211–215.
21. Kario K, Narita N, Matsuo T, Kayaba K, Tsutsumi A, Matsuo M, et al. Genetic determinants of plasma factor VII activity in the Japanese. *Thromb Haemost* 1995; **73:** 617–622.
22. Humphries SE, Lane A, Green FR, Cooper J, Miller GJ. Factor VII coagulant activity and antigen levels in healthy men are determined by interaction between factor VII genotype and plasma triglyceride concentration. *Arterioscler Thromb* 1994; **14:** 193–198.
23. Feng D, Tofler GH, Larson MG, O'Donnell CJ, Lipinska I, Schmitz C, et al. Factor VII gene polymorphism, factor VII levels, and prevalent cardiovascular disease: The Framingham Heart Study. *Arterioscler Thromb Vasc Biol* 2000; **20:** 593–600.
24. Bernardi F, Arcieri P, Bertina RM, Chiarotti F, Corral J, Pinotti M, et al. Contribution of factor VII genotype to activated FVII levels: Differences in genotype frequencies between northern and southern European populations. *Arterioscler Thromb Vasc Biol* 1997; **17:** 2548–2553.
25. Ogawa K, Numao T, Iizuka M, Yanagisawa A, Yoshino H, Ishikawa K, et al. Angiographic and coronary risk factor analyses of Japanese patients with ischemic heart disease before age 40: A multicenter cooperative study. *Jpn Circ J* 1996; **60:** 822–830.
26. Zimmerman FH, Cameron A, Fisher LD, Ng G. Myocardial infarction in young adults: Angiographic characterization, risk factors and prognosis (Coronary Artery Surgery Study Registry). *J Am Coll Cardiol* 1995; **26:** 654–661.
27. Choudhury L, Marsh JD. Myocardial infarction in young patients. *Am J Med* 1999; **107:** 254–261.
28. Yasuda T, Shimizu M, Ino H, Okeie K, Yamaguchi M, Fujino N, et al. Coronary lesion morphology and prognosis in young males with myocardial infarction with or without familial hypercholesterolemia. *Jpn Circ J* 2001; **65:** 247–250.
29. Saigo M, Abe S, Ogawa M, Yamashita T, Biro S, Minagoe S, et al. Imbalance of plasminogen activator inhibitor-1/tissue plasminogen activator and tissue factor/tissue factor pathway inhibitor in young Japanese men with myocardial infarction. *Thromb Haemost* 2001; **86:** 1197–1203.
30. Merlini PA, Ardissino D, Oltrona L, Broccolino M, Coppola R, Mannucci PM. Heightened thrombin formation but normal plasma levels of activated factor VII in patients with acute coronary syndromes. *Arterioscler Thromb Vasc Biol* 1995; **15:** 1675–1679.
31. Heywood DM, Ossei-Gerning N, Grant PJ. Association of factor VII: C levels with environmental and genetic factors in patients with ischaemic heart disease and coronary atheroma characterised by angiography. *Thromb Haemost* 1996; **76:** 161–165.
32. Ardissino D, Mannucci PM, Merlini PA, Duca F, Fetiveau R, Tagliabue L, et al. Prothrombotic genetic risk factors in young survivors of myocardial infarction. *Blood* 1999; **94:** 46–51.
33. Batalla A, Alvarez R, Reguero JR, González P, Alvarez V, Cubero GI, et al. Lack of association between polymorphisms of the coagulation factor VII and myocardial infarction in middle-aged Spanish men. *Int J Cardiol* 2001; **80:** 209–212.
34. Tamaki S, Iwai N, Nakamura Y, Tsujita Y, Kinoshita M. Variation of the factor VII gene and ischemic heart disease in Japanese subjects. *Coron Artery Dis* 1999; **10:** 601–606.
35. Iacoviello L, Di Castelnuovo A, de Knijff P, D'Orazio A, Amore C, Arboretti R, et al. Polymorphisms in the coagulation factor VII gene and the risk of myocardial infarction. *N Engl J Med* 1998; **338:** 79–85.
36. Girelli D, Russo C, Ferraresi P, Olivieri O, Pinotti M, Friso S, et al. Polymorphisms in the factor VII gene and the risk of myocardial infarction in patients with coronary artery disease. *N Engl J Med* 2000; **343:** 774–780.
37. Di Castelnuovo A, D'Orazio A, Amore C, Falanga A, Donati MB, Iacoviello L. The decanucleotide insertion/deletion polymorphism in the promoter region of the coagulation factor VII gene and the risk of familial myocardial infarction. *Thromb Res* 2000; **98:** 9–17.
38. Mrozikiewicz PM, Cascorbi I, Ziemer S, Laule M, Meisel C, Stangl V, et al. Reduced procedural risk for coronary catheter interventions in carriers of the coagulation factor VII–Gln[353] gene. *J Am Coll Cardiol* 2000; **36:** 1520–1525.
39. Li YH, Chen JH, Guo HR, Tsai WC, Chao TH. Genetic risk factors associated with the prognosis of myocardial infarction in young patients. *Thromb Haemost* 2002; **88:** 694–697.
40. Shimokata K, Kondo T, Ohno M, Takeshita K, Inden Y, Iino S, et al. Effects of coagulation factor VII polymorphisms on the coronary artery disease in Japanese: Factor VII polymorphism and coronary disease. *Thromb Res* 2002; **105:** 493–498.
41. Sawano M, Watanabe Y, Ohmura H, Shimada K, Daida H, Mokuno H, et al. Potentially protective effects of the Ser447–Ter mutation of the lipoprotein lipase gene against the development of coronary artery disease in Japanese subjects via a beneficial lipid profile. *Jpn Circ J* 2001; **65:** 310–314.
42. Takezako T, Zhang B, Serikawa T, Fan P, Nomoto J, Saku K. The D allele of the angiotensin-converting enzyme gene and reperfusion-induced ventricular arrhythmias in patients with acute myocardial infarction. *Jpn Circ J* 2001; **65:** 603–609.
43. Taniguchi I, Yamazaki T, Wagatsuma K, Kurusu T, Shimazu Y, Takikawa K, et al. The DD genotype of angiotensin-converting enzyme polymorphism is a risk factor for coronary artery disease and coronary stent restenosis in Japanese patients. *Jpn Circ J* 2001; **65:** 897–900.
44. Siscovick DS, Schwartz SM, Rosendaal FR, Psaty BM. Thrombosis in the young: Effect of atherosclerotic risk factors on the risk of myocardial infarction associated with prothrombotic factors. *Thromb Haemost* 1997; **78:** 7–12.
45. Ridker PM, Vaughan DE, Stampfer MJ, Manson JE, Hennekens CH. Endogenous tissue-type plasminogen activator and risk of myocardial infarction. *Lancet* 1993; **341:** 1165–1168.
46. Thompson SG, Kienast J, Pyke SD, Haverkate F, van de Loo JC. Hemostatic factors and the risk of myocardial infarction or sudden death in patients with angina pectoris: European Concerted Action on Thrombosis and Disabilities Angina Pectoris Study Group. *N Engl J Med* 1995; **332:** 635–641.
47. Hamsten A, Wiman B, de Faire U, Blomback M. Increased plasma levels of a rapid inhibitor of tissue plasminogen activator in young survivors of myocardial infarction. *N Engl J Med* 1985; **313:** 1557–1563.
48. Iacoviello L, Di Castelnuovo A, D'Orazio A, Donati MB. Cigarette smoking doubles the risk of myocardial infarction in carriers of a protective polymorphism in the blood coagulation factor VII gene. *Thromb Haemost* 1999; **81:** 658.
49. Marchetti G, Gemmati D, Patracchini P, Pinotti M, Bernardi F. PCR detection of a repeat polymorphism within the F7 gene. *Nucleic Acids Res* 1991; **19:** 4570.
50. Marchetti G, Patracchini P, Papacchini M, Ferrati M, Bernardi F. A polymorphism in the 5' region of coagulation factor VII gene (F7) caused by an inserted decanucleotide. *Hum Genet* 1993; **90:** 575–576.
51. Humphries S, Temple A, Lane A, Green F, Cooper J, Miller G. Low plasma levels of factor VIIc and antigen are more strongly associated with the 10 base pair promoter (–323) insertion than the Glutamine 353 variant. *Thromb Haemost* 1996; **75:** 567–572.
52. Dell'Acqua G, Iacoviello L, D'Orazio A, Di Bitondo R, Di Castelnuovo A, Donati MB. A polymorphic cluster in the 5' region of the human coagulation factor VII gene: Detection, frequency, and linkage disequilibrium. *Thromb Res* 1997; **88:** 445–448.
53. Peyvandi F, Mannucci PM, Bucciarelli P, Zeinali S, Akhavan S, Sacchi E, et al. A novel polymorphism in intron 1a of the human factor VII gene (G73A): Study of a healthy Italian population and of 190 young survivors of myocardial infarction. *Br J Haematol* 2000; **108:** 247–253.

THE JOURNAL OF BIOLOGICAL CHEMISTRY
© 2004 by The American Society for Biochemistry and Molecular Biology, Inc.

Vol. 279, No. 49, Issue of December 3, pp. 51182–51192, 2004
Printed in U.S.A.

Antiapoptotic Activity of Akt Is Down-regulated by Ca^{2+} in Myocardiac H9c2 Cells

EVIDENCE OF Ca^{2+}-DEPENDENT REGULATION OF PROTEIN PHOSPHATASE 2Ac*

Received for publication, June 28, 2004, and in revised form, September 3, 2004
Published, JBC Papers in Press, September 16, 2004, DOI 10.1074/jbc.M407225200

Chie Yasuoka‡§¶, Yoshito Ihara‡¶‖, Satoshi Ikeda§, Yoshiyuki Miyahara§, Takahito Kondo‡, and Shigeru Kohno§

From the ‡Department of Biochemistry and Molecular Biology in Disease, Atomic Bomb Disease Institute and the §Second Department of Internal Medicine, Nagasaki University Graduate School of Biomedical Sciences, Nagasaki 852-8523, Japan

Cell survival signaling of the Akt/protein kinase B pathway was influenced by a change in the cytoplasmic free calcium concentration ($[Ca^{2+}]_i$) for over 2 h via the regulation of a Ser/Thr phosphatase, protein phosphatase 2Ac (PP2Ac), in rat myocardiac H9c2 cells. Akt was down-regulated when $[Ca^{2+}]_i$ was elevated by thapsigargin, an inhibitor of the endoplasmic reticulum Ca^{2+}-ATPase, but was up-regulated when it was suppressed by 1,2-bis(o-aminophenoxy)ethane-*N*,*N*,*N*′,*N*′-tetraacetic acid tetra(acetoxymethyl)ester (BAPTA-AM), a cell permeable Ca^{2+} chelator. The inactivation of Akt was well correlated with the susceptibility to oxidant-induced apoptosis in H9c2 cells. To investigate the mechanism of the Ca^{2+}-dependent regulation of Akt via the regulation of PP2A, we examined the transcriptional regulation of PP2Acα in H9c2 cells with Ca^{2+} modulators. Transcription of the *PP2Acα* gene was increased by thapsigargin but decreased by BAPTA-AM. The promoter activity was examined and the cAMP response element (CRE) was found responsible for the Ca^{2+}-dependent regulation of PP2Acα. Furthermore, phosphorylation of CRE-binding protein increased with thapsigargin but decreased with BAPTA-AM. A long term change of $[Ca^{2+}]_i$ regulates *PP2Acα* gene transcription via CRE, resulting in a change in the activation status of Akt leading to an altered susceptibility to apoptosis.

Calcium (Ca^{2+}) plays a signaling role in many important cellular functions, such as fertilization, embryonic pattern formation, differentiation, proliferation, contraction, secretion, and metabolism (1). The versatility of the Ca^{2+}-signaling mechanism in terms of speed, amplitude and spatio-temporal patterning enables elevations of Ca^{2+} to regulate many processes of cell activity. Ca^{2+} exhibits cross-talk between a variety of signaling pathways (1). Ca^{2+} affects the protein kinase A pathway by regulating the metabolism of cAMP. It also activates nitric-oxide (NO) synthase to generate NO, which in turn activates the cGMP pathway through the activation of guanylyl cyclase. The Ras/mitogen-activated protein kinase (MAPK)[1] and Ca^{2+}/calmodulin/calmodulin kinase (CaMK) pathways are also controlled by Ca^{2+} (1, 2).

On the other hand, a cellular Ca^{2+} overload or the perturbation of intracellular Ca^{2+} compartmentalization can cause cytotoxicity and trigger apoptosis or necrosis (3, 4). Under such circumstances, various Ca^{2+}-dependent signaling cascades with kinases and phosphatases directly or indirectly influence cellular signaling. Protein kinase C family has been proposed to play an important role in the Ca^{2+}-mediated signaling of apoptosis (5). Calcineurin/PP2B, a Ca^{2+}-dependent Ser/Thr phosphatase (6), also appears to be involved in apoptosis (7). Together, these findings show that Ca^{2+} has a pivotal role in the regulatory mechanism of signaling pathways in cell survival and death, although the precise mechanism of Ca^{2+}-dependent cross-talk has not been fully clarified.

Akt/protein kinase B is a pleckstrin homology domain-containing Ser/Thr kinase (8, 9, 10). Akt is presently recognized as a cell survival or an antiapoptotic cellular signaling mediator. Akt is activated through a growth factor receptor-mediated activation of the phosphatidylinositol 3-kinase (PI3K) pathway (10). With growth factor signals, Akt is recruited to the plasma membrane and is activated through phosphorylation at Ser-473 and Thr-308 by phosphatidylinositol 3-phosphate-dependent protein kinase-1 (PDK1) or integrin-linked kinase (9, 10). Akt can phosphorylate Bad, caspase-9, and forkhead-related transcription factors, leading to their inactivation and to enhanced cell survival (8, 9, 10). Inhibitor of nuclear factor κB (IκB) kinase is also phosphorylated by Akt leading to an up-regulation of its activity and resulting in a promotion of the nuclear factor κB (NFκB)-mediated inhibition of apoptosis (8, 11, 12)

Akt has been found to be involved in cell death following the withdrawal of extracellular signaling factors, oxidative and osmotic stress, irradiation, treatment with drugs and ischemic stress (10). However, in spite that a variety of cellular stressors influence cells through Ca^{2+} signaling, the number of studies on Akt signaling and Ca^{2+} is limited. As for Akt, Ca^{2+}-dependent activation was reported in several studies (13, 14). On the other hand, there was a report that the activation of Akt is independent of Ca^{2+} (15). In contrast, we found that Akt was suppressed by an elevation of $[Ca^{2+}]_i$ in myocardiac H9c2 cells overexpressing the calreticulin gene (16). In the cells overexpressing calreticulin, protein phosphatase 2A (PP2A) was up-regulated by Ca^{2+} to decrease the phosphorylation level of Akt, and the inactivated status of Akt was well correlated with the susceptibility to apoptosis in H9c2 cells under conditions for differentiation induced by retinoic acid. Collectively, these results suggest that the Ca^{2+}-dependent regulatory mechanism of Akt signaling may be important to a variety of apoptotic signaling mechanisms, although how has not been fully clarified.

In the present study, to investigate the mechanism of the Ca^{2+}-dependent regulation of Akt signaling, we examined the influence of a change of $[Ca^{2+}]_i$ on susceptibility to oxidative stress-induced cell injury and on the Akt signaling pathway in myocardiac H9c2 cells. We show that the Ca^{2+}-dependent regulation of *PP2Acα* gene transcription is controlled through the cAMP responsive element (CRE), resulting in a change in the activation status of Akt leading to an altered susceptibility to apoptosis.

MATERIALS AND METHODS

Antibodies and Reagents—Antibodies against Akt, phospho-Akt (Ser-473), and phospho-Akt (Thr-309), CRE-binding protein (CREB), and phospho-CREB (Ser-133) were purchased from Cell Signaling Technology (Beverly, MA). The antibody against Sp1 was purchased from Santa Cruz Biotechnology (Santa Cruz, CA). The reagents used in the study were all of high grade and from Sigma or Wako Pure Chemicals (Osaka, Japan).

Cell Culture—H9c2 cells from embryonic rat heart (16, 17) were obtained from American Type Culture Collection (CRL-1446). H9c2 cells were cultured in Dulbecco's modified Eagle's medium supplemented with 10% fetal bovine serum in a humidified atmosphere of 95% air and 5% CO_2 at 37 °C. Before reaching confluence, the cells were split, and plated at low density in culture medium containing 10% fetal bovine serum.

Measurement of Cytoplasmic Free Ca^{2+}—The cytoplasmic free Ca^{2+} concentration, $[Ca^{2+}]_i$, was measured using Fura-2-AM essentially as described previously (16). Briefly, cultured cells on glass coverslips were loaded with 5 μM Fura-2-AM (Dojindo, Kumamoto, Japan) for 20 min in Earle's balanced salt solution (EBSS) in the presence of 0.01% pluronic acid F-127. After four washes with EBSS, the cover glass was positioned in a quartz cuvette containing 3.5 ml of fresh EBSS at a 45° angle to both excitation and emission light paths. The fura-2 fluorescence was determined at 37 °C using a spectrofluorophotometer operating at an emission wavelength of 505 nm with an excitation wavelength of 340 and 380 nm. The maximal signal (R_{max}) was obtained by adding ionomycin at a final concentration of 4 μM. Then the minimal signal (R_{min}) was obtained by adding EGTA at a final concentration of 7.5 mM, followed by Tris-free base to a final concentration of 30 mM, to increase the pH to 8.3. R is the ratio (F1/F2) of the fluorescence of Ex 340 nm, Em 505 nm (F1) to that of Ex 380 nm, Em 505 nm (F2). The actual Ca^{2+} concentration was calculated as $K_d \times (R - R_{min})/(R_{max} - R)$ with the K_d equal to 224 nM (18).

Lactate Dehydrogenase (LDH) Release Assay—After 4 h of treatment with 5 μM thapsigargin or 10 μM BAPTA-AM or not, cells were incubated with 75 μM hydrogen peroxide (H_2O_2) for 0–120 min. The LDH activity was assayed by using a MTX LDH kit (Kyokuto Seiyaku, Tokyo, Japan) according to the manufacturer's instructions. Briefly, 50 μl of supernatant was transferred to a 96-well plate, then 50 μl of coloring reagent was added and incubated for 45 min at room temperature. After 100 μl of stop solution was added, absorbance was measured at 560 nm with a microplate reader. The LDH release was shown as a rate of LDH released in the medium to total cellular LDH.

TUNEL Assay—Apoptosis was detected flow cytometrically by the terminal deoxynucleotidyltransferase-mediated dUTP nick-end labeling (TUNEL) method (19) using an ApopTag Plus Fluorescein *in situ* Apoptosis Detection kit (Serologicals, Norcross, GA). Briefly, cells were harvested and fixed in 70% ethanol, treated with terminal deoxynucleotidyl transferase for 1 h, and then with fluorescein isothiocyanate (FITC)-conjugated antidigoxigenin for 1 h at room temperature, and washed with phosphate-buffered saline (pH 7.0) (PBS) containing 0.1% Triton X-100. The fluorescence intensity was measured at 530 nm using a flow cytometer (BD Biosciences, San Jose, CA).

Northern Blot Analysis—The full-length rat PP1α catalytic subunit and PP2A catalytic α cDNAs were generously provided by Dr. Kunimi Kikuchi (Hokkaido University, Japan) (20, 21). A PstI-SmaI fragment of 600 bp and EcoRI-PvuII fragment of 680 bp were prepared from the cDNAs of PP1αc and PP2Acα, respectively, and used as cDNA probes. The probes were labeled with ^{32}P using a Random Primer Labeling kit (Takara Biomedicals, Shiga, Japan). The isolation of cytoplasmic RNA and Northern blotting were essentially performed as described before (16). Isolated RNAs (10 μg) were electrophoresed on a 1% agarose gel containing 0.6 M formaldehyde, transferred to a nylon membrane, and then hybridized with ^{32}P-labeled probes. Autoradiographed membranes were analyzed using a BAS5000 bioimage analyzer (Fuji Photo Film).

Immunoblot Analysis—Cultured cells were harvested and lysed for 20 min at 4 °C in lysis buffer (20 mM Tris-HCl, pH 7.5, 130 mM NaCl, 1% Nonidet P-40, and 10% glycerol including protease inhibitors (20 μM amidinophenylmethanesulfonyl fluoride, 50 μM pepstatin, and 50 μM leupeptin)). The supernatants obtained on centrifugation at 8,000 × *g* for 10 min were used in subsequent experiments. Protein samples were subjected to 10% SDS-PAGE under reducing conditions and then transferred to nitrocellulose membrane as described (22). The membrane was blocked with 5% skim milk or 3% bovine serum albumin in Tris-buffered saline (pH 7.5) containing 0.05% Tween 20. The blots were coupled with the peroxidase-conjugated secondary antibodies, washed, and then developed using the ECL chemiluminescence detection kit (Amersham Biosciences) according to the manufacturer's instructions.

Akt Activity Assay—Akt acitivity was assayed using an Akt assay kit (Cell Signaling Technology) according to the manufacturer's protocol. Briefly, Akt was immunoprecipitated from cell lysates using the anti-Akt antibody, and then the immunoprecipitates were incubated at 30 °C for 30 min in an assay mixture containing an Akt substrate, GSK-3α/β fusion protein. Phosphorylated proteins were separated by 12.5% SDS-PAGE and then transferred to nitrocellulose membrane to detect phosphorylated GSK-3α/β using an anti-phosphorylated GSK-3α/β (Ser-21/9) antibody.

Protein Phosphatase Assay—Protein Ser/Thr phosphatase activity was assayed photometrically using Ser/Thr phosphatase assay kit 1 (Upstate Biotechnology, Lake Placid, NY), according to the manufacturer's directions. The activity was assayed in the presence or absence of 10 nM okadaic acid, and the okadaic acid-sensitive activity was estimated as PP2A-specific activity. The phosphopeptide (RK(pT)IRR) was used as a phosphatase substrate. Protein concentrations were determined using a BCA assay kit (Pierce).

Generation of Luciferase Reporter Constructs—A ~1.6-kb fragment of rat *PP2Acα* gene promoter (−1350 to +258) (23) was amplified with rat genome by PCR using *Pfu* turbo DNA polymerase (Stratagene). The primers used are as follows; a forward primer (5′-GATCTCAGGTACTT-TCTTCCGGAACACTAG-3′) and a reverse primer (5′-GTCCAGCTCCT-TGGTGAACAACTTC-3′). The PCR product was subcloned into pUC18 to obtain pUC18-pro-PP2Ac. The nucleotide sequence was confirmed by sequencing with an ALFexpress II system (Amersham Biosciences). pUC18-pro-PP2Ac was digested with HindIII, and the resulting fragment containing the promoter region from −1209 to +258 was inserted into the HindIII site of the reporter vector pGLS-Basic (Stratagene) to give pGL3-pro-PP2Ac. To generate deleted mutants of the luciferase reporter construct, pGL3-pro-PP2Ac was digested with SacI and XhoI, and deletion mutants were made using a deletion kit for kilo sequence (Takara Biomedicals).

Site-directed Mutagenesis for Luciferase Vectors—*In vitro* mutagenesis was performed with pGL3-pro-PP2Ac-del (−279 to +258) and del (−145 to +258) as templates by using a QuikChange site-directed mutagenesis kit (Stratagene). Oligonucleotides used are as follows: GC box (−155), 5′-CCCTCCCCGCGGGAGGACCACAACCCAAAAGCGAA-GCCACTTCC-3′; CRE (−26), 5′-CCTGACGCCGGCGTGTGGTCACCA-CGCCGGGGCGGCCGCCATTAC-3′. The nucleotide sequences were confirmed by sequencing with an ALFexpress II system (Amersham Biosciences).

Luciferase Activity Assay—Each vector was transfected into H9c2 cells by using Lipofectamine2000 (Invitrogen) according to the manufacturer's instructions. After 24 h of transfection, cells were treated with thapsigargin (5 μM) or BAPTA-AM (10 μM), or left untreated for the periods indicated in the text. Then luciferase activity was assayed with cellular extracts by using a dual-luciferase reporter assay system (Promega).

* This work was supported in part by grants-in-aid from the Japanese Ministry of Education, Culture, Sports, Science, and Technology through the 21st Century COE program, and by a grant provided by the Ichiro Kanehara Foundation. The costs of publication of this article were defrayed in part by the payment of page charges. This article must therefore be hereby marked "*advertisement*" in accordance with 18 U.S.C. Section 1734 solely to indicate this fact.

The nucleotide sequence(s) reported in this paper has been submitted to the GenBank™/EBI Data Bank with accession number(s) AY749432.

¶ Both authors contributed equally to this work.

‖ To whom correspondence should be addressed: Dept. of Biochemistry and Molecular Biology in Disease, Atomic Bomb Disease Institute, Nagasaki University Graduate School of Biomedical Sciences, 1-12-4 Sakamoto, Nagasaki 852-8523, Japan. Tel.: 81-95-849-7099; Fax: 81-95-849-7100; E-mail: y-ihara@net.nagasaki-u.ac.jp.

[1] The abbreviations used are: MAPK, mitogen-activated protein kinase; BAPTA-AM, 1,2-bis (o-aminophenoxy) ethane-*N*,*N*,*N*′,*N*′-tetraacetic acid tetra (acetoxymethyl) ester; CRE, cAMP response element; CREB, CRE-binding protein; ER, endoplasmic reticulum; FITC, fluorescein isothiocyanate; PBS, phosphate-buffered saline; PI3K, phosphatidylinositol 3-kinase; LDH, lactate dehydrogenase; CaMK, calmodulin kinase; TUNEL, terminal deoxynucleotidyltransferase-mediated dUTP nick end-labeling; EMSA, electrophoretic mobility shift assay.

Electrophoretic Mobility Shift Assay—The electrophoretic mobility shift assay (EMSA) for the GC box and CRE was performed as described previously (24). Briefly, oligonucleotides were labeled with [γ-^{32}P]ATP using T4 polynucleotide kinase and then annealed to double-strand oligonucleotides. Specific oligonucleotides for the GC box and CRE were prepared according to the nucleotide sequences of the rat *PP2Acα* promoter region. Oligonucleotides used are as follows: GC box (−155), 5′-CGGGAGGACCACGCCCCAAAAGCGAAGC-3′; GC box (−155)-Mt, 5′-CGGGAGGACCACAACCCAAAAGCGAAGC-3′; CRE (−26), 5′-GACGCCGGCCTGACGTCACCACGCC-3′; CRE (−26)-Mt, 5′-GACGCCGGCCTGTGGTCACCACGCC -3′. Binding reactions were carried out in 15 μl of reaction mixture (25 mM Tris, pH 7.0, 6.25 mM $MgCl_2$, 0.5 mM EDTA, 0.5 mM dithiothreitol, 50 mM KCl, and 10% glycerol) containing 10 μg of nuclear extract, and 25 ng of labeled oligonucleotide. For the supershift assay, specific antibodies were added to the reaction mixture during the 30-min binding reaction.

Indirect Immunofluorescence Microscopy—After treatment with 5 μM thapsigargin or 10 μM BAPTA-AM for 2 h, cells incubated on Lab-Tek chamber slides (Nunc) were fixed with 3% paraformaldehyde for 20 min at room temperature and washed three times with PBS. Cells were permeabilized in 1% Triton X-100 in PBS for 10 min and washed three times with PBS. They were blocked with 1% bovine serum albumin in PBS for 30 min at room temperature, washed three times with PBS, and then incubated with antiphospho-CREB (Ser-133) overnight at 4 °C. Cells were washed with PBS four times and incubated with FITC-labeled anti-rabbit IgG antibody for 30 min in a dark room. The immunoreactive signals were visualized by indirect immunofluorescence microscopy.

RESULTS

Elevation of $[Ca^{2+}]_i$ Gradually Accelerates Cell Damage and Apoptosis in H9c2 Cells—To modify the level of $[Ca^{2+}]_i$ in H9c2 cells, the cells were treated with 5 μM thapsigargin (25), an inhibitor for sarcoplasmic/endoplasmic reticulum Ca^{2+} ATPase to increase $[Ca^{2+}]_i$, or with 10 μM BAPTA-AM (26), a cell permeable Ca^{2+} chelator to decrease $[Ca^{2+}]_i$, for 0–4 h. As shown in Fig. 1*A*, with thapsigargin, $[Ca^{2+}]_i$ shows a transient increase within the first 10 min. It then decreases to the basal level till 30 min, but again increases and retains elevated until 120 min, before gradually decreasing to the initial level. In contrast, with BAPTA-AM, $[Ca^{2+}]_i$ shows a continuous lowering during the treatment. To investigate the influence of the long term change of $[Ca^{2+}]_i$ on susceptibility to oxidative stress-induced cell injury, cells were treated with Ca^{2+} modulators (*i.e.* thapsigargin and BAPTA-AM) for 4 h then exposed to 75 μM hydrogen peroxide (H_2O_2) for 0–120 min, and cell damage was examined at predetermined times using the LDH release assay as described in the methods. In Fig. 1*B*, the release of LDH by H_2O_2 was observed only at 120 min in the medium of untreated cells. However, the release by H_2O_2 was initially observed at 60 min and increased at 120 min in the cells treated with thapsigargin. In contrast, BAPTA-AM treatment completely suppressed the release of LDH by H_2O_2 throughout the 120 min. Next, to investigate whether apoptosis is involved in the mechanism of thapsigargin-induced cell damage, cells were treated with Ca^{2+} modulators for 4 h then exposed to H_2O_2 (75 μM) for 2 h, and apoptosis was examined. Fig. 1*C* shows that TUNEL-positive fluorescence intensity was increased slightly by H_2O_2 (*upper*), but was significantly enhanced after the pretreatment with thapsigargin (*middle*). In contrast, no change was observed in the fluorescent intensity of the BAPTA-AM-treated cells with or without H_2O_2 (*lower*). Collectively, these results indicate that the susceptibility to apoptosis was enhanced with a long term elevation of $[Ca^{2+}]_i$, but was suppressed with the lowering of $[Ca^{2+}]_i$ in the cells under oxidative stress with H_2O_2, suggesting that the continuous change of $[Ca^{2+}]_i$ influences the susceptibility to apoptosis.

The Long Term Change of $[Ca^{2+}]_i$ Influences Akt Signaling in H9c2 Cells—To know the role of $[Ca^{2+}]_i$ in cell survival signaling, we focused on the effect of Ca^{2+} modulators on Akt signaling. Previously, we found that the Akt signaling pathway is responsible for the cytoprotective mechanism in H9c2 cells under conditions of stress such as serum starvation with retinoic acid (16), and oxidative stress with hydrogen peroxide (27). Although elevations in Ca^{2+} act as a signal, a prolonged increase in the concentration of Ca^{2+} can be lethal (1). Moreover, cell signaling molecules including transcription factors are activated differentially by the amplitude and duration of the response to Ca^{2+} (28). In the present study, H9c2 cells were treated with Ca^{2+} modulators such as thapsigargin (5 μM) and BAPTA-AM (10 μM) for over 2 h to induce a long term change of $[Ca^{2+}]_i$. After the treatments, the phosphorylation levels of Ser-473 and Thr-308 of Akt were examined. The phosphorylation of Thr-308 located in the kinase catalytic domain of Akt is necessary for the activation, and the phosphorylation of Ser-473 located in the regulatory domain of Akt supports the activation. As shown in Fig. 2, *A* (*right*) and *B*, the treatment with BAPTA-AM increased the phosphorylation of Akt both at Ser-473 and Thr-308, and the phosphorylation level increased to a maximum at 2 h, and was sustained thereafter till 4 h. In contrast, the phosphorylation of Akt decreased in a time-dependent manner with thapsigargin (Fig. 2, *A* (*left*) and *B*). Next we examined whether Ca^{2+} modulators also have an effect on the kinase activity of Akt. Fig. 2*C* shows that Akt activity is suppressed after the treatment with thapsigargin, but increased with BAPTA-AM. These results were consistent with the change in the phosphorylation status of Akt on treatment with Ca^{2+} modulators such as thapsigargin and BAPTA-AM. Together, Akt signaling was suppressed by the long term elevation of $[Ca^{2+}]_i$ with thapsigargin, but was enhanced by the long term lowering of $[Ca^{2+}]_i$ with BAPTA-AM. This suggests a Ca^{2+}-dependent regulation of Akt signaling in H9c2 cells. Furthermore, the Ca^{2+}-induced suppression of Akt signaling was compatible with the enhanced susceptibility to apoptosis in H9c2 cells treated with H_2O_2 (Fig. 1, *B* and *C*).

The Expression of PP2Acα Is Transcriptionally Regulated by Ca^{2+} Modulators—3-Phosphoinositide-dependent protein kinase (PDK1) is known to be responsible for phosphorylating Akt at Thr-308, and is activated by both phosphatidylinositol (3,4,5)-trisphosphate and phosphatidylinositol (3,4,)-bisphosphate, products of PI3K (9, 10). To investigate whether the upstream kinases are involved in the regulation of Akt by the change of $[Ca^{2+}]_i$, the activities for PI3K and PDK1 were measured in the cells treated with Ca^{2+} modulators. However, neither activities showed any significant change even if the cells were treated with thapsigargin or BAPTA-AM for 0–4 h (data not shown). Therefore, we focused on Ser/Thr protein phosphatases that could dephosphorylate and inactivate Akt to regulate the Akt signaling pathway (7). To investigate whether $[Ca^{2+}]_i$ levels affect the expression of protein Ser/Thr phosphatases, the cells were treated with 5 μM thapsigargin or 10 μM BAPTA-AM for 0–4 h, and transcriptional levels were estimated by Northern blot analysis for protein phosphatase 2A catalytic subunit α (PP2Acα) and protein phosphatase 1α catalytic subunit (PP1cα). In Fig. 3*A*, the level of PP2Acα mRNA was increased by thapsigargin but decreased by BAPTA-AM. In contrast, the mRNA level of PP1cα was not significantly changed by the Ca^{2+} modulators. In the immunoblot analysis, the protein level of PP2Acα was increased by thapsigargin but decreased by BAPTA-AM (Fig. 3*B*). However, the protein level of PP1cα was not influenced by thapsigargin or BAPTA-AM. The protein level of calcineurin/PP2B was not influenced by thapsigargin or BAPTA-AM either (data not shown). These results were consistent with results of the change of transcriptional levels for the phosphatases in the cells treated with each Ca^{2+} modulator. The enzymatic activity

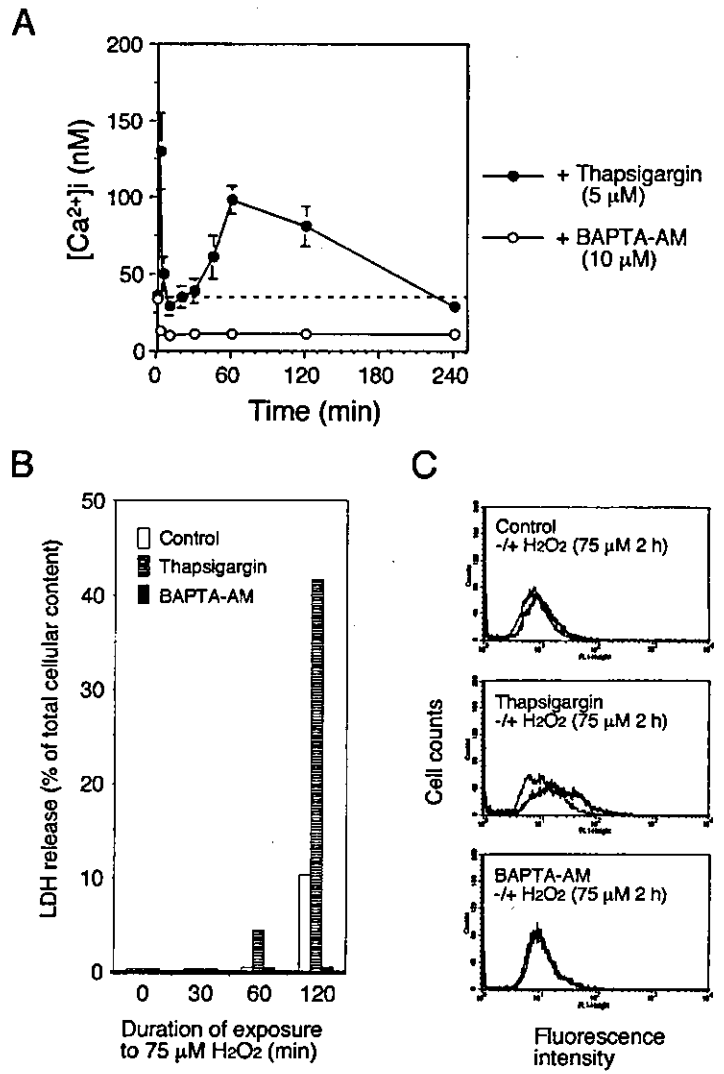

FIG. 1. **The long term elevation of $[Ca^{2+}]_i$ accelerates apoptosis in H9c2 cells under oxidative stress with H_2O_2.** *A*, H9c2 cells were treated with thapsigargin (5 μM) or BAPTA-AM (10 μM) for the periods indicated, and $[Ca^{2+}]_i$ was measured using Fura-2-AM as described under "Materials and Methods." Each value represents the mean ± S.D. of four independent experiments. *B*, after 4 h of treatment with thapsigargin (5 μM) or BAPTA-AM (10 μM) or not, the cells were incubated with H_2O_2 (75 μM) for the periods indicated. Cell injury was estimated by measuring the release of LDH in the culture medium as described under "Materials and Methods." The LDH release is shown as the proportion of total cellular LDH in the medium to total cellular LDH. Each value represents the mean of three experiments, and the S.D. was always within 10% of the mean. *C*, DNA double-stranded breaks were detected by the TUNEL method as described under "Materials and Methods." Cells were treated with either thapsigargin (5 μM) or BAPTA-AM (10 μM) for 4 h and untreated cells were prepared as a control. Then the cells were treated with (*thick lines*) or without (*thin lines*) H_2O_2 (75 μM) for 2 h. The results were reproducible in three independent experiments.

FIG. 2. **Ca^{2+} modulators influence the phosphorylation and kinase activity of Akt in H9c2 cells.** H9c2 cells were cultured in the presence of either thapsigargin (5 μM) or BAPTA-AM (10 μM) for the periods indicated. *A*, Akt phosphorylation was detected in the cell lysates by immunoblot analysis (*IB*) with anti-phospho-Akt (Ser-473), anti-phospho-Akt (Thr-308), and anti-Akt antibodies. *B*, quantitative data for the phosphorylation status of Akt shown in *A*. The band intensity was estimated densitometrically, and the phosphorylation rate is expressed as the relative intensity of the phosphorylated Akt (Akt-P/Akt. Each value represents the mean ± S.D. of four independent experiments. *C*, Akt kinase activity was assayed as described under "Materials and Methods" using GSK-3α/β as a substrate. Phosphorylated GSK-3α/β (Ser-21/9), the enzymatic products of Akt, was detected by immunoblot analysis using specific antibody. The data represent three independent experiments.

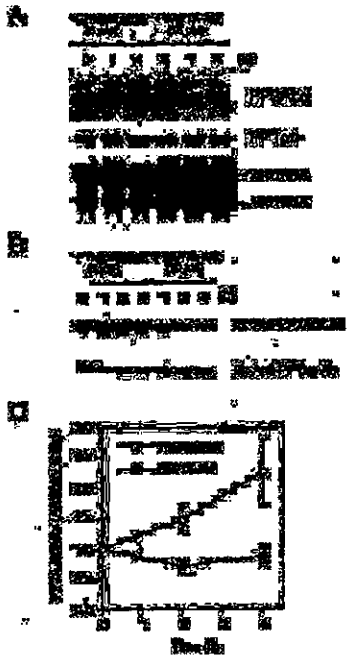

FIG. 3. **The expression and phosphatase activity of PP2Acα are regulated by Ca^{2+} modulators in H9c2 cells.** H9c2 cells were treated with thapsigargin (5 μM) or BAPTA-AM (10 μM) for the periods indicated. *A*, transcriptional levels of PP2Acα and PP1cα were evaluated by Northern blot analysis as described under "Materials and Methods." An EcoRI-PvuII fragment of 680 bp and a PstI-SmaI fragment of 600 bp were prepared from cDNAs for PP2Acα and PP1cα, respectively, and were used as cDNA probes after labeling with [α-^{32}P]dCTP. *B*, protein levels for PP2Acα and PP1cα were estimated by immunoblot analysis using specific antibodies. The data represent three independent experiments. *C*, protein phosphatase activity was assayed photometrically as described under "Materials and Methods." Each value represents the mean ± S.D. of four independent experiments.

of PP2A was also assayed in the cells treated with thapsigargin or BAPTA-AM for 0–4 h. As shown in Fig. 3*C*, the activity of PP2A increased with thapsigargin by ~2-fold compared with that of untreated cells. In contrast, the activity was slightly suppressed after 2 h treatment with BAPTA-AM. Collectively, these results indicate that PP2Acα expression is transcriptionally regulated by the long term change of $[Ca^{2+}]_i$ to control the phosphorylation status of target molecules including Akt.

Inhibition of PP2A Activity by Okadaic Acid Enhanced the Phosphorylation of Akt—Okadaic acid, a polyether toxin from the marine black sponge *Halichondria okadai* is a highly selective inhibitor of PP2A (29). To establish a link between Akt and PP2A, the influence of okadaic acid on Akt signaling was investigated with cells treated with okadaic acid. The cells were treated with okadaic acid (100 nM) for 0–30 min. The phosphorylation level of Akt was estimated by immunoblot analysis using specific antibodies. Akt kinase and PP2A activities were measured as described above. As shown in Fig. 4*A*, okadaic acid reduced the activity of PP2A by ~30%, and increased the phosphorylation level of Akt (both Thr-308 and Ser-473) and Akt kinase activity. Next, we examined whether the decrease in phosphorylation of Akt caused by thapsigargin could be reversed by okadaic acid. The cells were preincubated with thapsigargin (5 μM) for 4 h, and treated with or without okadaic acid (100 nM) for another 30 min, then the phosphorylation level of Akt was examined as described above. As shown in Fig. 4*B*, okadaic acid suppressed PP2A activity, and this reversed the decrease in phosphorylation of Akt with thapsigargin. Okadaic acid enhanced the phosphorylation of Akt at concentrations higher than 50 nM (data not shown). These results indicate that the function of PP2A can regulate the phosphorylation status of Akt in H9c2 cells.

Inhibition of PP2A Activity by Okadaic Acid Suppressed Apoptotic Cell Damage in H9c2 Cells Treated with Thapsigargin and H_2O_2—To establish a link between PP2A and Ca^{2+}-dependent enhancement of apoptosis, the influence of okadaic acid on apoptosis was investigated using cells treated with okadaic acid. In Fig. 5*A*, cells were treated with or without

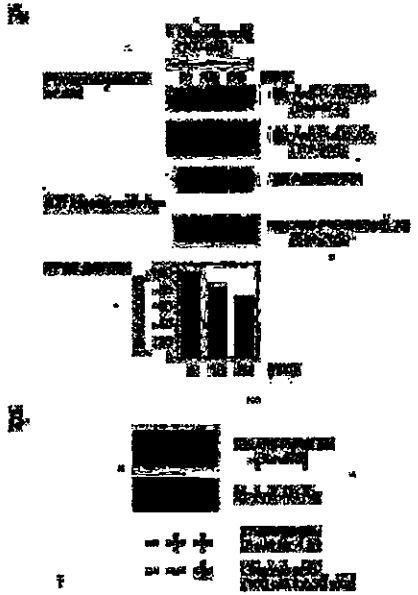

FIG. 4. **Inhibition of PP2A activity by okadaic acid enhances the phosphorylation of Akt in H9c2 cells.** *A*, H9c2 cells were incubated with 100 nM okadaic acid for 0–30 min. The phosphorylation level of Akt was estimated by immunoblot analysis using specific antibodies. The activities for Akt and PP2A were measured as described under "Materials and Methods." The data for PP2A activity represent the mean of three independent experiments. *B*, cells were preincubated with thapsigargin (5 μM) for 4 h then treated with or without okadaic acid (100 nM) for 30 min. The phosphorylation level of Akt (Ser-473) was examined by immunoblot analysis as described above. The data represent three independent experiments.

thapsigargin (5 μM) for 4 h then treated with okadaic acid (200 nM) for 30 min. Then cells were exposed to H_2O_2 (75 μM) for 0–2 h, and cell damage was examined at predetermined times using LDH release assay. The results showed that treatment with okadaic acid suppressed the Ca^{2+}-dependent enhancement of cell damage in cells treated with thapsigargin and H_2O_2. Fig. 5*B* shows a dose-dependent effect of okadaic acid on the Ca^{2+}-dependent enhancement of cell damage. Cells were treated with thapsigargin (5 μM) for 4 h then treated with different concentrations of okadaic acid (0–500 nM) for 30 min. Thereafter, cells were exposed to H_2O_2 (75 μM) for 2 h, and cell damage was examined using LDH release assay. Okadaic acid showed maximal cytoprotective effects at a limited concentration range around 100–200 nM. The protective effect of okadaic acid was rather diminished at concentrations higher than 500 nM (data not shown). Fig. 5*C* shows the effect of okadaic acid on Ca^{2+}-dependent enhancement of apoptosis. Cells were treated with thapsigargin (5 μM) for 4 h then treated with or without okadaic acid (100 nM) for 30 min. Then cells were exposed to H_2O_2 (75 μM) for 2 h, and apoptosis was examined by the TUNEL method. After thapsigargin treatment without okadaic acid, TUNEL-positive fluorescence intensity was significantly increased by H_2O_2 (Figs. 1*C* and 5*C*, Tg(+)OA(−)H_2O_2(+)). In contrast, okadaic acid reduced the TUNEL-positive fluores-

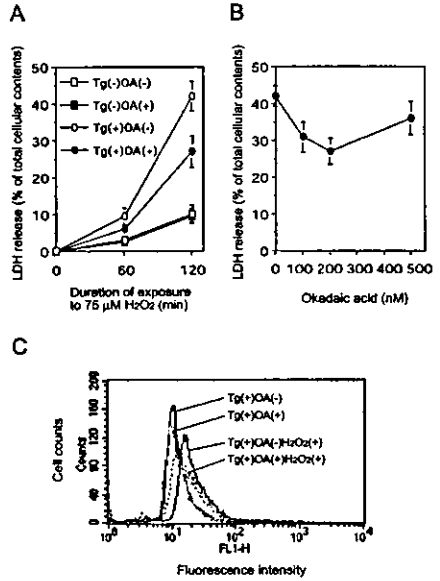

FIG. 5. **Inhibition of PP2A activity by okadaic acid suppresses apoptosis in H9c2 cells treated with thapsigargin and H_2O_2.** *A*, H9c2 cells were preincubated with or without thapsigargin (*Tg*, 5 μM) for 4 h then treated with or without okadaic acid (*OA*, 200 nM) for 30 min. Then the cells were treated with H_2O_2 (75 μM) for the periods indicated. Cell injury was estimated by measuring the release of LDH in the culture medium as described in Fig. 1*B*. Each value represents the mean ± S.D. of four independent experiments. *B*, cells were preincubated with thapsigargin (5 μM) for 4 h then treated with different concentrations of okadaic acid (0–500 nM) for 30 min. Then the cells were incubated with H_2O_2 (75 μM) for the periods indicated. Cell injury was estimated by measuring the release of LDH in the culture medium as described above. Each value represents the mean ± S.D. of four independent experiments. *C*, DNA double-stranded breaks were detected by the TUNEL method as described in Fig. 1*C*. Cells were treated with thapsigargin (5 μM) for 4 h then treated with or without okadaic acid (100 nM). Thereafter, the cells were treated with or without H_2O_2 (75 μM) for 2 h. The results were reproducible in three independent experiments.

cence intensity even in the cells treated with thapsigargin and H_2O_2 (Fig. 5*C*, Tg(+)OA(+)H_2O_2(+)) compared with that of cells treated with thapsigargin and H_2O_2 without okadaic acid. Okadaic acid did not solely affect the fluorescence intensity in cells with thapsigargin without H_2O_2 (Fig. 5*C*, Tg(+)OA(−) and Tg(+)OA(+)). However, it is noteworthy that okadaic acid shows an antiapoptotic effect at a limited concentration range around 100 nM. At concentrations above 500 nM, the antiapoptotic effect of okadaic acid was diminished or rather it showed enhancement of apoptosis in the cells treated with thapsigargin and H_2O_2 (data not shown). This may be explained by the dualistic effect of inhibiting the effects of PP1 and PP2A on both apoptosis and cell proliferation in cells exposed to okadaic acid or microcystin-LR (30). Together, these results indicate that okadaic acid, a specific inhibitor of PP2A, inhibits apoptotic cell damage in H9c2 cells treated with thapsigargin and H_2O_2, and strongly suggests that PP2A up-regulates the Ca^{2+}-dependent enhancement of apoptosis by dephosphorylating Akt to inhibit cell survival signaling.